

Nuclear Spin Effects in Nanostructures

Nuclear Spin Effects in Nanostructures

Proefschrift

ter verkrijging van de graad van doctor
aan de Technische Universiteit Delft,
op gezag van de Rector Magnificus prof. dr. ir. J. T. Fokkema,
voorzitter van het College voor Promoties,
in het openbaar te verdedigen op dinsdag 8 september 2009 om 12:30 uur

door

Jeroen DANON

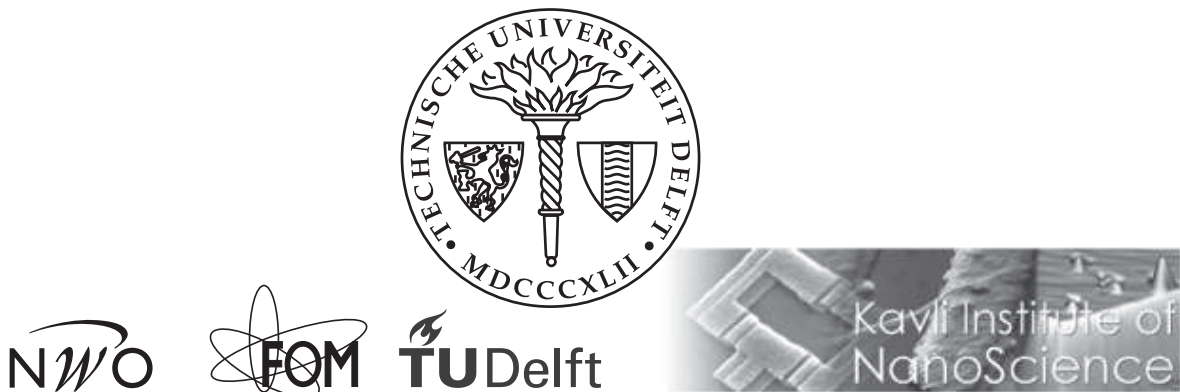
natuurkundig ingenieur
geboren te Delft.

Dit proefschrift is goedgekeurd door de promotor:

Prof. dr. Yu. V. Nazarov

Samenstelling van de promotiecommissie:

Rector Magnificus,	voorzitter
Prof. dr. Yu. V. Nazarov	Technische Universiteit Delft, promotor
Prof. dr. ir. L. M. K. Vandersypen	Technische Universiteit Delft
Prof. dr. ir. T. M. Klapwijk	Technische Universiteit Delft
Prof. dr. C. W. J. Beenakker	Universiteit Leiden
Prof. dr. G. Burkard	Universität Konstanz, Duitsland
Prof. dr. P. W. Brouwer	Freie Universität Berlin, Duitsland
Dr. P. A. Bobbert	Technische Universiteit Eindhoven
Prof. dr. ir. J. E. Mooij	Technische Universiteit Delft, reservelid



Published by: Jeroen Danon

Printed by: Ipskamp Drukkers B.V.

ISBN: 978-90-9024534-8

Casimir PhD Series, Delft-Leiden 2009-10

Copyright © 2009 by Jeroen Danon

An electronic version of this thesis is available at www.library.tudelft.nl/dissertations

Preface

In September 2003, my ninth year as a student at the TU Delft started. In the eight years before I had passed some exams, had been a fanatic musician in almost all student orchestras existing in the country, and had also spent a lot of time organizing tours and concerts for these orchestras. (In 2002 we managed to organize for the National Student Orchestra a tour to Carnegie Hall, New York!) So, I had a very busy life without spending too much of my time at studying physics, and I still did not have any definite plans to graduate in the near future.

Then, in the second week of September, something happened which might have been the first event in the chain of events finally leading to me writing this Ph.D. thesis. Somewhere in the physics building I bumped into a fellow student who had obviously lost his way. Probably he was a first or second year student, and indeed, if you don't understand the numbering in our building it is sometimes hard to find your way. He asked me where to find office C201, I explained him, and we both continued our way. Only later I realized that he had addressed me with the polite form 'U', which in Dutch you usually use for people of the age of your parents and older. When I thought some more about it, I started to feel a bit like an anachronism. I realized that I could not continue the way I was living for another eight years, and that the time had come to make serious decisions.

I decided to graduate. In the year 2003–2004 I finished (almost) all courses I still had to follow, and in the spring of 2004 I started to look for a final research project. After having visited several groups, I decided to join the Theory group and take a project Yuli offered me. The project seemed interesting and challenging to me, and I started working on it in May 2004. At that moment I was not sure yet what to do after my graduation: whether to consider to do a Ph.D. or to go to work in industry. About one thing however, I was absolutely sure: As soon as I would get my Master's degree, I would leave the TU Delft. I was born in Delft, lived all my life in or close to Delft, and had been at the TU for too many years. It was time to broaden my horizon.

However, it turned out completely different. I very much enjoyed doing research, and already halfway my year in the Theory group I had made my mind up that I wanted to find a Ph.D. position after my graduation. When my year of

research was nearing its end, Yuli offered me the possibility to stay in the group as a Ph.D. student. My first thought was: “Of course not. After all, I already decided that I need to flee far away from Delft after my graduation.” But then I realized how much I enjoyed working with Yuli, and what a seemingly infinite amount of things I still could learn from him. It became a tough decision, but in the end I decided that doing a Ph.D. was about physics and not about living in Delft or not. So I accepted Yuli’s offer, and started in September 2005 as a Ph.D. student in the group.

Now, four years later, I can say that this was indeed the right decision. I learned a lot in the past four years, and enjoyed very much being part of the Theory group. Of course, the fact that it all turned out so well is not at all just my own accomplishment. Many people — colleagues, family, friends — played an important role in this, and it would be unfair not to mention them here.

When I started, my colleagues Xuhui, Izak, Wouter, Sijmen, Omar, Rachid, Richard, Gabriele, Alex, Jens and Oleg made the Theory group a lively place, where it was fun to work. As in any research group, many people come and go every year, and all colleagues mentioned above have left the group by now. Since I started, Henri, Fabian, Rutger, Dima, Moosa, Vitaly, Marnix, Jiang, Hongduo, Kevin, Stefan, Martijn, Chris, Giorgi, Mariya, Alina, Kim, Tungky, Ciprian, Fatemeh Mirjani, Mireia and Fatemeh Joibari joined the group as new Master students, Ph.D. students and postdocs, some of them already left again. They all contributed to the pleasure I had working in this group.

I am also very grateful to the scientific and administrative staff of the group. I bothered Gerrit, Yaroslav, Jos and Miriam regularly to ask advice, sometimes about physics, sometimes about other issues. I am very happy that they were always willing to help me. Last November our secretary Yvonne retired, who had been an indispensable force in the group for so many years that no one knew exactly how many. We had some difficulty finding a new secretary, but in the end it turned out all right. Several months ago Marjolein started as our new secretary, and I am sure that she will manage our group as well as Yvonne did.

During my four years of research, I also had the great privilege of collaborating with colleagues from the Quantum Transport group ‘downstairs’. One of the main goals of my research project was to understand some aspects of a series of experiments which had been performed by Frank. In my first years I regularly met Frank to discuss his data and my models. Already then, he really was an expert on the subject, and I learned a lot from him. Finally, in my last year, this collaboration resulted in two publications. Since Frank had already left Delft in 2007, the publications were prepared in close collaboration with his colleagues Ivo, Katja and Lieven. I think that half of the understanding of my own work

resulted from the discussions I had with them, I am very grateful for that.

In my last year I also developed an interest in some specific issues in related nanowire experiments. Again I was lucky: in the Quantum Transport group, Stevan and Sergey were performing exactly the kind of experiments about which I was thinking. In the past few months we regularly met to discuss our work, which I found very stimulating. I very much hope the we can continue our collaboration also after my graduation.

I should also thank my ‘formal’ boss, Leo, for his sincere interest in my work and my progress. I experienced our yearly evaluation meetings as very valuable and motivating.

Finally, I want to thank Yuli: I honestly cannot imagine a better supervisor. At almost any time I could bother him with my questions, most of them related to physics but sometimes about anything. Always he would take as much time for me as was needed to answer them: even during weekends or holidays, an e-mail sent to Yuli would mostly be answered within a day. His great insight in physics and incredible patience in explaining me things I did not understand are amazing. After working together with Yuli for in total five years, the feeling persists that there still is an almost infinite amount of things left that I could learn from him. On the other hand, it is also hard to overstate how much I already did learn from him. Yuli, thank you very much for that.

Apart from all my colleagues at the TU, also my family and friends have been indispensable. Geert, Pieter, Marco, and many more: without all my friends close by, the past four years would have been much more difficult. It is also hard for me to imagine how I could have done this all without the love and support I get from my parents, my brother Bart, and, during the last year, my girlfriend Anna. If I would try to explain them how much they contributed to my successful completion of this work, they would probably not believe me.

And, last but not least, I should thank the anonymous student addressing me with ‘U’ in September 2003. If it were not for him, my life might have been completely different.

Jeroen Danon
July 2009

Contents

1	Introduction	1
1.1	Nanosopic physics	2
1.2	Quantum information	3
1.3	Outline of this thesis	5
2	Spin Devices	7
2.1	Quantum dots	7
2.1.1	Single quantum dots	9
2.1.2	Double quantum dots	10
2.1.3	Pauli spin blockade	11
2.2	Spin qubits in quantum dots	12
2.3	Interaction of a localized spin with its environment	14
2.3.1	Relaxation and dephasing	14
2.3.2	Spin-orbit interaction	16
2.3.3	Hyperfine interaction	19
2.3.4	Feedback effects of hyperfine interaction: DNSP	22
2.4	Spin valves	24
2.4.1	Spin-polarized transport in spin valves	25
2.4.2	Hyperfine interaction in spin valves	26
3	Useful theoretical concepts	27
3.1	Rotating frame	27
3.2	Perturbation theory	28
3.3	Stochastics of the nuclear spin dynamics	30
4	Nuclear tuning and detuning of the electron spin resonance in a quantum dot: Theoretical consideration	35
4.1	Introduction	36
4.2	Model	37
4.3	Results	40
4.4	Conclusion	43

5	Multiple nuclear polarization states in a double quantum dot	45
5.1	Introduction	46
5.2	Experimental observations	47
5.3	Model	50
5.4	Results	51
5.5	Conclusion	54
5.6	Appendix	54
5.6.1	Sample	54
5.6.2	Measurements	56
5.6.3	Candidate mechanisms	56
5.6.4	Theory	58
5.6.5	More detailed results	61
6	Locking electron spins into magnetic resonance by electron-nuclear feedback	65
6.1	Introduction	66
6.2	ESR detection scheme	67
6.3	Locking to the spin resonance condition	67
6.4	Locking characteristics	70
6.5	Dependence on sweep and excitation parameters	70
6.6	A phenomenological model	73
6.7	Implications for electron spin dephasing	75
6.8	Acknowledgments	76
6.9	Appendix	76
6.9.1	Tuning the double dot	76
6.9.2	Suppression of fluctuations	77
6.9.3	Statistics of switching	79
6.9.4	Analysis of ESR current levels	80
6.9.5	Pump-probe measurements	82
7	Pauli spin blockade in the presence of strong spin-orbit coupling	85
7.1	Introduction	86
7.2	Model and approach	88
7.3	Results	91
7.4	Conclusion	93

8 Nuclear spin effect in a metallic spin valve	95
8.1 Introduction	96
8.2 Overview	96
8.3 Model	97
8.4 Approach	99
8.5 Conclusion	103
Bibliography	105
Summary	117
Samenvatting	119
Curriculum Vitae	123
Publications	125

Chapter 1

Introduction

In 1687 Isaac Newton published his famous *Philosophiæ Naturalis Principia Mathematica*, in which he laid the foundations of our understanding of classical mechanics. For over 200 years, Newton's laws seemed to provide a rigid description of all mechanical motion, on small as well as large scales. When James Clerk Maxwell formulated his theory of electromagnetism in 1873, it was widely believed that our understanding of the physical laws of the universe was nearing its completion: there was no doubt that all remaining open issues would soon be clarified within the existing theories

However, as experimental techniques advanced, a growing number of observations could not be fit in Newton's and Maxwell's 'classical' theories. A study of the radiation spectra of excited atoms led Max Planck in 1900 to the hypothesis that the atomic energy levels are discrete, and that an atom can only radiate separate, well-defined quanta of energy. In 1905 Albert Einstein explained the photoelectric effect by proposing that also light consists of individual discrete quanta, which later came to be called photons. In the following decades, these ideas of 'quantization' evolved into the revolutionary theory of *quantum mechanics*, describing physical phenomena on the atomic scale. The classical laws turned out to be only a limiting case of this quantum theory.

Despite its success in explaining and predicting phenomena on the small scale, the interpretation of quantum mechanics has been subject of intensive debate. A lot of the elementary building blocks of quantum theory do not appeal to common sense very much: fitting quantum mechanics with our picture of the everyday world is difficult if not impossible. For example, the principle of *superposition* tells us that particles can have mutually excluding properties at the same time. Erwin Schrödinger explained the strangeness of this idea once using the analogue of a cat which is dead and alive simultaneously. Another curious concept is that of *entanglement*: multiple particles can be in a sort of 'joint' quantum state, in

which each particle carries information about all others. Even after separating them far apart, manipulating one of the entangled particles will immediately affect all the other particles.

Most physicists however appreciate the practical power of quantum theory, and consider the interpretation of the theory, if important at all, to belong to the realm of philosophy rather than physics. The brilliant physicist and Nobel prize winner Richard Feynman once even stated: “I think I can safely say that nobody understands quantum mechanics.” Indeed, without worrying about the philosophical implications of the theory, we can use quantum theory to accurately describe the world at the atomic scale. It has proven to be a very rigid theory: it provided an explanation for many phenomena which could not be understood within any other theoretical framework, and it was at the source of several major technological advances.

1.1 Nanoscopic physics

In the last century, fabrication techniques have experienced a huge development, allowing experimentalists to design and build increasingly small devices.

One of the intriguing aspects of this development is that, as devices become smaller and smaller, at some point they will no longer obey the classical laws of physics, but rather those of quantum mechanics. Already in the 1980s, physicists could fabricate electronic systems which manifested quantum mechanical effects such as interference of electrons [1]. These systems were typically of micrometer size, which is still very large compared to the atomic scale ($\sim 1 \text{ \AA} = 10^{-4} \text{ \mu m}$), but comparable to the electronic correlation length. This implies that electrons typically can travel through the whole system without their quantum mechanical state being changed, and therefore can interfere coherently with electrons traveling via another path. Nowadays, state-of-the-art fabrication produces electronic systems rather of nanometer scale and quantum effects such as superposition and entanglement can be clearly observed in some experiments.

A field which has recently emerged in the rapid advance of experimental techniques is that of *spintronics*, its central theme being the active manipulation of spin degrees of freedom in nanoscopic solid state systems. Although spin is a quantum mechanical property of particles, most of the spintronic devices involve rather the average spin of large ensembles, which is manifested by spin density or magnetization. These properties, being collective, macroscopic variables, behave mainly classically: they usually can be described by a single vector giving the strength and direction of a magnetization or of a local spin density. Quantum effects, such

as superposition or entanglement of these vectors have never been observed.

The field of spintronics has produced some important scientific discoveries, e.g. the spin Hall effect [2] and magnetic semiconductors [3]. Some spintronic phenomena, such as magnetoresistance, led to widely used applications: the giant magnetoresistance effect, only discovered in 1988 [4, 5], is nowadays commonly used for the read-out of the bits stored on a hard disk. For an excellent review of the field of spintronics, we refer to [6].

1.2 Quantum information

In the 1980s, theorists already speculated that quantum systems might be able to perform certain information processing tasks much more efficiently than classical systems [7]. Based on clever exploitation of the quantum concepts of superposition and entanglement, several futuristic applications were invented, such as schemes to transfer information encoding complete quantum states (*quantum teleportation* [8]), infallible cryptography of messages (*quantum cryptography* [9]), and performing complex calculations using quantum states as computational units (*quantum computation* [10]).

Let us focus on quantum computation, and give a simplified picture of the difference between a ‘classical’ and a quantum computer. As mentioned above, the superposition principle tells us that a quantum system can be in several distinct states at a time. Where a classical two-level system can only occupy one out of the two levels (such as a classical bit being either 0 or 1), a quantum two-level system can be in any superposition of the two states. A computational operation f performed on a classical bit will give as result $f(0)$ or $f(1)$, depending on the input state of the bit. Using a quantum bit (*qubit*), one could perform the same operation on a superposition of $|0\rangle$ and $|1\rangle$ and get as result a superposition of $f(|0\rangle)$ and $f(|1\rangle)$, i.e. both possibilities are evaluated simultaneously. For a multi-qubit system, the gain becomes even more significant: it can be shown [11] that the computing power of a quantum computer scales exponentially with the number of bits, whereas this scaling is only linear for a classical computer. Therefore, a large enough quantum computer could outperform any classical computer.

Based on this simple idea, several quantum algorithms have been developed, such as for factoring integers [10], simulating quantum systems [12] and searching databases [13]. From a theoretical point of view the quantum computer seems to be feasible, the challenge being rather a technical one.

A major fundamental problem is the interaction of the qubit with its (uncontrolled) environment. This interaction inevitably leads to ‘decoherence’, i.e.

unwanted evolution of the qubit states, introducing errors in the computation. After some time, typically the *decoherence time*, the states of the qubits are significantly different from what they should be, this setting a practical length limit for quantum computations. To overcome this problem, some algorithms for detecting and correcting errors have been developed [14, 15]. These algorithms however still impose an accuracy boundary on single quantum operations, for which an optimistic estimate gives around 10^{-4} , implying that the decoherence time of a qubit must be minimally equal to the time it takes to do roughly 10^4 operations. This defines two important challenges: (i) to reduce the coupling of the qubit with its environment, thereby extending the decoherence time, and (ii) to develop ‘fast’ quantum operations.

Apart from the fundamental problem of the environment, there also exist several technical difficulties. First of all, the number of coupled qubits needed to do a useful computation is at least of the order of 100. This demands from a qubit design that it should be easily scalable to large numbers. Also, the physical implementation of single quantum operations is not always straightforward, since any error due to inaccurate operations adds effectively to decoherence.

Motivated by all these different constraints, a number of physical implementations of the qubit have been proposed in the past few decades, part of which is presently under experimental investigation. Among them are atomic systems (such as atoms in optical lattices [16], ions in electrostatic traps [17], and ensembles of nuclear spins in a liquid [18]) and solid state systems (such as superconducting circuits containing Josephson junctions [19] and single electron spins trapped in quantum dots [20], in impurities [21], or in nitrogen defects in diamond [22]). Each of these approaches has its own advantages and disadvantages.

The ‘conflicting’ requirements of good controllability and weak decoherence create an interesting tension in the design of the qubit: on the one hand one wants to have accurate control over the states of the qubits, which demands for an effective coupling to some environmental degrees of freedom, but on the other hand, from the point of view of decoherence, one would rather have qubits which are completely isolated from their environment. An attempt to meet both requirements in one design is, for instance, the electron spin qubit in a quantum dot: most fluctuations in the environment couple to the *charge* of the electron, and therefore do not influence the qubit states, which are encoded in the *spin* degree of freedom of the electrons. The qubit states could then be effectively addressed by applying well controllable magnetic fields to the sample. A third requirement, already mentioned above, is that of scalability of the qubit, i.e. it should be not fundamentally more difficult to create a circuit of 100 qubits than just one. Most microscopic qubit proposals (such as trapped atoms or ions, or nuclear spins in

a liquid) have very good coherence properties, but are badly scalable. Although the most remarkable realization of quantum computing to date is the factoring of the number 15 in a liquid-state NMR quantum computer [23], there exists no systematic way for scaling up these systems to work for a larger number of qubits. Larger, artificially engineered systems on the other hand, such as solid state devices, are in principle easily scalable, but usually have bad coherence properties or do not give accurate control over the qubit states. To meet all these different criteria in a single design is a major challenge: the perfect qubit still has to be invented.

Of course, apart from the more ‘fundamental’ challenges, also practical aspects of a qubit design such as the complexity and economic cost of the fabrication process should be taken into account. If scaling up from a single qubit to multiple qubits would involve an exponential growth of fabrication costs, the gain in information processing power would be completely canceled out by the economic drawbacks. Presently however, most research is still focused on creating operational single and double qubits: the specific problems which will arise when a certain design has to be scaled up to a multiple qubit system do not yet get too much attention.

1.3 Outline of this thesis

In this thesis we investigate effects of interaction between electron spins and nuclear spins in two nanoscopic devices, the *quantum dot* and the *spin valve*.

In Chapter 2 we will introduce the devices. First, we discuss the quantum dot and its derivative, the double quantum dot. We explain its basic physics and one of its proposed applications, which is the implementation of electron spin qubits. We discuss a number of possible types of interaction of an electron spin in a quantum dot with its environment, and explain how these will lead to decoherence of the spin qubit. We focus on the interaction which dominates decoherence: the hyperfine interaction of the electron spin with all the nuclear spins in the quantum dot host material. We finally show how this interaction not only affects the electron spin, but also can lead to the build-up of large nuclear polarizations. In the last Section, we introduce the spin valve, one of the basic spintronic devices. It consists of a small ferromagnet-normal metal-ferromagnet junction which exhibits strong magnetoresistive effects: the conductance of the junction can vary strongly when changing the directions of magnetization in the two ferromagnets. We also discuss what is generally seen as the role of hyperfine interaction in metallic spintronic devices.

In Chapters 4–8 we investigate in more detail effects of hyperfine interaction in quantum dots and spin valves. A few specific theoretical techniques we apply in these Chapters are introduced and briefly explained in Chapter 3.

In Chapter 4 we start by investigating the coupled electron-nuclear spin dynamics in a single quantum dot under conditions of electron spin resonance. We show how the non-equilibrium electron spin dynamics can cause strong nuclear spin pumping. The resulting nuclear spin polarization feeds back to the electron spin, and will thereby be clearly observable in experiment. Then, in Chapters 5 and 6, we turn to the same effect in a double quantum dot. We develop a model taking into account experimental complications such as electrical side-effects of magnetic driving, and support our results with extensive experimental data. In Chapter 7 we present the first step of our analysis of similar effects which have been observed in quantum dots in materials with strong spin-orbit coupling, even without driving the electron spin resonance. We show that the presence of spin-orbit coupling drastically modifies the basic spin physics in the dots, and we explain several unexpected experimental observations.

Finally, in Chapter 8, we investigate nuclear spin effects in a metallic spin valve. It is widely believed that in metallic devices hyperfine interaction manifests itself merely as a weak source of spin relaxation and that it does not influence the electronic transport properties of the devices directly. We propose a simple experiment in which a feedback effect of the interaction is expected to produce clearly observable current oscillations.

Chapter 2

Spin devices

In this chapter we will introduce the systems which we investigate further in Chapters 4–8, the *quantum dot* and the *spin valve*. After explaining the basic physics of the quantum dot, we will focus on electron spin qubits in quantum dots and discuss the most important interactions of the qubit with its environment. We show that the nuclear spins in the quantum dot are an important source of decoherence and we discuss ideas to overcome this problem. In the last Section of this Chapter, we will introduce the spin valve, and explain what is commonly believed to be the role of the nuclear spins in this device.

2.1 Quantum dots

Generally, a quantum dot is a small quantum well in which one can trap electrons. The dot can be coupled by tunnel barriers to reservoirs or to other quantum dots, with which it can exchange electrons (see e.g. Fig. 2.1). With gate electrodes one can tune the electrostatic potential of the dot with respect to the leads, as well as the strength of the tunnel barriers (not shown in the Figure).

Being such a general kind of system, quantum dots of many different sizes and materials exist. A few examples of experimental realizations of quantum dots are:

- *Self-assembled quantum dots* [25] are small three-dimensional islands of a low-bandgap material embedded in a high-bandgap material, such as InAs islands in a GaAs environment. Under certain conditions the dots nucleate spontaneously during growth, due to the lattice mismatch between the two materials ($\sim 7\%$ for an InAs-GaAs system). The dots have typical dimensions between 5 and 50 nm. With an applied gate voltage over the sample one can accurately tune the average number of electrons in the dots. Ex-

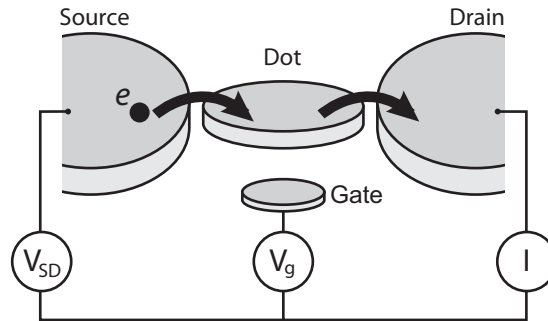


Figure 2.1: Schematic picture of a quantum dot coupled to a source and drain reservoir via tunnel barriers. With a gate voltage V_g the electrochemical potential of the electrons on the dot can be tuned. In response to a bias voltage V_{SD} a current I can flow through the device. (Picture adapted from [24].)

perimental access to the dots is usually obtained by shining with a laser on the dots, thereby creating excitons (excited electron-hole pairs), and subsequently measuring the photoluminescence from the dots. These dots have potential application in quantum cryptography since they can behave as single-photon sources. An important limitation of the self-assembled dots is the lack of control over positioning of individual dots.

- *Semiconductor lateral dots* [26] are created in a two-dimensional electron gas (2DEG) formed at the interface of two materials in a semiconductor heterostructure. When a negative voltage is applied to gate electrodes on top of the heterostructure, the 2DEG is depleted below the electrodes. This allows to design barriers in the 2DEG, thereby creating separate islands connected to each other or to large reservoirs by tunnel barriers. These quantum dots have typically lateral dimensions exceeding 100 nm. They are mainly of interest for experiments and applications involving electron or hole transport, i.e. electrical currents.
- *Semiconducting nanowires* [27] provide a natural one-dimensional confinement for electrons and holes, and are therefore interesting candidates for hosting quantum dots. The wires have a typical diameter of several tens of nanometers and can be gated with electrodes to create tunnel barriers, thereby forming quantum dots typically smaller than the dots defined in a 2DEG. When the two ends of the wire are contacted to large reservoirs, one can do similar transport measurements as on lateral dots. Since the nanowire dots are not embedded in a large piece of host material, one could also optically address the dots, or possibly use them as single-photon

sources. In recent years the techniques for growing, contacting and gating nanowires have improved rapidly.

Let us also refer to some of the many excellent reviews written on the topic of quantum dots [24, 28, 29].

2.1.1 Single quantum dots

We start by considering the simple case of a single quantum dot. The electronic properties of a quantum dot are mainly determined by two factors. (i) Due to the small size of the dot, the electrons in it experience a strong confinement in all directions. This confinement leads to a discrete energy spectrum of electronic levels, so that the dot resembles, in a way, an atom [30]. (ii) A similar, but typically stronger effect results from the Coulomb repulsion between single electrons: for adding an extra electron to the dot, one has to overcome the electrostatic potential set up by all other electrons on the dot. This effect can lead to a complete blockade of electron transport through the dot, also known as *Coulomb blockade*, and it provides a practical way to tune the exact number of electrons on the dot.

Both of these effects can in principle be observed if one measures the current through the dot when varying the gate voltage V_g , with a very small but finite

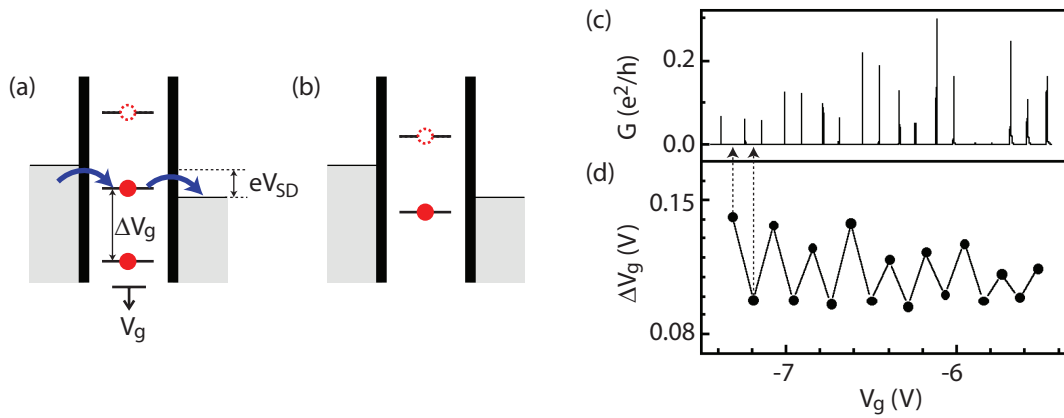


Figure 2.2: A single quantum dot coupled to two leads. (a,b) Schematic energy diagrams for two different gate voltages V_g . In (a) there exists an electronic level with its electrochemical potential lying within the bias window eV_{SD} , causing current to flow. In diagram (b) there is no available level within the bias window: the system is in Coulomb blockade. (c) The conductance of the dot as a function of V_g with a small bias voltage applied. (d) The distance between adjacent all peaks in (c). (The experimental data in (c,d) are taken from [31].)

bias voltage V_{SD} applied (see Fig. 2.2). The current peaks observed in Fig. 2.2.c indicate for which gate voltages a discrete electronic energy level lies within the bias window (Fig. 2.2.a). The spacing between the peaks is therefore proportional to the spacing of the levels.

The alternation of the spacings (Fig. 2.2.d) can be understood as follows: to add a new electron to the dot, one always has to overcome the Coulomb repulsion, causing all current peaks to be spaced in terms of energy by E_C , the electrostatic charging energy of the dot. However, if the total number of electrons on the dot is even, in principle one expects them all to form pairs of spin singlets, and the next electron added to the dot will have to occupy an empty orbital state with a higher energy. Therefore every second peak spacing is expected to be $E_C + \Delta$, where Δ is the spacing of the orbital levels involved. This implies that also for larger numbers of electrons on the dot, the spin states might be well approximated by a one-electron Zeeman doublet (when the number of electrons on the dot N is odd) or by two-electron singlet or triplet states (when N is even).

2.1.2 Double quantum dots

A double quantum dot is a slightly more complex device consisting of two quantum dots connected with a tunnel barrier, and both coupled to a reservoir (see Fig. 2.3.a). With two gates V_{g1} and V_{g2} one can shift the electrochemical potential of the electronic levels in the two dots separately.

If one applies a small bias and measures the current through the double dot (or the differential conductance dI/dV_{g1}) as a function of V_{g1} and V_{g2} , again electronic transport is only observed for distinct gate voltages. In these points all potentials of the charge states involved in transport lie within the bias window (Fig. 2.3.b). Outside of these points the number of electrons on both dots is in principle well defined: the numbers (n, m) in Fig. 2.3.c denote a charge state with $n(m)$ electrons on the left(right) dot. (The numbers in the Figure are fictitious and only meant for illustrational purposes. One can in principle determine the electron numbers exactly by depleting the dots with large negative gate voltages and then adding electrons one by one.) We can now identify e.g. the transport in the green circle as the cycle $(1, 1) \rightarrow (2, 1) \rightarrow (1, 2) \rightarrow (1, 1)$, and transport in the blue circle as $(2, 2) \rightarrow (2, 1) \rightarrow (1, 2) \rightarrow (2, 2)$.

The distances ΔV_{g1} and ΔV_{g2} observed in Fig. 2.3.c again correspond to the spacing of the electronic energy levels in the left and right dot. For both dots an electronic shell filling as in the single dot case can be expected. One complication in the energy spectrum of the double dot is that due to the interdot tunnel coupling two doublet states in the two dots can form a two-dot singlet or triplet.

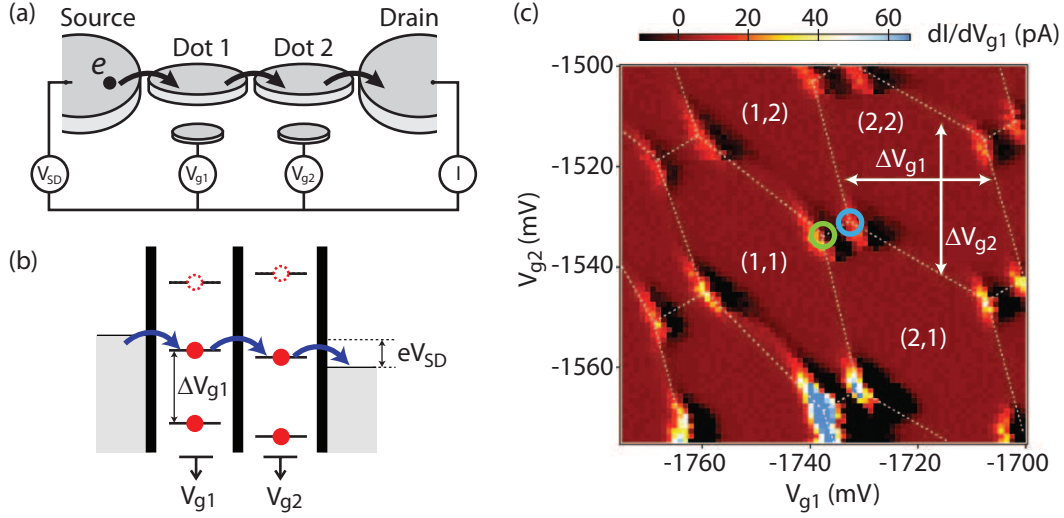


Figure 2.3: (a) A double quantum dot coupled to two leads. (b) Schematic energy diagram of the double dot. Electrons can flow from the left lead to the right lead as long as the electrochemical potentials of all charge states involved in the transport lie within the bias window. (c) The differential conductance of a double quantum dot as a function of the two gate voltages V_{g1} and V_{g2} . (Experimental data taken from [32].)

If such a (1,1) singlet or triplet is close to degeneracy with the corresponding (0,2) spin state, the two states will hybridize.

2.1.3 Pauli spin blockade

An interesting regime of the double dot is where electron transport involves the cycle $(0,1) \rightarrow (1,1) \rightarrow (0,2)$, also known as the Pauli spin blockade regime [33]. As explained above, the (0,2) as well as the (1,1) states can form spin singlets and triplets, which are coupled by the interdot tunnel coupling t . Let us investigate the regime where the (0,2) singlet state $|S_{02}\rangle$ (which is typically the (0,2) ground state) is close to degeneracy with the (1,1) singlet state $|S\rangle$. In this case, for not too large external magnetic fields B_{ext} , all three (1,1) triplet states, $|T_{\pm}\rangle$ and $|T_0\rangle$, are usually far from degeneracy with the (0,2) triplet, i.e. this energy difference is much larger than t . Therefore charge transitions from $|T_{\pm}\rangle$ or $|T_0\rangle$ to the (0,2) triplets are very unlikely, and for describing transport we can focus on the subspace of the four (1,1) states and $|S_{02}\rangle$.

The Hamiltonian describing the energy spectrum of the five states then reads

$$\hat{H} = g\mu_B B_{\text{ext}} \{ |T_+\rangle \langle T_+| - |T_-\rangle \langle T_-| \} - \Delta_{\text{LR}} |S_{02}\rangle \langle S_{02}| + t \{ |S\rangle \langle S_{02}| + |S_{02}\rangle \langle S| \}, \quad (2.1)$$

where g is the effective g -factor of the electrons, μ_B the Bohr magneton, and Δ_{LR} the energy difference between $|S\rangle$ and $|S_{02}\rangle$. In Fig. 2.4.a we plotted the resulting energy spectrum as a function of the detuning Δ_{LR} , where we chose $g\mu_B B_{\text{ext}} = 3t$. If one would tune the system to a finite detuning (e.g. as indicated by the vertical dashed line), one can sketch the relevant energy levels as in Fig. 2.4.b.

The mechanism of spin blockade is now easy to understand. If $\Delta_{LR} < 0$, no transport is expected as the system is in Coulomb blockade. For $\Delta_{LR} \geq 0$ we have to distinguish two situations. (i) An electron entering the left dot forms a $(1,1)$ singlet state with the electron in the right dot. Then the state $|S_{02}\rangle$ is energetically favorable over $|S\rangle$ and an electron will tunnel from the left to the right dot. This transition can be the result of coherent coupling between the states, or inelastic relaxation (for larger detuning). Finally $|S_{02}\rangle$ decays to a $(0,1)$ state, thereby contributing to the current through the double dot. (ii) The electron entering the left dot forms a $(1,1)$ triplet state with the one in the right dot. As the $(0,2)$ triplet states are inaccessible due to their high energy (Fig. 2.4.b), the left electron cannot move to the right dot and the current is blocked.

This spin-selective blockade can be harnessed such that it serves as a practical tool for the read-out of single electron spin states [34, 35, 36, 37, 38].

2.2 Spin qubits in quantum dots

In 1998, Loss and DiVincenzo [20] proposed to use the spin up and down states of electrons trapped in quantum dots as qubit states. As most environmental

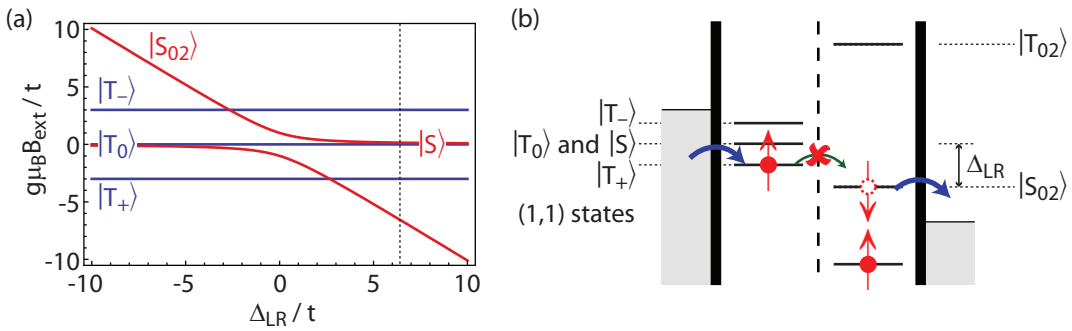


Figure 2.4: A double quantum dot in the spin blockade regime. (a) The energy spectrum of the double dot in vicinity of the degeneracy point of $|S\rangle$ and $|S_{02}\rangle$, following from (2.1). (b) Energy diagram for finite detuning Δ_{LR} . The $(0,2)$ triplets are split far apart in energy, so the only accessible $(0,2)$ state is a spin singlet: charge transitions from any $(1,1)$ triplet state to a $(0,2)$ state are forbidden and the current is blocked.

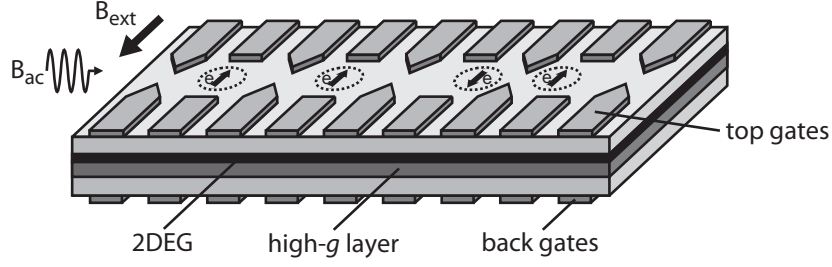


Figure 2.5: Electron spin qubits in a multi-quantum dot structure defined in a two-dimensional electron gas (Figure adapted from [39]). By changing the voltages on the top gates one can couple or decouple two neighboring qubits. Single qubit rotations can be performed by applying microwave excitation B_{ac} resonant with the Zeeman splitting of the qubit states.

fluctuations only couple to the *charge* of the electrons in a quantum dot, it was expected that quantum dot *spin* qubits would be well isolated from their environment, therefore possibly combining the properties of a long coherence time and scalability. Motivated by this proposal, several systems for isolating and manipulating single electron spins have been investigated, such as N-V centers in diamond, self-assembled quantum dots, quantum dots defined in one-dimensional structures as carbon nanotubes or semiconducting nanowires, and quantum dots defined in a two-dimensional electron gas.

To distinguish the two spin qubit basis states in experiment, one can apply an external magnetic field B_{ext} , which splits the spin up and down state by the Zeeman energy E_Z . Using this splitting, one can think of ways to initialize or read-out the qubit spin-selectively. To complete the set of requirements for quantum computation, one needs a universal set of quantum operations, i.e. a set of basic qubit operations from which any quantum operation can be compiled. Single qubit rotations can be achieved by applying a small oscillating magnetic field $B_{ac} \cos(\omega t)$ perpendicular to B_{ext} : when the frequency of this oscillating field matches the Zeeman splitting of an electron, i.e. $\hbar\omega = g\mu_B B_{ext}$, its spin will be coherently rotated between up and down. Two-qubit operations can be achieved by varying the coupling strength between a pair of quantum dots. In the case of quantum dots defined in a two-dimensional electron gas (2DEG), this could be carried out purely electrically, by varying the top gate voltage that controls the potential barrier between two dots (see Fig. 2.5). When two neighboring quantum dots are coupled via a tunnel barrier, single spins in the two dots will interact via the Heisenberg exchange interaction, $\hat{H}_{ex} = J\hat{\mathbf{S}}_1 \cdot \hat{\mathbf{S}}_2$, where $\hat{\mathbf{S}}_{1(2)}$ is the electron spin operator in dot 1(2) and J the strength of the coupling [20].

By turning on this interaction for a certain time, the two spins can be swapped or even entangled. The combination of single spin rotations and this two-spin interaction forms a universal set of quantum operations [20].

In recent years, all the ingredients for quantum computation have separately been realized in semiconducting quantum dots: in self-assembled InAs/GaAs quantum dots it was shown that with optical cooling one can initialize a qubit in one of the two spin states with a fidelity exceeding 99.8 % [40]. Coherent single qubit rotations have been demonstrated in GaAs quantum dots defined in a two-dimensional electron gas, using a microwave magnetic [34] or electric [35] field. In the same type of system, coherent interactions of two spins in two coupled quantum dots were observed [36], and also a spin read-out scheme was implemented which yielded a single-shot visibility of more than 80 % [41].

This all seems to be very promising, and has motivated many more experiments on spin qubits in semiconducting quantum dots. However, although not foreseen by all, the main drawback of the semiconducting quantum dot spin qubit turned out to be the short spin coherence time. Even for high-purity GaAs quantum dots this time was measured to be in the ns range [37, 36, 38]. In the next section we will discuss the most important interactions of the quantum dot spin qubit with its environment, leading to this short coherence time.

2.3 Interaction of a localized spin with its environment

As explained earlier, the information stored in a qubit is in general very fragile and easily lost in interactions with the environment. In this section we explain the concepts of relaxation and dephasing of the qubit in the context of coupling to a general fluctuating environment. We will then focus on spin-orbit interaction and hyperfine interaction, which are believed to play an important role in relaxation and dephasing of quantum dot spin qubits.

2.3.1 Relaxation and dephasing

The information stored in a qubit can be lost in two different ways. To understand this, let us consider a qubit which is prepared in an arbitrary superposition state

$$|\Psi_{\text{qubit}}\rangle = \cos \frac{\theta}{2} |\uparrow\rangle + e^{i\varphi} \sin \frac{\theta}{2} |\downarrow\rangle.$$

As there are only two degrees of freedom θ and φ , one can represent this state uniquely by a point on a sphere where the two poles represent the basis states

$|\uparrow\rangle$ and $|\downarrow\rangle$, as in Fig. 2.6.a. The first way in which this qubit can lose its information, is by energy relaxation. If coupled to a dissipative environment, the qubit will after some time relax to its ground state, here taken to be $|\uparrow\rangle$ (Fig. 2.6.b). This loss of information involves the transfer of energy from the qubit to the environment. Another way to lose its information is shown in Fig. 2.6.c: the qubit loses merely its phase information φ , though its energy is conserved. This process is generally called dephasing and obviously does not involve transfer of energy to the environment.

To understand the nature of the processes leading to relaxation and dephasing, let us present a simple model Hamiltonian describing the interaction of a single spin qubit with a general environment,

$$\hat{H}_{\text{env}} = \frac{E_Z}{2} \hat{\sigma}_z + \mathbf{q}(t) \cdot \hat{\boldsymbol{\sigma}}, \quad (2.2)$$

where E_Z is the Zeeman splitting of the spin up and down states,

$$\hat{\sigma}_x = \begin{pmatrix} 0 & 1 \\ 1 & 0 \end{pmatrix}, \quad \hat{\sigma}_y = \begin{pmatrix} 0 & -i \\ i & 0 \end{pmatrix}, \quad \text{and} \quad \hat{\sigma}_z = \begin{pmatrix} 1 & 0 \\ 0 & -1 \end{pmatrix}$$

are the Pauli spin matrices, and $\mathbf{q}(t)$ represents the environmental degrees of freedom coupling to the three components of the electron spin operator. As this Hamiltonian treats the environment as a classical vector (e.g. a fluctuating magnetic field) acting on the electron spin, it is in many cases a too simple representation. For example, if the electron spin is coupled to a bath of other spins the electron spin can affect the bath spins as well, leading to much richer dynamics than described by (2.2) [42]. To illustrate the basics of relaxation and dephasing, this Hamiltonian however satisfies.

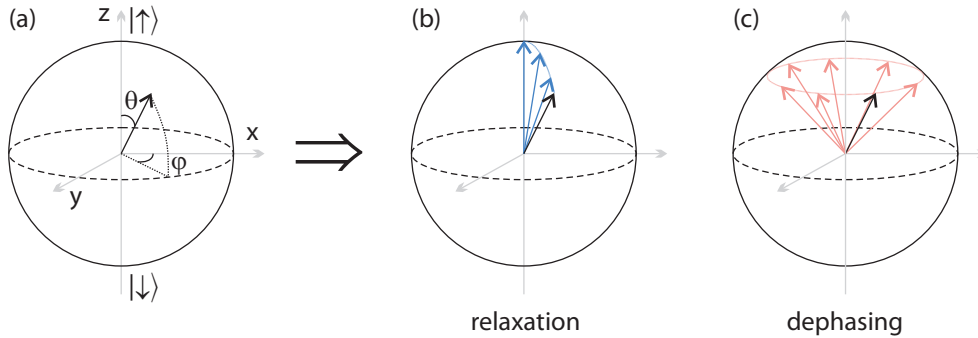


Figure 2.6: Relaxation and dephasing of a qubit. (a) A Bloch sphere representation of the state $\cos \frac{\theta}{2} |\uparrow\rangle + e^{i\varphi} \sin \frac{\theta}{2} |\downarrow\rangle$. (b) Relaxation of the qubit to the ground state $|\uparrow\rangle$. (c) Dephasing of the qubit: the phase information φ is lost.

We can now identify the origin of relaxation and dephasing as follows: (i) As the environmental degrees of freedom $q_{x,y}(t)$ couple to $\hat{\sigma}_{x,y}$, they can cause transitions between spin up and down. However, following energy conservation arguments, only the frequency component E_Z/\hbar in the noise power spectral density $S_{x,y}(\omega) \equiv \int_{-\infty}^{\infty} \int_{-\infty}^{\infty} q_{x,y}(t+\tau)q_{x,y}^*(t) dt e^{-i\omega\tau} d\tau$ can contribute to relaxation. For example, the x -component of the fluctuations in an applied magnetic field can cause relaxation from $|\downarrow\rangle$ to $|\uparrow\rangle$ only when the field has a frequency component matching the Larmor frequency E_Z/\hbar . The time scale on which any arbitrary qubit state relaxes to its ground state is usually denoted by T_1 . (ii) Any change in the total term coupling to $\hat{\sigma}_z$ leads to a loss of phase information. Suppose we have measured the total Zeeman splitting $E_Z + 2q_z(t_0)$ at a certain moment of time t_0 . This leads us to the prediction that the phase of any qubit state will constantly evolve with a frequency $E_Z/\hbar + 2q_z(t_0)/\hbar$. However, since the term q_z fluctuates in time, at a later moment of time t_1 the total Zeeman splitting will be different. Generally, only in a short time interval after the measurement (short compared to the time scale of the fluctuations in q_z) we know that the total splitting is close to $E_Z + 2q_z(t_0)$. After this time interval there will be a random offset with typical magnitude $\sim q_z$, which causes the phase to change in an unpredictable way. We say that the phase information is completely lost on a time scale $T_2 \sim h/2q_z$, which corresponds to an extra unpredictable phase change of $\sim \pi$.

One can think of many processes that in principle could contribute to relaxation and dephasing of a quantum dot spin qubit. In the next Sections we will concentrate on two processes which are believed to dominate in well isolated, high-purity quantum dots: spin-orbit interaction and hyperfine interaction. For specific circumstances, however, other processes can play an important role as well. For example, in the regime of strong tunnel coupling between the dot and a lead, one can expect cotunneling processes to contribute significantly to spin relaxation: the electron carrying the qubit information tunnels from the dot to the lead and simultaneously another electron with random spin tunnels from the lead onto the dot. At low temperatures this process effectively relaxes the electron spin in the dot to the ground state on a time scale which is $\propto (\Gamma/E_{\text{det}})^2 E_Z$, Γ being the typical tunneling rate between the dot and the lead and E_{det} the detuning of the electron levels in the dot relative to the Fermi level of the lead.

2.3.2 Spin-orbit interaction

Both spin-orbit and hyperfine interaction as manifested in quantum dots are relativistic corrections to the non-relativistic Pauli-Schrödinger equation. To derive

the spin-orbit and hyperfine Hamiltonians, let us start from the Dirac equation for a relativistic electron in a potential $V(\mathbf{r})$,

$$i\hbar \frac{\partial \Psi}{\partial t} = \hat{H}_{\text{Dirac}} \Psi \equiv \{ \hat{\boldsymbol{\alpha}} \cdot \hat{\boldsymbol{\pi}} + \beta mc^2 - eV(\mathbf{r}) \} \Psi, \quad (2.3)$$

where m is the rest mass of the electron, c the speed of light, $-e$ the electron charge, and $\hat{\boldsymbol{\pi}}$ the ‘long’ momentum $c(\hat{\mathbf{p}} + e\hat{\mathbf{A}})$ of the electron in an electromagnetic field. The matrices

$$\hat{\boldsymbol{\alpha}} \equiv \begin{pmatrix} 0 & \hat{\boldsymbol{\sigma}} \\ \hat{\boldsymbol{\sigma}} & 0 \end{pmatrix} \quad \text{and} \quad \beta \equiv \begin{pmatrix} \mathbb{1} & 0 \\ 0 & -\mathbb{1} \end{pmatrix} \quad (2.4)$$

are the 4×4 Dirac matrices.

Let us now search for solutions of the Dirac equation $\hat{H}_{\text{Dirac}} \Psi = E\Psi$, where E is the total energy of the electron $E = mc^2 + \varepsilon$. We can split the four-component spinor Ψ in two two-component spinors Ψ_A and Ψ_B , yielding the two coupled linear equations

$$\left\{ \frac{(\hat{\boldsymbol{\sigma}} \cdot \hat{\boldsymbol{\pi}})(\hat{\boldsymbol{\sigma}} \cdot \hat{\boldsymbol{\pi}})}{2mc^2 + eV(\mathbf{r}) + \varepsilon} - eV(\mathbf{r}) \right\} \Psi_A = \varepsilon \Psi_A \quad (2.5)$$

$$\Psi_B = \frac{\hat{\boldsymbol{\sigma}} \cdot \hat{\boldsymbol{\pi}}}{2mc^2 + eV(\mathbf{r}) + \varepsilon} \Psi_A. \quad (2.6)$$

It is clear that in the non-relativistic limit follows that $|\Psi_A| \gg |\Psi_B|$, which allows us to derive the Pauli-Schrödinger equation $\hat{H}_{\text{PS}} \Psi_A = \varepsilon \Psi_A$, with

$$\hat{H}_{\text{PS}} = \frac{1}{2m} (\hat{\mathbf{p}} + e\mathbf{A})^2 + \frac{e\hbar}{2m} (\nabla \times \mathbf{A}) \cdot \hat{\boldsymbol{\sigma}} - eV(\mathbf{r}), \quad (2.7)$$

where we used that $2mc^2 + eV(\mathbf{r}) + \varepsilon \approx 2mc^2$. In the presence of a magnetic field \mathbf{B} , this equation thus adds a term $\propto \mathbf{B} \cdot \hat{\boldsymbol{\sigma}}$ to the standard Schrödinger equation. One can correct equation (2.7) in higher orders of p^2/m^2c^2 in a systematic way using a Foldy-Wouthuysen transformation [43], yielding in first order $\hat{H}_{\text{PS}}^{(1)} \Psi_A = \varepsilon \Psi_A$ with

$$\hat{H}_{\text{PS}}^{(1)} = \hat{H}_{\text{PS}} + \frac{e\hbar}{4m^2c^2} \{ \mathbf{E} \times (\hat{\mathbf{p}} + e\mathbf{A}) \} \cdot \hat{\boldsymbol{\sigma}} + \frac{e\hbar^2}{8m^2c^2} \nabla \cdot \mathbf{E}, \quad (2.8)$$

where we used $\mathbf{E} = -\nabla V$. The correction consists of two terms, the first describing spin-orbit interaction, and the second being the so-called Darwin term [44].

If we now focus on the spin-orbit term and assume $\mathbf{A} = 0$, i.e. no magnetic fields present, we note that it effectively describes a magnetic field $\propto \mathbf{E} \times \mathbf{p}$ acting on the electron spin, which scales with the electric field \mathbf{E} experienced by

the electron. For an electron trapped in a quantum well in a semiconducting crystal, there generally are two important contributions to this electric field: (i) If the crystal structure lacks inversion symmetry (as the zinc-blende structure of GaAs does), the electron experiences a net local electric field set up by the atoms in the crystal lattice. For electrons in a 2DEG in a heterostructure grown along the (001) direction, this leads to the so-called Dresselhaus spin-orbit interaction term [45], which in leading order of p reads

$$\hat{H}_D = \beta \{-\hat{p}_x \hat{\sigma}_x + \hat{p}_y \hat{\sigma}_y\}, \quad (2.9)$$

β depending on material properties and the confinement in the z -direction. (ii) An electron can also experience an electric field due to an asymmetric confining potential of the quantum well. Although the average electric field in the conduction band is zero, this effect adds to spin-orbit interaction due to mixing between different bands. For a confining field in the z -direction, this yields to a contribution to spin-orbit coupling known as the Rashba term [46]

$$\hat{H}_R = \alpha \{-\hat{p}_y \hat{\sigma}_x + \hat{p}_x \hat{\sigma}_y\}, \quad (2.10)$$

α depending also on material properties and the confining potential.

As is clear from the spin-orbit Hamiltonian $\hat{H}_{SO} = \hat{H}_D + \hat{H}_R$, it causes the electron spin to rotate while the electron moves through the 2DEG. The speed of this rotation is proportional to the speed of the electron, and therefore the length over which the spin performs a π rotation is independent of $p_{x,y}$. This length, known as the spin-orbit length l_{SO} , is estimated to be 1–10 μm in GaAs 2DEGs. The size of a typical quantum dot (~ 100 nm) is much smaller than l_{SO} , and therefore one expects in principle no strong spin-orbit effects in GaAs quantum dots.

Indeed, closer investigation of \hat{H}_{SO} tells us that spin-orbit interaction in quantum dots does not couple the Zeeman-split sublevels of a quantum dot orbital state. As the average momenta $\langle p_x \rangle$ and $\langle p_y \rangle$ are zero, one finds that $\langle nl \downarrow | \hat{H}_{SO} | nl \uparrow \rangle = 0$, where n and l are the quantum numbers of the orbital state. The effect of spin-orbit interaction manifests itself merely as a perturbation of the wave functions, for e.g. a spin up state in first order approximated by

$$|nl \uparrow\rangle^{(1)} = |nl \uparrow\rangle + \sum_{n'l' \neq nl} \frac{\langle n'l' \downarrow | \hat{H}_{SO} | nl \uparrow \rangle}{E_{nl} - E_{n'l'} - E_Z} |n'l' \downarrow\rangle. \quad (2.11)$$

This implies that the doublet states in a quantum dot are not pure spin up and down states, but rather admixtures of spin and orbital states [47]. One effect of

this mixing is that it renormalizes the Zeeman energy of the electrons, observed as a different effective g -factor.

Another effect, important in the context of spin relaxation, is that the perturbed doublet states $|nl \uparrow\rangle^{(1)}$ and $|nl \downarrow\rangle^{(1)}$ can be coupled by electric fields, whereas the fields cannot mix *pure* spin states. Therefore, fluctuating electric fields can now contribute to relaxation between the doublet states. This mechanism, being a second order process involving electric fields and spin-orbit coupling, is not very efficient. Indeed, in experiments on GaAs quantum dots, very long relaxation times have been observed even approaching ~ 1 s [41, 48].

In general, fluctuating electric fields could have many sources. Apart from externally applied fields, one could think of fluctuations of gate potentials, background charge fluctuations [49], or lattice phonons [50, 51]. The latter are believed to be the dominating source of spin-orbit induced spin relaxation, and are therefore extensively studied in theory and experiment. An estimate of the dependence of the resulting relaxation rate on the Zeeman splitting E_Z involves the phonon density of states ($\propto E_Z^2$ [52]) and the electric field amplitude from single deformation or piezo-electric phonons ($\propto E_Z^{\pm 1/2}$). The result is that $1/T_1 \propto E_Z^5$ for piezo-electric phonons [47] and $1/T_1 \propto E_Z^7$ for deformation phonons. This dependence of $1/T_1 \propto B_{\text{ext}}^5$ has indeed been observed in experiment [53].

Let us also briefly comment on the effect of spin-orbit coupling on spin dephasing. Of course, any spin relaxation implies inevitably also the loss of phase information on the same time scale, so $T_2 \leq T_1$ always holds. However, as \hat{H}_{SO} only contains the spin operators $\hat{\sigma}_x$ and $\hat{\sigma}_y$, one expects to first approximation no phase randomization due to spin-orbit interaction. Therefore one can say that dephasing due to spin-orbit coupling takes place with $T_2 = T_1$.

2.3.3 Hyperfine interaction

Another effect present in most quantum dot structures is hyperfine interaction. In materials with non-zero nuclear spin, the electron spins experience a small magnetic field set up by the magnetic dipole moments of the nuclear spins. If we zoom in on the interaction between a single electron and a single nucleus, the vector potential describing this magnetic field reads

$$\mathbf{A} = \frac{\mu_0}{4\pi} \frac{\hat{\boldsymbol{\mu}} \times \mathbf{r}}{r^3}, \quad (2.12)$$

where $\hat{\boldsymbol{\mu}}$ is the nuclear magnetic dipole moment, \mathbf{r} is the vector pointing from the nucleus to the electron, and $\mu_0 = 4\pi \cdot 10^{-7}$ N/A² is the permeability of free space. This vector potential can be substituted in the Pauli-Schrödinger Hamiltonian

(2.7), yielding the coupling Hamiltonian

$$\hat{H} = \frac{e\hbar}{2m}(\nabla \times \mathbf{A}) \cdot \hat{\boldsymbol{\sigma}} = \frac{e\hbar\mu_0}{8\pi m} \left\{ \frac{3(\hat{\boldsymbol{\mu}} \cdot \mathbf{r})(\hat{\boldsymbol{\sigma}} \cdot \mathbf{r})}{r^5} - \frac{\hat{\boldsymbol{\mu}} \cdot \hat{\boldsymbol{\sigma}}}{r^3} \right\}. \quad (2.13)$$

As long as the two dipoles are sufficiently far apart (which holds for e.g. electronic p - and d -orbitals), one can evaluate this interaction straightforwardly by averaging over the electron wave function. The electrons in s -orbitals however, like the conduction band electrons in all systems investigated in this thesis, have a non-zero wave function at the position of the nuclei. The large electrostatic potential at these points causes the relativistic correction $(e^2\hbar/4m^2c^2)(\mathbf{E} \times \mathbf{A}) \cdot \hat{\boldsymbol{\sigma}}$ (see Eq. 2.8) to dominate the electron-nuclear spin-spin interaction instead of (2.13). The electrostatic potential created by a charged nucleus reads

$$V(\mathbf{r}) = \frac{Ze}{4\pi\epsilon_0 r}, \quad (2.14)$$

where $\epsilon_0 = 8.85 \cdot 10^{-12} \text{ C}^2/\text{Nm}^2$ is the permittivity of free space. With this potential it is straightforward to calculate the relativistic correction, and after integrating over s -type wave functions, one finds [54]

$$\hat{H}_{\text{HF}} = \frac{2}{3}\mu_0 g_0 \mu_B \gamma_n \hbar \hat{\mathbf{S}} \cdot \hat{\mathbf{I}} |\Psi(0)|^2, \quad (2.15)$$

where g_0 is the free electron g -factor, γ_n the nuclear gyromagnetic ratio, $\hat{\mathbf{S}}$ and $\hat{\mathbf{I}}$ the electron and nuclear spin operators, and $|\Psi(0)|$ the magnitude of the electron wave function $\Psi(\mathbf{r})$ at the position of the nucleus. If a single electron is in contact with many nuclei, as in the case of a quantum dot, we can sum over the contributions of all N nuclei, yielding

$$\hat{H}_{\text{HF}} = \sum_k^N A_k \hat{\mathbf{S}} \cdot \hat{\mathbf{I}}_k, \quad (2.16)$$

where the A_k denote the coupling constants as in (2.15). In quantum dots in GaAs 2DEGs typically $N \sim 10^6$, in other structures such as self-assembled dots and dots in semiconducting nanowires this number can be one or two orders of magnitude smaller. The coupling constants can be written as $A_k = A\nu|\Psi(r_k)|^2$ with ν being the volume of a crystal unit cell and A the average hyperfine coupling constant. The coupling A is independent of N , and is for GaAs $A \sim 90 \mu\text{eV}$ [54].

As is clear from \hat{H}_{HF} , the state of the nuclear spins affects the electron spin, but on the other hand, the electron spin can also affect the nuclear spins. Further, both type of spins being quantum objects, one can also think of quantum effects

such as entanglement between the electron spin and the nuclear spin bath [55]. These two effects can in principle lead to very rich and complex dynamics. Fortunately, however, the time scales of typical nuclear field fluctuations and the manifestation of quantum effects are large compared to those of the electron spin dynamics. This allows for a semi-classical approximation in which the nuclear spin bath is treated as an effective magnetic field, $\hat{H}_{\text{HF}} = g\mu_B \mathbf{B}_N \cdot \hat{\mathbf{S}}$, where \mathbf{B}_N denotes the effective field, also known as Overhauser field.

In the semiclassical description, the nuclear field is maximal when all nuclear spins are fully polarized. This yields an effective field of $B_N^{\text{max}} = IA/g\mu_B$ T, where I is the nuclear spin. In GaAs this would correspond to $B_N^{\text{max}} \sim 5$ T [54]. However, under most experimental conditions (as in GaAs, when the temperature $T \gtrsim 10$ mK and the external field $B_{\text{ext}} \lesssim 12$ T), the thermal energy $k_B T$ dominates the nuclear Zeeman splitting by far, and the nuclear spin system is in thermodynamic equilibrium. The resulting average field is zero, but has a Gaussian distribution with a width $\sigma_N = IA/g\mu_B\sqrt{N}$ T: the nuclear field will fluctuate in time and has a typical magnitude $B_N \sim \sigma_N$. In GaAs quantum dots σ_N has been measured [37, 38], giving values in the range of a few mT, which agrees with $N \sim 10^6$.

As we explained in Section 2.3.1, an unknown offset in the z -component of the externally applied magnetic field always leads to dephasing of the electron spin. A typical z -component of a nuclear field in a quantum dot $B_N^z \sim 2$ mT changes the precession frequency of the electron by $\sim 10^7$ Hz (using $g = 0.35$) and causes the electron spin to pick up an extra phase of π on a time scale of ~ 50 ns. As any particular precession frequency added by the nuclear field is sampled from a Gaussian distribution, the effective qubit dephasing is best described by averaging the spin precession over this distribution $\int_{-\infty}^{\infty} \frac{1}{\sqrt{2\pi}\sigma_N} \exp\{-(B_N^z/\sqrt{2}\sigma_N)^2\} \cos(g\mu_B B_N^z t/\hbar) dB_N^z = \exp\{-(t/T_2^*)^2\}$, with $T_2^* = \hbar\sqrt{2}/g\mu_B\sigma_N$ [56]. For the same parameters as above, this gives $T_2^* \sim 23$ ns. Several ways to suppress this rapid dephasing have been proposed, such as Hahn echo sequences [57], strong polarization of the nuclear system [42], or measuring B_N^z before operating the quantum dot as a spin qubit [58].

The transverse components of the nuclear fields $B_N^{x,y}$ are in principle expected to play a role only for small external fields, $B_{\text{ext}} \lesssim B_N^{x,y}$. In this regime they can cause transitions between the electron spin up and down states, whereas for larger fields these transitions are strongly suppressed [37, 38]. However, since the exact magnitude and orientation of \mathbf{B}_N depends on the specific set of nuclei that the electron wave function overlaps with, fluctuating electric fields can cause $B_N^{x,y}$ to fluctuate as well. If the frequency of these fluctuations matches the Zeeman splitting of the electron spin, the nuclear fields can cause electron spin-flip transitions for larger external fields as well [59].

Let us now turn to the dynamics of the nuclear fields. Methods to suppress dephasing, such as a Hahn echo or a measurement of B_N^z , would work perfectly if the nuclear field \mathbf{B}_N would be static during the whole experiment. The fact that the nuclear field also evolves in time reduces their efficiency significantly. The time scale of the nuclear field fluctuations t_{nuc} is believed to be mainly determined by two mechanisms [24]: (i) The internuclear dipole-dipole interaction couples the spins of neighboring nuclei [60, 61]. This leads to an evolution of $B_N^{x,y}$ on a $100 \mu\text{s}$ time scale, and predicts for B_N^z an even slower scale. (ii.a) Due to the hyperfine interaction, each nucleus also experiences a small magnetic field set up by the electron, known as the Knight field. The coupling of the z -components of spin changes $B_N^{x,y}$ on a $10 \mu\text{s}$ time scale, B_N^z will only be affected near $B_{\text{ext}} = 0$. (ii.b) The same hyperfine interaction can also affect \mathbf{B}_N indirectly. By a virtual process, two nuclear spins can interact simultaneously with the electron spin, thereby leaving the electron spin in its original state and in general effectively modifying \mathbf{B}_N [62].

Altogether it is believed that \mathbf{B}_N fluctuates on moderate time scales ($t_{\text{nuc}} \sim 10 - 100 \mu\text{s}$), although the fluctuations of the z -component B_N^z can be much slower at high magnetic fields. Remarkably, this t_{nuc} does not set the scale of the dephasing time when applying Hahn echo sequences or measuring the nuclear field. The reason is that dephasing not only depends on t_{nuc} , but also on specific stochastic properties of the nuclear fluctuations. The real dephasing time solely due to the fluctuations of the nuclear field is hard to calculate, but can be estimated in various regimes to be $1 - 100 \mu\text{s}$.

2.3.4 Feedback effects of hyperfine interaction: DNSP

Let us now turn in more detail to the bi-directional nature of the hyperfine Hamiltonian \hat{H}_{HF} . We rewrite (2.16) as

$$\hat{H}_{\text{HF}} = \sum_k^N A_k \hat{\mathbf{S}} \cdot \hat{\mathbf{I}}_k = \frac{1}{2} \sum_k^N A_k \left\{ 2\hat{S}^z \hat{I}_k^z + \hat{S}^+ \hat{I}_k^- + \hat{S}^- \hat{I}_k^+ \right\}. \quad (2.17)$$

From the so-called flip-flop terms $\hat{S}^\pm \hat{I}^\mp$ in this representation it is clear that any hyperfine induced electron spin flip is always accompanied by a nuclear spin flip. This suggests that non-equilibrium electron spin dynamics in principle can lead to dynamic nuclear spin polarization (DNSP).

Based on this idea, Overhauser predicted in 1953 that driving the electron spin resonance (ESR) in a metal would lead to dynamical polarization of the nuclear spins [63]. If one applies an external magnetic field B_{ext} , the spin-up and spin-down conduction bands are split by the Zeeman energy. In equilibrium this

causes the low-energy band to be more populated than the high-energy band. A perpendicular oscillating magnetic field $B_{ac} \cos(\omega t)$ matching the ESR condition $\hbar\omega = g\mu_B B_{ext}$ causes rapid transitions from spin-up to spin-down and vice versa, creating a non-equilibrium excess population of the electron spin excited state. Several processes compete with this ESR driving and try to restore the equilibrium situation: they flip electron spins from the overpopulated high-energy band to the low-energy band. Hyperfine induced flip-flops are one of these processes, so flip-flops preferably flip an electron spin from high to low energy, leading to a preferred direction of DNSP. The resulting sign of nuclear polarization is parallel to the excited electron spin state. This prediction by Overhauser was confirmed experimentally already in 1956 [64], and since then the Overhauser effect became a widely used tool to increase the nuclear polarization in metals, e.g. to enhance NMR peaks in experiment.

One can in principle expect the same kind of mechanism of DNSP in quantum dots. If there is a process which drives the electron spin out of equilibrium, causing the spin to populate an excited state, one can expect the build-up of nuclear polarization parallel to that of the excited electron spin.

Let us briefly explain the direct analogue of Overhauser's original proposal: DNSP due to ESR excitation of a doublet state in a single quantum dot (we investigate this further in Chapter 4 of this thesis). Assuming $g < 0$ and low temperatures, the electron spin prefers to be in its ground state $|\uparrow\rangle$ (see Fig. 2.7.a). ESR driving of the electron causes a rapid coherent evolution between $|\uparrow\rangle$ and $|\downarrow\rangle$ (Fig. 2.7.b) and thereby creates a non-zero probability to find the electron in its excited state $|\downarrow\rangle$. Several relaxation processes compete with the ESR driving, causing transitions from $|\downarrow\rangle$ to $|\uparrow\rangle$. In such a process, (i) the excess

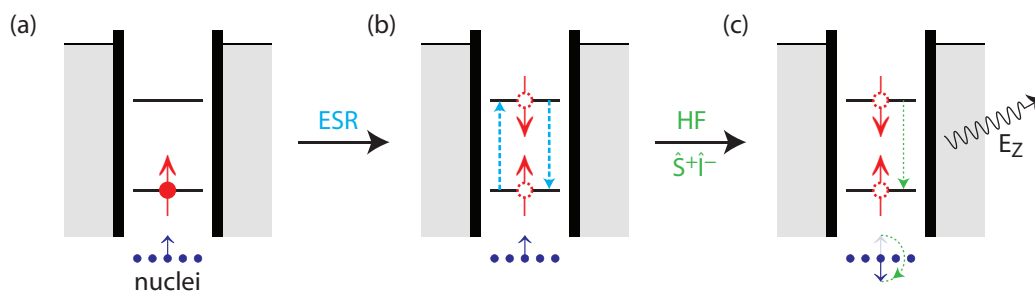


Figure 2.7: The Overhauser effect in a single quantum dot occupied by a single electron. (a) In equilibrium the electron occupies its ground state. (b) ESR driving causes coherent transitions between the two spin states. (c) While relaxing from the excited state, the electron spin can transfer its angular momentum to one of the nuclei.

Zeeman energy E_Z is absorbed by the leads or by lattice phonons, and (ii) the excess angular momentum is transferred to the electrons in the leads or, via the hyperfine coupling $\sum_k A_k \hat{S}^+ \hat{I}_k^-$, to one of the nuclei (Fig. 2.7.c). The resulting nuclear polarization P is again expected to be parallel to the spin of the excited electrons, that is $P < 0$.

The Overhauser effect in quantum dots has indeed been observed in ESR experiments on self-assembled GaAs quantum dots [65], yielding a sign of nuclear polarization as predicted above. Under optical pumping conditions the same effect has been observed [66], the actual sign of DNSP then being determined by the polarization of the pump laser as this sets the spin direction of the optically excited electrons.

As any build-up of nuclear polarization also changes the Overhauser field B_N acting on the electron, these mechanisms of DNSP can be expected to lead to complex feedback effects such as bistabilities and hysteresis [37, 67]. Let us give a simple intuitive example: if ESR excitation ultimately leads to DNSP, the resulting nuclear field adds to the external field B_{ext} and thereby changes the ESR condition to $\hbar\omega = g\mu_B(B_{\text{ext}} + B_N)$. Obviously, this could lead to mechanisms of nuclear self-tuning or -detuning of the ESR condition. This specific effect is further investigated in Chapter 4 of this thesis.

However, one could also think of applications of this DNSP, since the nuclear spin bath in a quantum dot was identified to be the main source of electron spin dephasing. As mentioned in Section 2.3.3, strong polarization of the nuclear spins could significantly improve the dephasing time of the electron spin [42]. The degrees of polarization needed, however, are probably too large to be feasible: to improve T_2 by a factor of 100, a polarization of 99.99 % is needed. Another way to improve coherence using DNSP could be to narrow the width of the statistical distribution of nuclear fields σ_N (the dephasing time scales as $\propto 1/\sigma_N$). The strongly accelerated nuclear spin dynamics under conditions of DNSP could possibly result in a significant narrowing of σ_N . These considerations motivated in recent years much experimental and theoretical work on the coupled electron-nuclear spin dynamics in quantum dots [58, 68, 69].

2.4 Spin valves

A *spin valve*, which is the subject of Chapter 8 of this thesis, is one of the basic magnetoelectronic devices [6]. It consists of a small normal metallic island, which is contacted to two ferromagnetic leads with magnetization directions \mathbf{m}_L and \mathbf{m}_R (see Fig. 2.8.a). If a bias voltage is applied over this system, the current flowing

through the system creates a spin accumulation in the normal metal island, the size and direction of which depend on the specific configuration of the two lead magnetizations.

If the dimensions of the island do not exceed the spin diffusion length in the metal, this spin accumulation can strongly affect net electron transport properties such as the conductance of the device. To understand this in simple terms, we can consider the two simplest cases of lead magnetizations: (i) Suppose the two leads have parallel magnetization vectors, both pointing ‘up’ (see Fig. 2.8.b). Both leads then have an electronic density of states at the Fermi level which is larger for spin up than spin down electrons. The current flowing from the left lead into the metallic island is therefore carried by a majority of spin up electrons. Due to the same difference in densities of states in both leads, the majority spin up electrons can enter the right lead more easily than spin down electrons, resulting in relatively good conductance. (ii) The two magnetization vectors are anti-parallel (Fig. 2.8.c). In this case, most electrons arriving at the interface of the right lead have the ‘wrong’ spin and will be scattered back into the metallic island. The conductance of the spin valve will thus be suppressed as compared to the case with parallel magnetizations.

2.4.1 Spin-polarized transport in spin valves

Let us describe the spin-polarized transport through the spin valve more formally. Each FN-contact can be completely characterized by four conductance parameters: the conductance for spin up electrons $G^{\uparrow\uparrow}$, the conductance for spin down electrons $G^{\downarrow\downarrow}$, and a complex ‘mixing conductance’ $G^{\uparrow\downarrow} = \text{Re } G^{\uparrow\downarrow} + i\text{Im } G^{\uparrow\downarrow}$.

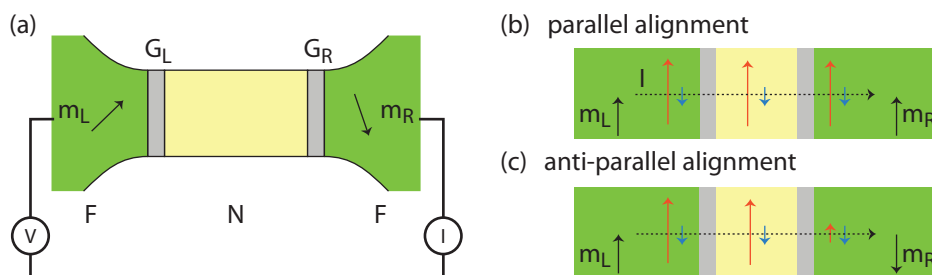


Figure 2.8: (a) A spin valve is a metallic island (N), coupled to two ferromagnetic reservoirs (F) with magnetization vectors \mathbf{m}_L and \mathbf{m}_R . (b,c) The current I for a given bias voltage V can depend on the relative orientation of \mathbf{m}_L and \mathbf{m}_R .

These parameters are microscopically defined as

$$G^{\alpha\beta} = \frac{e^2}{h} \sum_{mn} \{ \delta_{mn} - r_{\alpha}^{mn} (r_{\beta}^{mn})^* \}, \quad (2.18)$$

where $r_{\uparrow(\downarrow)}^{mn}$ is the reflection coefficient of the interface for reflection of spin up(down) electrons from transport channel n to m . The charge and spin currents flowing through the FN-interface then can be expressed as [70]

$$\begin{aligned} I_c &= GV - PG\mathbf{m} \cdot \mathbf{V}_s \\ \mathbf{I}_s &= (PGV - GV_s \cdot \mathbf{m}) \mathbf{m} + 2\text{Re} G^{\uparrow\downarrow} \mathbf{m} \times (\mathbf{V}_s \times \mathbf{m}) + 2\text{Im} G^{\uparrow\downarrow} (\mathbf{V}_s \times \mathbf{m}), \end{aligned} \quad (2.19)$$

where we introduced the total conductance $G = G^{\uparrow\uparrow} + G^{\downarrow\downarrow}$ and the contact polarization $P = (G^{\uparrow\uparrow} - G^{\downarrow\downarrow})/G$. Further, V denotes the bias voltage applied over the contact, \mathbf{m} the magnetization vector of the ferromagnet, and \mathbf{V}_s the spin accumulation in the normal metal. Using magnetoelectronic circuit theory [70, 71, 72], one can then derive an expression for the total conductance of a symmetric spin valve as a function of the angle θ between \mathbf{m}_L and \mathbf{m}_R

$$G_{\text{sv}}(\theta) = \frac{G}{2} \left(1 - P^2 \frac{\tan^2 \theta/2}{\alpha + \tan^2 \theta/2} \right), \quad (2.20)$$

where the dimensionless parameter $\alpha = (2[\text{Re} G^{\uparrow\downarrow}]^2 + 2[\text{Im} G^{\uparrow\downarrow}]^2)/G \text{Re} G^{\uparrow\downarrow}$. As expected, this function has a maximum at $\theta = 0$ and a minimum at $\theta = \pi$.

2.4.2 Hyperfine interaction in spin valves

Also in metals, the spins of conduction electrons interact with the nuclear spins via the hyperfine interaction as introduced in Section 2.3.3. For the case of metallic spintronic devices, two aspects of this interaction have been investigated. (i) The contribution to electron spin relaxation or dephasing due to the randomly polarized nuclear spins is believed to be negligible [73], mainly due to the itinerant nature of the conduction electrons. Electron spin decoherence in metals is probably dominated by other processes involving spin-orbit interaction and the electron-hole exchange interaction [6]. (ii) Under conditions of non-equilibrium electron spin dynamics, hyperfine interaction can significantly affect the nuclear spins in a metal, e.g. causing strong dynamical nuclear spin polarization [63].

In Chapter 8 we investigate the coupled electron-nuclear spin dynamics in the normal metal part of a spin valve. Due to the non-equilibrium electron spin accumulation in the normal metal part, a significant nuclear polarization can be built up locally, which in turn can affect the electronic transport properties of the system. We propose an experiment in which the driven nuclear spin dynamics will manifest themselves as oscillations in the net current through the spin valve.

Chapter 3

Useful theoretical concepts

In this Chapter we will discuss some of the theoretical concepts we will use in Chapters 4–8. The methods described here are relatively simple and widely used in many fields. We will briefly outline the methods, and also discuss some of the specific issues when applying the methods in the following Chapters.

3.1 Rotating frame

In Chapters 4 and 5 we investigate the coupled electron-nuclear spin dynamics in quantum dots under conditions of electron spin resonance. As this resonance is driven by a small oscillating magnetic field, the most convenient description of the problem is in a reference frame rotating at the same frequency as that of the oscillating field.

To appreciate this, let us start by considering an electron in the presence of both a static magnetic field and a perpendicular *rotating* magnetic field, i.e. $\mathbf{B}_{\text{tot}} = B_0\hat{\mathbf{z}} + B_1\{\cos(\omega t)\hat{\mathbf{x}} + \sin(\omega t)\hat{\mathbf{y}}\}$. We can transform the corresponding Schrödinger equation $i\hbar\dot{\psi} = \{g\mu_B\mathbf{B}_{\text{tot}} \cdot \hat{\mathbf{S}}\}\psi$ to a rotating frame of coordinates by the substitution $\psi_r = \exp\{i\omega\hat{S}_z t\}\psi$. In this new basis one readily obtains the effective Hamiltonian

$$\hat{H}_{\text{RF}} = (g\mu_B B_0 - \hbar\omega)\hat{S}_z + g\mu_B B_1\hat{S}_x, \quad (3.1)$$

which is no longer time-dependent.

In experiment however, rather *oscillating* than rotating fields are used. A linearly polarized oscillating field $B_1 \cos(\omega t)\hat{\mathbf{x}}$ can be considered as a superposition of two counterrotating fields, both with amplitude $B_1/2$ and frequency ω . A common approach, known as the rotating wave approximation, is to disregard one of those fields and approximate $B_1 \cos(\omega t)\hat{\mathbf{x}} \approx \frac{1}{2}B_1\{\cos(\omega t)\hat{\mathbf{x}} + \sin(\omega t)\hat{\mathbf{y}}\}$. In

terms of the rotating frame Hamiltonian (3.1), this corresponds to neglecting a field rotating with frequency 2ω .

In the regime of interest, i.e. close to the electron spin resonance condition, both energies in (3.1) are comparable: $g\mu_B B_0 - \hbar\omega \sim g\mu_B B_1$. As long as $B_1 \ll B_0$, a field with frequency 2ω in (3.1) is far from resonance with the other energies, and can justly be neglected. If one calculates the effect of this rapidly rotating component to lowest order [60], one finds that it (i) shifts the resonance condition to $\hbar\omega = g\mu_B B_0 \{1 + (B_1/4B_0)^2\}$ and (ii) has a component $\sim \frac{1}{2}B_1(3B_1/8B_0)^2$ which is resonant with the eigenstates of (3.1) at the frequency $3\omega \approx g\mu_B B_0$. Indeed, both effects can be disregarded in the limit $B_1 \ll B_0$.

3.2 Perturbation theory

In many cases we are interested in effects of small perturbations, such as hyperfine interaction, on a system which is otherwise in (quasi-)equilibrium. More precisely, we would like to calculate rates at which this perturbation causes transitions between the eigenstates of an unperturbed Hamiltonian. To do this, we use the convenient tool of perturbation theory.

Let us briefly outline how to calculate transition rates from perturbation theory. We consider a system described by the Hamiltonian \hat{H}_0 which is perturbed by a small term \hat{V} . We assume that the system was in an eigenstate $|i\rangle$ of \hat{H}_0 at time $t = -\infty$ and we would like to calculate the transition rate to the state $|f\rangle$, another eigenstate of \hat{H}_0 . We use the Schrödinger equation in the interaction picture [74] and expand the time evolution operator for the wave function of the system in powers of \hat{V} . The first and second order corrections to the probability amplitude for finding the system in $|f\rangle$ can then be expressed as

$$\begin{aligned}
 a_f^{(1)}(t) &= -\frac{i}{\hbar} \int_{-\infty}^t d\tau \langle f | e^{\frac{i}{\hbar}\hat{H}_0\tau} \hat{V} e^{-\frac{i}{\hbar}\hat{H}_0\tau} | i \rangle \\
 a_f^{(2)}(t) &= -\frac{1}{\hbar^2} \int_{-\infty}^t d\tau \int_{-\infty}^{\tau} d\tau' \sum_v \langle f | e^{\frac{i}{\hbar}\hat{H}_0\tau} \hat{V} e^{-\frac{i}{\hbar}\hat{H}_0\tau} | v \rangle \langle v | e^{\frac{i}{\hbar}\hat{H}_0\tau'} \hat{V} e^{-\frac{i}{\hbar}\hat{H}_0\tau'} | i \rangle,
 \end{aligned} \tag{3.2}$$

where the summation in the second order term is performed over all eigenstates of \hat{H}_0 . The real probability to find the system in state $|f\rangle$ is given by the modulo square of $a_f(t)$, and the transition rate from $|i\rangle$ to $|f\rangle$ is then calculated as the time derivative $\Gamma_{i \rightarrow f} = \partial_t |a_f(t)|^2$.

The fact that $e^{-\frac{i}{\hbar}\hat{H}_0 t} |n\rangle = e^{-\frac{i}{\hbar}E_n t} |n\rangle$ for any eigenstate of \hat{H}_0 (with E_n the energy of state $|n\rangle$) allows us to explicitly evaluate all integrals. The resulting

first and second order transition rates for a time-independent perturbation read

$$\begin{aligned}\Gamma_{i \rightarrow f}^{(1)} &= \frac{2\pi}{\hbar} |\langle f | \hat{V} | i \rangle|^2 \delta(E_i - E_f) \\ \Gamma_{i \rightarrow f}^{(2)} &= \frac{2\pi}{\hbar} \left| \sum_v \frac{\langle f | \hat{V} | v \rangle \langle v | \hat{V} | i \rangle}{E_v - E_i} \right|^2 \delta(E_i - E_f).\end{aligned}\tag{3.3}$$

The first order rate, also known as Fermi's golden rule, describes direct transitions from $|i\rangle$ to $|f\rangle$ caused by the perturbation \hat{V} . The delta function represents energy conservation: a transition is only allowed if the initial and final state have the same energy. The second order rate describes processes which involve a so-called *virtual* state. This rate can dominate if the perturbation does not couple the states $|i\rangle$ and $|f\rangle$ directly, or if the first-order transitions would violate energy conservation.

For the case of hyperfine induced electron-nuclear flip-flops in a quantum dot, the perturbing terms $\hat{S}^\pm \hat{I}^\mp$ couple states like $|\uparrow_e \downarrow_k\rangle$ and $|\downarrow_e \uparrow_k\rangle$, where the index $e(k)$ stands for electron(nucleus). Since the electron and nuclear Zeeman energies differ by three or four orders of magnitude, these states are roughly split by the electron Zeeman energy. Therefore the first order rate vanishes and one has to consider second order transitions in which another perturbation (e.g. interaction with the leads or with lattice phonons) takes care of the energy mismatch. The total perturbation thus reads $\hat{V} = \hat{H}_{\text{HF}} + \hat{H}_{\text{env}}$, where \hat{H}_{env} describes the interaction with the dissipative environment. The relevant terms in the second order transition rate are then of the kind $\langle f | \hat{H}_{\text{env}} | v \rangle \langle v | \hat{H}_{\text{HF}} | i \rangle$.

Let us mention two complications which arise when calculating hyperfine flip-flop rates in a quantum dot under conditions of electron spin resonance:

1. The operators \hat{S}^\pm in the hyperfine flip-flop terms fully consist of transversal electron spin operators, i.e. $\hat{S}^\pm = \hat{S}^x \pm i\hat{S}^y$. In the rotating reference frame discussed in Section 3.1, these operators will become *time-dependent* operators $\hat{S}^\pm e^{\pm i\omega t}$.

To implement this time-dependence, we derive a general second order transition rate for a perturbation consisting of two oscillating components $\hat{V} = \hat{H}_1 e^{i\omega_1 t} + \hat{H}_2 e^{i\omega_2 t}$. After substituting the time-dependence in equations (3.2), we find the modified second order transition rate

$$\Gamma_{i \rightarrow f}^{(2)} = \frac{2\pi}{\hbar} \left| \sum_v \frac{\langle f | \hat{H}_1 | v \rangle \langle v | \hat{H}_2 | i \rangle}{E_v - \hbar\omega_2 - E_i} \right|^2 \delta(E_f - E_i - \hbar\omega_1 - \hbar\omega_2).\tag{3.4}$$

As can be seen from this expression, an oscillating perturbation effectively changes the energy splitting of two states that it couples.

2. In Chapter 5 of this thesis we investigate the effect of the small oscillating electric field unavoidably accompanying the magnetic driving field in the experimental setup considered. We include these electrical side-effects by introducing an oscillating component in the hyperfine coupling parameters, i.e. $A_k \rightarrow A_k + \tilde{A}_k \cos(\omega t)$. In the rotating frame this now introduces *time-independent* flip-flop terms $\tilde{A}_k \hat{S}^\pm \hat{I}_k^\mp$.

The two eigenstates of the rotating frame Hamiltonian (3.1) are both mixtures of spin up and down. As a result, the operators \hat{S}^\pm in the basis of these eigenstates have non-vanishing diagonal matrix elements, i.e. generally $\langle n | \hat{S}^\pm | n \rangle \neq 0$ for an eigenstate $|n\rangle$ of \hat{H}_{RF} . This implies that there exist contributions to the nuclear spin flip rate like $\tilde{A}_k \langle n_e \downarrow_k | \hat{S}^+ \hat{I}_k^- | n_e \uparrow_k \rangle$, which are split in energy only by the nuclear Zeeman energy E_k . This could lead to very small denominators in the transition rates, and therefore also other small contributions to the electron spin dynamics have to be considered: there exist dissipative processes which are negligible on the scale B_1 of \hat{H}_{RF} , but become relevant on the scale E_k . The correct denominators are found by using a full propagator $\hat{U}(t, 0)$, including the small dissipative terms, instead of the basic time evolution $e^{-\frac{i}{\hbar} \hat{H}_{\text{RF}} t}$ in (3.2).

3.3 Stochastics of the nuclear spin dynamics

As explained in Chapter 2, the fluctuating nuclear field in a quantum dot is believed to be the main source of electron spin dephasing. In Section 2.3.4 we suggested that the strongly accelerated nuclear spin dynamics in the presence of dynamical nuclear spin polarization could possibly result in a significant suppression of these fluctuations. In Chapters 4–6 we investigate the nuclear spin dynamics under conditions of electron spin resonance in a single and double quantum dot. We calculate the nuclear spin flip rates $\Gamma_\pm(x)$ as a function of the nuclear spin polarization $x \equiv (N_\uparrow - N_\downarrow)/(N_\uparrow + N_\downarrow)$, where $N_{\uparrow(\downarrow)}$ denotes the number of nuclei with spin up(down)¹. The nuclear spin system is most likely to be found in one of the stable polarizations x_0 defined by $\Gamma_+(x_0) - \Gamma_-(x_0) = 0$ and $\partial_x \{\Gamma_+(x) - \Gamma_-(x)\}|_{x_0} < 0$. In this section we explain how we derive from the spin flip rates $\Gamma_\pm(x)$ estimates for the typical magnitude of nuclear field fluctuations around the stable points as well as for the typical switching time between different stable points.

We consider all possible configurations of the nuclear spin system in the dot as

¹In this Section we assume for simplicity nuclei with spin 1/2. In GaAs $I = 3/2$, which generally gives rise to extra numerical prefactors in the results.

discrete points, labeled n , defining $n \equiv x/2N$, where $N = N_{\uparrow} + N_{\downarrow}$. To investigate the stochastic properties we derive a Fokker-Planck equation for the probability distribution function $\mathcal{P}(n)$, starting from a simple master equation

$$\frac{\partial \mathcal{P}(n)}{\partial t} = -\mathcal{P}(n)[\Gamma_+(n) + \Gamma_-(n)] + \mathcal{P}(n-1)\Gamma_+(n-1) + \mathcal{P}(n+1)\Gamma_-(n+1). \quad (3.5)$$

In this equation $\mathcal{P}(n)$ gives the chance of finding the system in state n , and $\Gamma_{\pm}(n)$ is the rate at which the spin bath flips from the configuration n to $n \pm 1$. We go over to the continuous limit, justified by the large number of nuclei $N \sim 10^6$ [75], and expand all functions around n up to second order. We find

$$\frac{\partial \mathcal{P}}{\partial t} = \frac{\partial}{\partial n} \left\{ (\Gamma_- - \Gamma_+) \mathcal{P} + \frac{1}{2} \frac{\partial}{\partial n} (\Gamma_- + \Gamma_+) \mathcal{P} \right\}, \quad (3.6)$$

a Fokker-Planck equation where all rates Γ_{\pm} are still functions of n .

We assume that, due to the large number of nuclei, the spin flip rates Γ_{\pm} do not change on their full scale when increasing n by only ± 1 . In the cases we investigate, the features of Γ_{\pm} occur on the scale of the width of the resonance $\sim B_1 \sim 1$ mT, whereas changing n by ± 1 corresponds to $A/g\mu_B N \sim 5$ μ T. This implies that $|\partial_n \Gamma_{\pm}| \ll \Gamma_{\pm}$, which allows us to neglect one of the cross terms resulting from the last term in (3.6). With this assumption we rewrite equation (3.6) in terms of the polarization x

$$\frac{\partial \mathcal{P}}{\partial t} = \frac{2}{N} \frac{\partial}{\partial x} \left\{ (\Gamma_- - \Gamma_+) \mathcal{P} + \frac{1}{N} (\Gamma_- + \Gamma_+) \frac{\partial}{\partial x} \mathcal{P} \right\}, \quad (3.7)$$

where now \mathcal{P} and all Γ_{\pm} are functions of x . In this continuity equation, the right-hand side corresponds to the derivative of a probability flux. In equilibrium this probability flux must vanish, yielding the equilibrium equation

$$\frac{\partial \ln \mathcal{P}}{\partial x} = N \frac{\Gamma_+ - \Gamma_-}{\Gamma_+ + \Gamma_-}, \quad (3.8)$$

with the solution

$$\mathcal{P}(x) = \exp \left\{ \int^x N \frac{\Gamma_+ - \Gamma_-}{\Gamma_+ + \Gamma_-} dx' \right\}. \quad (3.9)$$

Maxima and minima of this distribution are found at the zeros of the derivative of the exponent, indeed where $\Gamma_+(x) - \Gamma_-(x) = 0$.

Suppose the point x_0 is one of these solutions corresponding to a maximum of $\mathcal{P}(x)$ (i.e. the second derivative in the point x_0 is negative). We then expand the

exponent of $\mathcal{P}(x)$ up to second order around the maximum, giving a Gaussian approximation for $\mathcal{P}(x)$,

$$\begin{aligned} \mathcal{P}(x) &\approx \exp \left\{ \int^{x_0} N \frac{\Gamma_+ - \Gamma_-}{\Gamma_+ + \Gamma_-} dx' + \frac{N}{2} \frac{\partial}{\partial x} \frac{\Gamma_+ - \Gamma_-}{\Gamma_+ + \Gamma_-} \Big|_{x_0} (x - x_0)^2 \right\} \\ &\equiv \mathcal{P}(x_0) \exp \left\{ - \frac{(x - x_0)^2}{2\sigma^2} \right\}, \end{aligned} \quad (3.10)$$

where σ gives the width of the distribution. Using that $\Gamma_+(x_0) - \Gamma_-(x_0) = 0$ we find an expression for σ^2 in terms of the nuclear spin flip rates

$$\sigma^2 = \frac{1}{N} \left(- \frac{\partial}{\partial x} \frac{\Gamma_+ - \Gamma_-}{\Gamma_+ + \Gamma_-} \Big|_{x_0} \right)^{-1} = \frac{1}{N} \frac{\Gamma_+ + \Gamma_-}{\frac{\partial}{\partial x} (\Gamma_- - \Gamma_+) \Big|_{x_0}}. \quad (3.11)$$

We also would like to estimate the rate $\Gamma_{A \rightarrow B}$ at which the nuclear spin system typically switches from one stable polarization x_a to another x_b . We do this using a method initiated by Kramers [76], which we will briefly outline here.

First, we suppose that the two maxima of the probability distribution are sharply peaked and can be approximated locally by a Gaussian as in (3.10). We then define $P_{A(B)}$ as the probability to find the system in the neighborhood of the stable point $x_{a(b)}$, which we approximate by integrating the local Gaussian approximation over $x \in [-\infty, \infty]$, yielding

$$P_{A,B} \approx \mathcal{P}(x_{a,b}) \sqrt{2\pi} \sigma_{a,b}. \quad (3.12)$$

We then define the function $\Pi(x) \equiv \int_{-\infty}^x \mathcal{P}(x') dx'$ giving the probability to find the system with a polarization smaller than or equal to x . We take the time-derivative of $\Pi(x)$ and write, using (3.7),

$$\frac{\partial \Pi(x)}{\partial t} = \int_{-\infty}^x \frac{\partial \mathcal{P}(x')}{\partial t} dx' = \frac{2}{N} \left\{ \gamma(x) \mathcal{P}(x) + \frac{1}{N} D(x) \frac{\partial \mathcal{P}(x)}{\partial x} \right\}, \quad (3.13)$$

where we use the notations $\gamma(x) \equiv \Gamma_-(x) - \Gamma_+(x)$ and $D(x) \equiv \Gamma_-(x) + \Gamma_+(x)$. We use the relation (3.13) to write

$$\begin{aligned} &\int_a^b \frac{\partial \Pi(x')}{\partial t} \frac{N^2}{D(x')} \exp \left\{ \int_0^{x'} N \frac{\gamma(x'')}{D(x'')} dx'' \right\} dx' \\ &= \int_a^b \left(\frac{2\gamma(x')}{N} \mathcal{P}(x') + \frac{2D(x')}{N^2} \mathcal{P}'(x') \right) \frac{N^2}{D(x')} \exp \left\{ \int_0^{x'} N \frac{\gamma(x'')}{D(x'')} dx'' \right\} dx', \end{aligned} \quad (3.14)$$

where we take to points a and b close to the two maxima x_a and x_b . We perform all integrations and assume again that $\mathcal{P}(x)$ is sharply peaked around x_a and x_b and that $1/\mathcal{P}(x)$ has a sharp maximum at x_{\min} , where $\mathcal{P}(x)$ is minimal. Around these points, we approximate $\mathcal{P}(x)$ and $1/\mathcal{P}(x)$ by Gaussians with corresponding variances $\sigma_{a,b,\min}$. This finally yields the expression

$$\frac{\partial P_A}{\partial t} = \frac{2D(x_{\min})}{N^2} \left(\frac{\mathcal{P}(x_{\min})}{\mathcal{P}(x_b)} \frac{P_B}{2\pi\sigma_{\min}\sigma_b} - \frac{\mathcal{P}(x_{\min})}{\mathcal{P}(x_a)} \frac{P_A}{2\pi\sigma_{\min}\sigma_a} \right), \quad (3.15)$$

which we can interpret as a master equation describing switching between two stable states

$$\frac{\partial P_A}{\partial t} = \Gamma_{B \rightarrow A} P_B - \Gamma_{A \rightarrow B} P_A. \quad (3.16)$$

From this we extract e.g.

$$\Gamma_{A \rightarrow B} = \frac{1}{\pi N} \sqrt{\frac{D(x_{\min})}{D(x_b)}} \sqrt{\left. \frac{\partial \gamma}{\partial x} \right|_{x_b} \left. \frac{\partial \gamma}{\partial x} \right|_{x_{\min}}} \exp \left\{ - \int_{x_a}^{x_{\min}} N \frac{\gamma(x')}{D(x')} dx' \right\}. \quad (3.17)$$

All parameters in this expression can be written in terms of $\Gamma_{\pm}(x)$. If the flip rates are known, we can thus find estimates for switching rates between the different stable points.

Chapter 4

Nuclear tuning and detuning of the electron spin resonance in a quantum dot: Theoretical consideration

We study nuclear spin dynamics in a quantum dot close to the conditions of electron spin resonance. We show that at small frequency mismatch the nuclear field detunes the resonance. Remarkably, at larger frequency mismatch its effect is opposite: the nuclear system is bistable, and in one of the stable states the field accurately tunes the electron spin splitting to resonance. In this state the nuclear field fluctuations are strongly suppressed and nuclear spin relaxation is accelerated.¹

¹This chapter has been published in Physical Review Letters **100**, 056603 (2008).

4.1 Introduction

Electrons confined in semiconductor quantum dots are being investigated intensively in recent years. Much research is inspired by the possibility to use their spin to implement *qubits*, i.e. the computational units in a quantum computer [20]. At present, the main obstacle for this development is the short spin coherence time T_2^* in high-purity quantum dots, measured to be in the ns range [38, 36, 37]. Hyperfine coupling of the electron spin to randomly fluctuating nuclear spins was identified to be the main source of this fast decoherence [38, 36, 77].

It was shown recently that hyperfine interaction in semiconductor quantum dots can lead to much richer physics than just dephasing. Various experiments have demonstrated a set of novel phenomena: random switching between two stable states [37], current oscillations on a time scale of minutes [33], and strong hysteresis [67]. All new effects were attributed to hyperfine induced dynamical nuclear spin polarization (DNSP) resulting from a non-equilibrium electron spin polarization. The nuclear polarization built up then feeds back to the electron spin splitting and is thereby observed. Optical excitation of quantum dots exhibited fine mode locking at multiples of the electron spin resonance frequency [78]. The large magnitude of the signal and slow dynamics suggest that DNSP tunes the resonance in individual dots [66]. Numerical simulations seem to support this point of view, but do not immediately supply a comprehensive picture of the underlying physics [79].

These findings triggered ideas to try to make use of the strong feedback [80], and several experiments were designed to optimize the effect of DNSP [81, 69]. It was observed that in a polarized state the fluctuations of the nuclear field are strongly suppressed and their relaxation is accelerated. Both effects may result in a significant improvement of T_2^* . On the other hand, controlled DNSP might open up the possibility of processing quantum information in robust nuclear spin ensembles [82]. All this feeds intensive research on the coupled electron-nuclear spin dynamics in quantum dots [83, 68].

Recently, electron spin resonance (ESR) in a double quantum dot [34], has been used to perform single electron spin rotations. Besides the demonstration of spin rotations, the experiment gave a clear indication of DNSP. The resonant response extended to a rather broad frequency interval without any amplitude reduction. Remarkably, this broadening was asymmetric with respect to the ESR frequency $g\mu_B B_0/\hbar$. Besides, a significant hysteresis was observed: the response depended on the sweep direction of frequency or magnetic field, suggesting that the resonant condition is shifted during the sweep, as if something tunes the electron splitting. While these effects have been speculatively attributed to DNSP,

their exact mechanisms are not yet understood.

In this Chapter we present a simple model to study the coupled electron-nuclear spin dynamics in a *single* quantum dot close to the ESR condition, assuming that the ac driving is sufficiently strong to saturate the resonance. We find that ESR polarizes the nuclei in a preferred direction. We show that this results in tuning as well as detuning of the resonance by DNSP, depending on the mismatch between the driving frequency and $g\mu_B|B_0|/\hbar$: at small mismatch, the nuclear field built up simply detunes the spin splitting away from ESR. At larger mismatch, competition between ESR pumping and nuclear spin relaxation causes a bistability, and in one of the stable states the nuclear field actually tunes the system back to ESR. With this model, we find a number of recently observed effects (strong asymmetric hysteresis [34, 67] and a reduction of nuclear field fluctuations and accelerated dynamics [69]), and we provide a clear explanation of the mechanisms involved. To achieve a quantitative agreement with the experiments, one would have to use more detailed and specific models to account for, e.g. the presence of two coupled dots [34] or the possibility of substantial electric contributions to the ESR signal [59].

4.2 Model

In our model, a single electron is confined in a quantum dot with its energy well below the Fermi levels of the nearby leads. To achieve ESR, one combines a dc and ac magnetic field, $\mathbf{B}_{\text{tot}} = B_0\hat{z} + B_1\cos(\omega t)\hat{x}$, the ESR condition being $\hbar\omega = g\mu_B|B_0|$. The interaction of the total magnetic field and the electron spin $\hat{\mathbf{S}}$ is given by the Hamiltonian $\hat{H} = -g\mu_B\mathbf{B}_{\text{tot}} \cdot \hat{\mathbf{S}}$.

It is natural to assume that the ESR frequency mismatch $\Delta f \equiv \omega - g\mu_B|B_0|/\hbar$ as well as the Rabi frequency $\tilde{B}_1 \equiv g\mu_B B_1/\hbar$ are much smaller than ω . This justifies a rotating wave approximation. In a rotating frame, we can write the Hamiltonian as

$$\hat{H}_0 = \hbar(\Delta f)\hat{S}^z + \frac{\hbar}{2}\tilde{B}_1\hat{S}^x. \quad (4.1)$$

This \hat{H}_0 determines the effective electron spin eigenstates in the rotating frame, $|+\rangle = \cos\frac{1}{2}\theta|\uparrow\rangle + \sin\frac{1}{2}\theta|\downarrow\rangle$ and $|-\rangle = \sin\frac{1}{2}\theta|\uparrow\rangle - \cos\frac{1}{2}\theta|\downarrow\rangle$, where $\theta = \pi/2 + \arctan(2\Delta f/\tilde{B}_1)$. To determine the probabilities ρ_{\pm} to be in one of the eigenstates, we have to take into account dissipative processes accompanied by a spin-flip. Those are due to the coupling to the environment, that very generally can be represented as

$$\hat{H}_{\text{coup}} = \hat{H}_e^z\hat{S}^z + \frac{1}{2}\left\{\hat{H}_e^-\hat{S}^+e^{i\omega t} + \hat{H}_e^+\hat{S}^-e^{-i\omega t}\right\}, \quad (4.2)$$

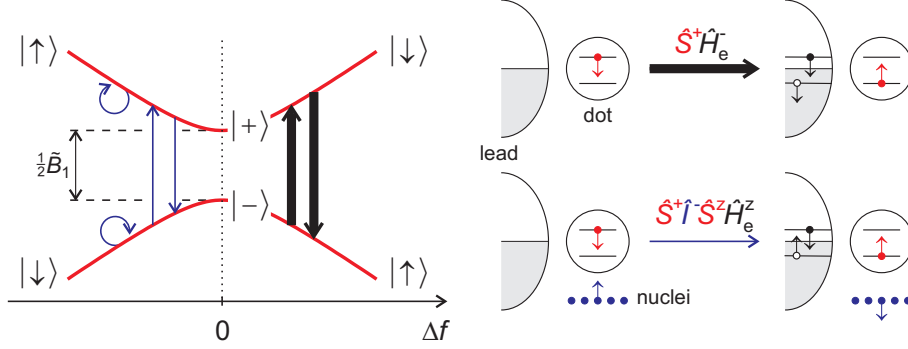


Figure 4.1: A quantum dot under ESR conditions. Left: The spin-split levels $|+\rangle$ and $|-\rangle$ in the rotating wave approximation. The arrows show the *first-order* transitions with a dissipative electron spin-flip (thick) and *second-order* transitions with a nuclear spin-flip (thin). Right: The initial and final states of the transitions for the case when dissipation is dominated by co-tunneling to the leads.

where $\hat{H}_e^{z,\pm}$ represent the environmental degrees of freedom coupled to corresponding electron spin components. It is convenient to consider the environment in the rest frame, while $\hat{\mathbf{S}}$ is defined in the rotating frame. This makes the coupling explicitly time-dependent. For quantum dots, relevant dissipation mechanisms are: (i) electron-hole pair creation in a nearby lead by a co-tunneling process [84], (ii) spin-orbit interaction with phonons [47], (iii) direct coupling to phonons perturbed by Zeeman energy. Mechanisms (i) and (ii) can lead to an electron spin-flip in the z -direction in first order, not causing any nuclear spin flips. Mechanism (iii) couples only to S_z and therefore it can flip the electron spin only through a second-order process involving the nuclei [85].

We assume temperatures lower than $\hbar\omega$. We then find from energy consideration that the terms proportional to $\hat{H}_e^- \hat{S}^+ e^{i\omega t}$ dominate the transition rates between $|+\rangle$ and $|-\rangle$, since they correspond to the maximum energy transfer $\approx g\mu_B|B_0| \approx \hbar\omega$ from the dot to the environment (see Fig. 4.1). To find the steady state probabilities ρ_+ and ρ_- , we compute these rates and solve the master equation $\Gamma_r^-[\omega](-M_{-+}\rho_+ + M_{+-}\rho_-) = 0$, where Γ_r^- is the maximum relaxation rate, $\Gamma_r^-[\omega] = \int \langle \hat{H}_e^-(0) \hat{H}_e^+(\tau) \rangle e^{-i\omega\tau} d\tau / 4\hbar^2$. For mechanism (i) $\Gamma_r^- \propto \omega$, while for (ii) $\Gamma_r^- \propto \omega^5$. The matrix elements $M_{\alpha\beta} \equiv |\langle \alpha | \hat{S}^+ | \beta \rangle|^2$ are calculated from $|+\rangle$ and $|-\rangle$, and this yields $\rho_{\pm} = \frac{1}{2} \pm \cos\theta / (1 + \cos^2\theta)$. Far from the resonance (if $\theta \rightarrow 0, \pi$) the spin is in the ground state $|\uparrow\rangle$ (corresponding with $\rho_+ \rightarrow 1$ or $\rho_- \rightarrow 1$, see Fig. 4.1), while exactly at resonance ($\theta = \pi/2$) one finds $\rho_{\pm} = 1/2$. This approach is valid provided that the energy splitting in the rotating frame is sufficiently big, i.e. $\tilde{B}_1 \gg \Gamma_r^-[\omega]$.

Let us now consider the nuclear spins $\hat{\mathbf{I}}$, which are coupled to the electron spin via hyperfine interaction [54],

$$\hat{H}_{\text{hf}} = \frac{E_n}{2N} \sum_k \left\{ 2\hat{S}^z \hat{I}_k^z + \hat{S}^+ e^{i\omega t} \hat{I}_k^- + \hat{S}^- e^{-i\omega t} \hat{I}_k^+ \right\}, \quad (4.3)$$

where the sum runs over all nuclei. For simplicity we assume that all nuclear spins are equally strongly coupled to the electron spin, so that the prefactor reduces to the hyperfine coupling energy (for bulk GaAs $IE_n \sim 100 \mu\text{eV}$ [54]) divided by the effective number of nuclei N . For quantum dots, this number is big ($N \sim 10^6$), and this distinguishes the situation in quantum dots from that of a single paramagnetic ion [86].

The effect of the hyperfine interaction is twofold. Firstly, the nuclei affect the electron dynamics via the Overhauser field $\langle I^z \rangle E_n$, that adds to the static z -component of the external magnetic field. Secondly, the interaction can cause electron spin flips to be accompanied by flips of nuclear spins. If there is a preferential direction for these flips, they can be the source of DNSP.

Let us evaluate the rate of the hyperfine induced nuclear spin flips. We keep in mind that hyperfine interaction by itself cannot cause spin exchange between the electron and the nuclear system owing to the energy mismatch $\approx \hbar\omega$ between the initial and final state. The rate thus arises from a second-order process, the corresponding amplitude incorporating \hat{H}_{coup} and \hat{H}_{hf} . In principle, there are six processes capable of flipping nuclear spins. To estimate their relative magnitude, we note that the environment favors large positive energy absorption. This brings us to the conclusion that the dominant process comes from combination of $\hat{S}^+ e^{i\omega t} \hat{I}^-$ in \hat{H}_{hf} , and $\hat{S}^z \hat{H}_e^z$ in \hat{H}_{coup} (see Fig. 4.1). The corresponding energy transfer is $\approx \hbar\omega$. This means that nuclear spins *only* flip from the ‘up’ to the ‘down’ state: there is a preferential direction, needed for DNSP.² The resulting polarization is negative, $P \equiv (N_\uparrow - N_\downarrow)/N < 0$, $N_{\uparrow(\downarrow)}$ being the number of nuclei with spin ‘up’(‘down’).

The pumping rate is proportional to $\Gamma_r^z[\omega] = \int \langle \hat{H}_e^z(0) \hat{H}_e^z(\tau) \rangle e^{-i\omega\tau} d\tau / \hbar^2$, accounting for the dissipation of $\hbar\omega$. For mechanism (i), $\Gamma_r^- = \Gamma_r^z$ owing to SU(2) symmetry in spin space. For spin-orbit mechanism (ii), Γ_r^- and Γ_r^z are of the same order of magnitude [47]. The total pumping rate reads

$$\Gamma_p = -\frac{\Gamma_r^z[\omega] E_n^2}{4N^2 (\hbar\omega)^2} N_\uparrow \sum_{k,l \in \{+,-\}} M_{kl} \rho_l. \quad (4.4)$$

We assume $P \ll 1$, so that $N_\uparrow = N/2$ (even small polarizations are enough to (de)tune the resonance in a wide frequency range). At this stage we incorporate

²Although $I = 3/2$ in GaAs, this only gives rise to a difference in numerical prefactors.

the effect of the Overhauser field: it is a simple shift of the frequency mismatch, and we define the resulting mismatch $\Delta = \Delta f + IE_n P/\hbar$. We note that the validity of the rotating wave approximation now requires $|\Delta| \ll \omega$. The matrix elements in (4.4) and ρ_{\pm} are now functions of Δ and the pumping rate assumes a Lorentzian shape

$$\Gamma_p(\Delta) = -\frac{5\Gamma_r^z[\omega]E_n^2}{32N(\hbar\omega)^2} \frac{1}{1 + 8(\Delta/\tilde{B}_1)^2}, \quad (4.5)$$

with the same width as e.g. $\langle S_z(\Delta) \rangle$. The numerical factor accounts for $I = 3/2$ for GaAs. We see that $\Gamma_p \ll \Gamma_r$, provided the Zeeman splitting $\hbar\omega$ exceeds the typical fluctuations of the nuclear field $\hbar\Omega = IE_n/\sqrt{N}$. This sets the limits of validity of our perturbative approach.

4.3 Results

The resulting nuclear polarization follows from the competition between spin pumping and intrinsic nuclear spin relaxation characterized by the rate $1/\tau_n$. In terms of P , the balance equation reads

$$\frac{dP}{dt} = \frac{2\Gamma_p(\Delta)}{N} - \frac{1}{\tau_n}P, \quad (4.6)$$

which is in combination with the Lorentzian in Eq. (4.5) the main result of our work.

To proceed, let us note that the nuclear relaxation rate is very low, $\tau_n \sim 10$ s [87]. We express this smallness in terms of a dimensionless parameter $\alpha = (18/5\sqrt{2})(\tau_n\Gamma_r^z[\omega])^{-1}\sqrt{N}(\tilde{B}_1\omega^2/\Omega^3)$. As $\alpha \propto \tilde{B}_1/\Gamma_p(0)\tau_n$, a small α means that Γ_p is sharply peaked compared to the slow relaxation rate $1/\tau_n$. Although the theory outlined is valid for any α , a strong DNSP feedback requires $\alpha \ll 1$. We assume this from now on.

Let us consider *detuning* first. The natural measure for the frequency mismatch is the resonance width $\tilde{B}_1/\sqrt{2}$. If the initial frequency mismatch is small, $\Delta f/\tilde{B}_1 \lesssim 1$, then the weak relaxation stops the building of nuclear polarization only at significantly large $\Delta/\tilde{B}_1 = 2^{-3/2}\alpha^{-1/3} \gg 1$, that is, far from the resonance (see Fig. 2a).

Counterintuitively, a larger frequency mismatch results in *tuning*. If $\Delta f/\tilde{B}_1 > 3 \cdot 2^{-13/6}\alpha^{-1/3}$, then Eq. (4.6) has three zeros, and the polarization becomes bistable, as in Fig. 2b. This bistability is preserved till much bigger mismatches, with upper boundary $(\Delta f)_{\max} \equiv \tilde{B}_1 2^{-3/2}\alpha^{-1}$. In one of the stable configurations

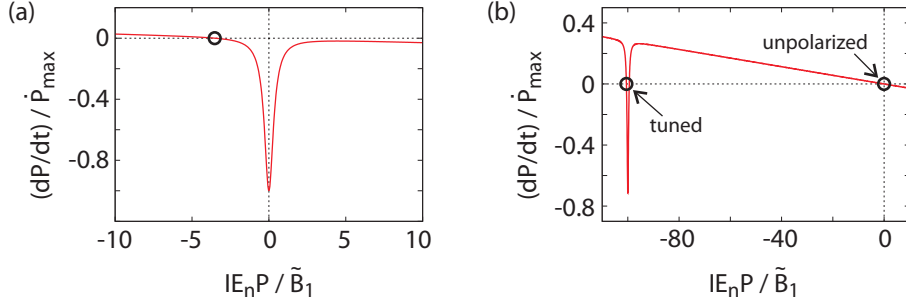


Figure 4.2: Two plots of dP/dt normalized by the maximum ESR pumping rate $\dot{P}_{\max} = 2\Gamma_p(0)/N$, versus the nuclear polarization P . The circles indicate the stable configurations. (a) Detuning at small frequency mismatch ($\Delta f = 0$). (b) Bistability and tuning at large frequency mismatch ($\Delta f = 100\tilde{B}_1$). For both plots $\alpha = 10^{-3}$.

$\Delta \simeq \tilde{B}_1$, and the system is tuned to resonance. The other stable state is unpolarized and thus far away from the ESR condition. We stress that the bistability is asymmetric: if $E_n > 0$, as in GaAs (an antiparallel arrangement of electron and nuclear spins is energetically favorable), the bistability occurs *only* at $\Delta f > 0$. If on the other hand $E_n < 0$, it occurs only at ω lower than $g\mu_B|B_0|/\hbar$.

Such a bistability implies also hysteretic behavior. Let us adiabatically sweep the frequency starting at $\omega < g\mu_B|B_0|$ far from the resonance (see Fig. 3). Upon increasing ω we first cross $g\mu_B|B_0|$ (i.e. the line $\Delta f = 0$), and then get to the tuned state at $\Delta f \simeq \tilde{B}_1\alpha^{-1/3}$. We remain in this state until the frequency mismatch reaches $(\Delta f)_{\max}$, provided that our sweep speed is much smaller than the typical nuclear spin pumping rate, i.e. $\dot{\omega} \ll 2E_n\Gamma_p(0)/N\hbar$. If we cross $(\Delta f)_{\max}$, nuclear relaxation becomes stronger than DNSP: the tuning ceases and the only stable state is again the unpolarized one, which will be reached on a time scale of τ_n . If we then go backwards decreasing ω , we will not get into the tuned state but remain in the stable unpolarized state.

The overall structure in the (B_0, ω) -plane is sketched in Fig. 3, where the bistability occurs in the gray-shaded region. An experimentally accessible quantity is the width of this region. It is equal to the maximum frequency mismatch $(\Delta f)_{\max} \propto \alpha^{-1} \propto \Gamma_r^z[\omega]/\omega^2$, so it exhibits dependence on ω . At lower frequencies, mechanism (i) (interaction with the leads) dominates the dissipative spinflips and $\Gamma_r^z[\omega] \propto \omega$, so that $(\Delta f)_{\max} \propto 1/\omega$. At larger frequencies mechanism (ii) takes over, resulting in $(\Delta f)_{\max} \propto \omega^3$. This together implies that $(\Delta f)_{\max}$ reaches a minimum at a finite ω_c . We illustrate this behavior in Fig. 3, choosing $(\Delta f)_{\max} = 0.04\omega_c[3(\omega_c/\omega) + (\omega/\omega_c)^3]$. The separate contributions of mechanism (i) and (ii) are indicated with thin dashed lines.

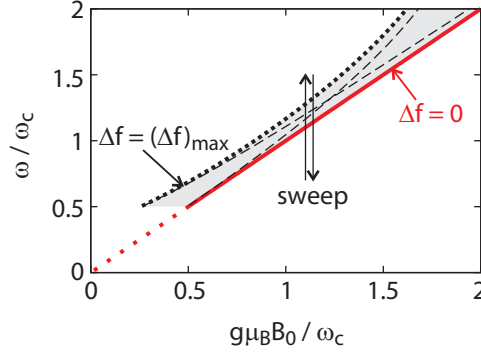


Figure 4.3: Stability diagram in the (ω, B_0) -plane for ESR induced DNSP. Bistability and tuning to the resonance occur in the gray-shaded region. The arrows show an adiabatic frequency sweep leading to the tuned state. The dashed lines present the separate contributions of mechanism (i) and (ii). This diagram qualitatively agrees with [15], Fig. 2C

Let us give a numerical example supporting the assumptions made. Based on typical experimental parameters [34], we use $\tau_n = 15$ s, $N = 10^6$, $\tilde{B}_1 = 1.5$ mT, $\omega = 120$ mT and $\Omega = 5$ mT (for $|g| = 0.35$ [34], 1 mT $\approx 3 \cdot 10^7$ s $^{-1}$). We take $\Gamma_r^z = 2 \cdot 10^6$ s $^{-1}$, this is in accordance with a lower bound estimate set by the typical leakage current of 100 fA [34]. We find that $\alpha \approx 1.5 \cdot 10^{-2}$, so it is small indeed, and this suggests strong DNSP. The same set of parameters gives $(\Delta f)_{\max} \approx 24\tilde{B}_1$, which is much bigger than the resonance width and even comparable to the driving frequency $(\Delta f)_{\max} \approx 0.3\omega$. This gives 40 mT, a value that agrees well with experimental observations in a double dot ([34], Fig. 2C). The maximum polarization is achieved at the edge of the region, where $P_{\max} \approx 7.2 \cdot 10^{-3}$, so that $P \ll 1$ indeed.

We also investigated both the switching rates between the tuned and the unpolarized state, and the small fluctuations near these stable states. To estimate the fluctuations, we use a Fokker-Planck equation for the distribution function of the polarization $\mathcal{P}(P)$. To derive the equation, we regard the nuclear dynamics as a random walk on a discrete set of spin values $n = \frac{1}{2}(N_{\uparrow} - N_{\downarrow})$. The pumping rate Γ_p only causes transitions from n to $n - 1$, while the spin relaxation causes transitions in both directions with almost equal rates $(1/2\tau_n)N_{\uparrow,\downarrow} \gg \Gamma_p$. We go to the continuous limit, justified by the large number of nuclei ($\sim 10^6$) to obtain [75]

$$\frac{\partial \mathcal{P}}{\partial t} = \frac{\partial}{\partial P} \left\{ \mathcal{P} \left[\frac{1}{\tau_n} P + \frac{2}{N} \Gamma_p \right] + \frac{\partial}{\partial P} \mathcal{P} \frac{1}{N\tau_n} \right\}. \quad (4.7)$$

From the steady state solution of (4.7) we evaluate the small fluctuations around the unpolarized and tuned states. While $\langle (\Delta P)^2 \rangle_{\text{unp}} = 1/N$ is not affected

by ESR, the fluctuations in the tuned state are suppressed roughly by a factor α^{-1} (67 for the numerical example), more precisely $\langle(\Delta P)^2\rangle_{\text{tun}} = \frac{1}{2}\alpha\{q^3(1-q)\}^{-1/2}\langle(\Delta P)^2\rangle_{\text{unp}}$, where $q \equiv \Delta f/(\Delta f)_{\text{max}} \sim 1$. Importantly, this factor also determines the *acceleration* of the nuclear dynamics: the local nuclear spin relaxation time in the tuned state, τ_n^{tun} , is shorter than τ_n by the same factor.

This quenching of the fluctuations is also a justification for neglecting them. If the fluctuations would have been fully developed, one could only neglect them if the resonance width $\tilde{B}_1 \gg \Omega$. Since the fluctuations are suppressed, this condition is now achieved at much smaller driving fields $\tilde{B}_1 \gg \Omega\sqrt{\alpha}$. The same condition guarantees that spontaneous switching between the tuned and unpolarized state occurs with an exponentially small rate. We evaluate this rate from (4.7) with Kramers method [75] to obtain

$$\Gamma_{t \rightarrow u} = \frac{1}{2\pi\tau_n^{\text{tun}}} \exp\left(-\frac{\tilde{B}_1^2}{4\Omega^2\alpha}f(q)\right), \quad (4.8)$$

where $f(q) = \arctan \sqrt{q^{-1}-1} - \sqrt{q(1-q)} \simeq 1$. The values from our numerical example give $1/\Gamma_{t \rightarrow u} \simeq 4$ s at $q = \frac{1}{2}$. The inverse rate $\Gamma_{u \rightarrow t}$ is yet smaller, so that if the dot has switched to the unpolarized state, it is unlikely to switch back by itself. One would have to make again a frequency sweep as described above.

4.4 Conclusion

To conclude, we have investigated DNSP under ESR conditions to find both detuning and bistability-related tuning of the resonance. The simple model in use explains qualitatively a set of recent experimental findings. The authors gladly acknowledge useful communications with F.H.L. Koppens, L.M.K. Vandersypen, M.S. Rudner, L.S. Levitov, D.R. Yakovlev and D.J. Reilly. This work was supported by the Dutch Foundation for Fundamental Research on Matter (FOM).

Chapter 5

Multiple nuclear polarization states in a double quantum dot

We observe multiple stable states of nuclear polarization and nuclear self-tuning over a large range of fields in a double quantum dot under conditions of electron spin resonance. The observations can be understood within an elaborated theoretical rate equation model for the polarization in each of the dots, in the limit of strong driving. This model also captures unusual features of the data, such as fast switching and a ‘wrong’ sign of polarization. The results reported enable applications of this polarization effect, including accurate manipulation and control of nuclear fields.¹

¹This chapter has been published in Physical Review Letters **103**, 046601 (2009).

5.1 Introduction

Great experimental progress in the last decade enabled the confinement, initialization and read-out of single spins in quantum dots [41, 40]. Controlled coherent single-spin rotations — a key ingredient for quantum manipulation — were demonstrated recently using the electron spin resonance (ESR) [34, 35, 59, 65, 88]. The weak hyperfine coupling of the electron spin to the nuclear spins in the host material appeared to be of great importance in this field. It was identified as the main source of qubit decoherence and provides a significant hybridization of the spin states [37, 36, 77]. This has stimulated intensive theoretical and experimental research focusing on nuclear spin dynamics in quantum dots [38, 58, 67, 89, 69, 90].

Overhauser pointed out already in the the 1950s [63, 86] that ESR may provide the buildup of significant nuclear spin polarization. Indeed, most ESR experiments on quantum dots, aimed at demonstrating electron spin rotations, also clearly demonstrated dynamical nuclear spin polarization (DNSP) [34, 35, 59, 65].

For ESR driving of a single spin in an almost isolated quantum dot, or an ensemble of such dots, the scenario is similar to that of the usual Overhauser effect: the direction of DNSP is parallel to the spin of the excited electrons [63, 86] (see also Chapter 4 of this thesis). Recent ESR experiments on self-assembled quantum dots have confirmed this picture [65], and a similar reasoning holds for spin experiments with optically pumped dots [66]. In some cases, a bistability has been observed: under the same conditions, the nuclear spins in the dot can be either polarized or unpolarized [67].

However, several issues can complicate the situation. In recent ESR experiments in double quantum dots [34, 35, 59] (i) electrons participate in *transport* during ESR driving, and (ii) there can be different nuclear spin dynamics in the two dots. Furthermore, a driving magnetic field is in practice accompanied by an electric field which modulates the electron-nuclear spin coupling at the resonance frequency [59]. All this makes a straightforward extension of existing models (as the one presented in Chapter 4) impossible and promises richer and more interesting physics, which we indeed reveal.

In this Chapter, we report a study of ESR in a double quantum dot focusing on DNSP. We have observed multiple stable states of nuclear polarization (up to four states), not seen in single-dot experiments, nuclear self-tuning to the ESR condition over a large range of magnetic fields ($\gtrsim 100$ mT), and a sign of DNSP opposite to that following from the Overhauser argument. We identify the most probable mechanism governing DNSP and present a theoretical model explaining our findings. The results reported enable applications of this self-tuning effect, including accurate manipulation and control of the nuclear polarization

(see Chapter 6 of this thesis) and use of this for improving the electron spin coherence time, possibly by orders of magnitude.

5.2 Experimental observations

The double quantum dot system is electrostatically defined in a two-dimensional electron gas, located 90 nm below the surface of a GaAs/AlGaAs heterostructure, by applying negative voltages to metal surface gates. The dots are tuned to the Pauli spin blockade regime [91, 92], where the transport sequence of charge states is $(1, 1) \rightarrow (0, 2) \rightarrow (0, 1) \rightarrow (1, 1)$, (n, m) denoting the charge state with $n(m)$ excess electrons in the left(right) dot. The current through the double dot depends on the spin orientation of the electrons in the $(1, 1)$ state since the only accessible $(0, 2)$ state is a spin singlet (Fig. 5.1).

Magnetic spin resonance is achieved by sending an alternating current through a coplanar stripline (CPS) which lies on top of the surface gates, separated by a thin dielectric layer. This current produces a small oscillating magnetic field $B_1 \simeq 1$ mT perpendicular to the external magnetic field $B_0 \simeq 100$ mT. The experimental data are obtained with the same device and in the same measurement run as the data presented in Ref. [34]. The difference is that the device is tuned

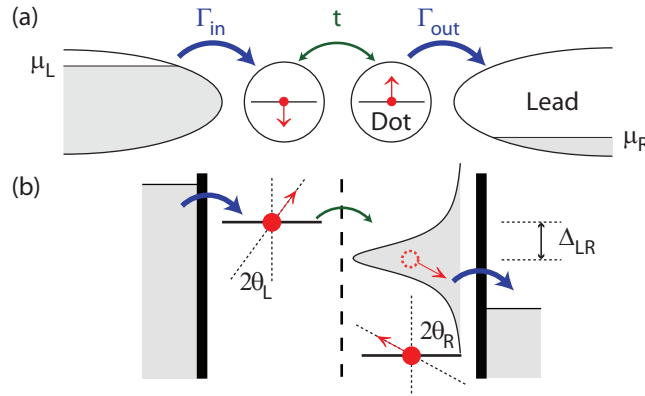


Figure 5.1: Double dot setup. (a) The double quantum dot is coupled to two leads. Due to a voltage bias, electrons can only run from the left to the right lead, implementing the transport sequence $(1, 1) \rightarrow (0, 2) \rightarrow (0, 1) \rightarrow (1, 1)$. (b) Energy diagram. The four possible $(1, 1)$ states differ in spin projections on the quantization axes (red arrows). Under ESR conditions the axes can be different in the two dots and do not coincide with the direction of the external magnetic field. These states are coherently coupled (green arrow) to the $(0, 2)$ singlet that decays quickly (broadened line), leaving the system in $(0, 1)$.

to a higher interdot tunnel coupling and coupling to the right lead.

When we apply a continuous wave RF current with fixed frequency ω to the CPS and sweep the external magnetic field B_0 passing the resonance condition $B_0 = B_{\text{res}} \equiv \hbar\omega/g\mu_B$, we make a remarkable observation. One would expect that the resonance manifests itself as a peak in the current [34]. Indeed, if the external field is swept from low to high values, the current jumps up upon achieving the resonance condition. Unexpectedly, this resonant response extends over a wide range of magnetic fields, that exceeds B_{res} by a factor of 2 (see Fig. 5.2a upper panel). If the field is swept in opposite direction (Fig. 5.2a lower panel), the current remains low till B_0 is several mT above B_{res} . This indicates a strong hysteresis for $B_0 > B_{\text{res}}$, whereas the hysteresis below B_{res} is much less pronounced.

Another unexpected observation is made at fixed $B_0 \approx B_{\text{res}}$. Instead of a single value of the current corresponding to the maximum value of the ESR satellite peak, we observe clearly distinguishable *multiple* stable values of the current. Switching between these values gives rise to a random telegraph signal (RTS) with time scales ranging from seconds to minutes. Typical time-resolved measurements of the RTS are presented in Fig. 5.2b for three different values of the energy level detuning Δ_{LR} (Fig. 5.1).

We associate both the hysteresis and RTS with DNSP induced by the non-equilibrium electron spin dynamics under conditions of ESR and transport in the dots. Nuclear polarization is known to provide an extra effective magnetic field B_N acting on the electron spin [63, 86]. Where high current is observed in the hysteresis region, this extra field should be such that the total field $B_0 + B_N \approx B_{\text{res}}$, i.e. the nuclear field ‘tunes’ the system to the resonance condition (compare Chapter 4). Low current indicates that the total field $B_0 + B_N$ significantly deviates from B_{res} : the nuclei are unpolarized. Both polarized and unpolarized states are stable in the interval of hysteresis. Fluctuations of any kind could provide spontaneous switching between stable states, leading to the RTS.

A number of experimental details does not fit into this simple picture. Firstly, there are *multiple* values of the current observed, three are clearly visible in Fig. 5.2b (labeled *A-C*). This implies multiple stable states of nuclear polarization with a total field close to B_{res} . Actually, we think that the RTS traces provide evidence for the existence of a fourth state. There is a number of current dips observed (labeled *D*) too big to be statistical fluctuations. We interpret those dips as signatures of a fourth state that decays on the scale of a second, i.e. different from state *A*, which decays on a larger time scale. Secondly, switching between the different current levels is rather fast. The nuclear spin dynamics are known to be slow, with a typical relaxation time $\tau_n \sim 15$ s [37, 89, 69]. If the current is a direct measure of the nuclear polarization, then why is the duration

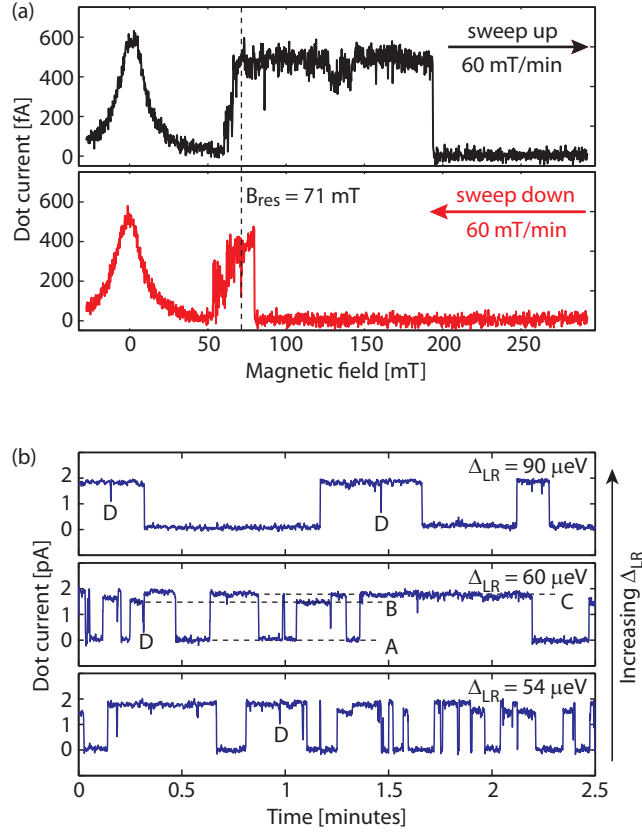


Figure 5.2: (a) Magnetic field sweeps for ω fixed at 350 MHz. Upper panel: magnetic field sweep from low to high values resulting in an ESR peak width exceeding 100 mT. Lower panel: sweep in the opposite direction, showing a much narrower ESR peak. Another peak is observed at zero field which manifests the mixing of the four (1,1) states by the fluctuating nuclear fields [34, 37]. An offset of ~ 7 mT of the external magnetic field due to the superconducting magnet is compensated for in both traces. The nominal resonance condition $B_{\text{res}} = \hbar\omega/g\mu_B$ is met at $B_0 \approx 71$ mT for $\omega = 350$ MHz and $g = 0.35$ [34] (see dashed line). Note that in both traces the nuclear bath is unpolarized at the onset of electron spin resonance (see Section 5.6). (b) Multiple values of the current through the double dot approximately at resonance. The current switches between at least three stable values on a time scale of seconds to minutes. The three panels correspond to three different values of the energy level detuning Δ_{LR} (increasing from the bottom to the upper panel). The values given for Δ_{LR} may have a constant offset, as photon assisted tunneling processes broaden the interdot transition which makes it difficult to separate resonant and inelastic transport. In both (a) and (b) the lowest value of current was subtracted as offset. The data in (b) were taken for a larger Γ_{in} and Γ_{out} than the data in (a).

of the switching events so short? A third point is the *sign* of the polarization. Usually, in ESR experiments the dominating mechanism of DNSP is described by the Overhauser effect: the ESR excitation drives the electron spin(s) out of equilibrium, and hyperfine induced electron-nuclear spin exchange is one of the mechanisms contributing to electron spin relaxation. As reasoned by Overhauser, on grounds of spin conservation, the direction of nuclear polarization should be parallel to the spin of excited electrons, whatever its orientation is with respect to the magnetic field applied. This is the case for most DNSP experiments, e.g. [34, 65, 67]. Given the negative g -factor and positive hyperfine coupling in GaAs [54], this would give a B_N *parallel* to B_0 (see Chapter 4). In our experiment, its direction is clearly *opposite*, as high current is seen for $B_0 > B_{\text{res}}$. All three points are captured by the theory given below.

5.3 Model

The electron spin $\hat{\mathbf{S}}$ and nuclear spins $\hat{\mathbf{I}}_k$ in each dot are coupled by hyperfine interaction [54]

$$\hat{H}_{\text{hf}} = \frac{1}{2} \sum_k A_k \left\{ 2\hat{S}^z \hat{I}_k^z + \hat{S}^+ \hat{I}_k^- + \hat{S}^- \hat{I}_k^+ \right\}, \quad (5.1)$$

where the sum runs over all $N \sim 10^6$ nuclei in the dot. The energy A_k is proportional to the probability to find the electron at the position of nucleus k , $A_k \simeq 10^{-10}$ eV. With an external field applied in the z -direction, the ‘flip-flop’ terms $\hat{S}^\pm \hat{I}_k^\mp$ provide spin exchange between the electrons and nuclei. Owing to energy conservation, these exchange transitions must be second-order processes involving a mechanism supplying or absorbing the excess Zeeman energy. Conventionally, the electron-nuclear spin exchange is due to the time-independent hyperfine coupling A_k . However, as recently has been pointed out [34, 59], in this setup a significant a.c. electric field moves the electrons in the dots with respect to the nuclei. This can be accounted for by introducing a *time-dependent* component in the hyperfine coupling $A_k \rightarrow A_k + \tilde{A}_k e^{i\omega t} + \tilde{A}_k^* e^{-i\omega t}$. We estimate that under the present conditions $\tilde{A}_k/A_k \simeq 0.1$ [59, 93].

We have considered six candidate mechanisms for DNSP (see Section 5.6.3), assuming a saturated ESR. We concluded that the dominant one involves the time-dependent hyperfine coupling, which allows for ‘photon assisted flip-flops’. These flip-flops not have a preferred direction set by a large energy mismatch: now the spin asymmetry is now provided by internal spin relaxation causing the spin ground state (parallel to the external field) to be more populated than the excited state.

The theoretical consideration includes the following steps: (i) We consider the four $(1, 1)$ states using a rotating wave approximation, assuming a saturated ESR and a negligible exchange splitting, i.e. $\min\{t, t^2/\Delta_{LR}\} \ll B_1, B_N$. The eigenstates in a rotating frame are mixtures of spin-up and spin-down states, with a mixing angle $\theta_{L,R} = \frac{1}{2} \arctan\{\tilde{B}_{L,R}/2f_{L,R}\}$ which can be different in both dots (see Fig. 5.1), due to e.g. different coupling of the electrons to the CPS. The Rabi frequency in each dot $\tilde{B}_{L,R} \equiv g\mu_B B_1^{(L,R)}/\hbar$ gives the width of the saturated resonance, and the ESR frequency mismatch $f_{L,R} \equiv |g\mu_B(B_0 + B_N^{L,R})/\hbar| - \omega$ depends on the nuclear polarization in each dot. (ii) We evaluate the transition rates between these states to obtain their quasi-stationary population and the current through the double dot. We include tunneling (characterized by $\Gamma_s = t^2/\Gamma_{\text{out}} \simeq 1 - 10$ MHz) and single electron spin relaxation (c.f. Chapter 4) ($\propto \Gamma_r \simeq 1$ MHz at zero temperature, which will be enhanced by a thermal factor $k_B T/g\mu_B B_0 \equiv \xi \simeq 5$, in accordance with a lower bound estimate set by the typical leakage current of 100 fA). This approach is valid in the limit $\tilde{B} \gg \Gamma_{s,r}$. (iii) We compute the rates of hyperfine-induced spin exchange. In the first approximation we find rates symmetric with respect to nuclear spin, their scale set by $\Gamma_2 \simeq \tilde{A}_k^2/(64\hbar^2\xi\Gamma_r) \sim 0.5$ Hz. Being symmetric, these rates do not contribute to DNSP. They merely enhance the relaxation of the nuclear fields. (iv) The small spin-asymmetric part of these rates $\Gamma_1 \simeq \frac{5}{3}(\tilde{A}_k/8\hbar\tilde{B})^2(\Gamma_s/\xi) \sim 10^{-2}$ Hz, due to electron spin relaxation, introduces a preferential direction of nuclear spin pumping in each dot. (v) We construct equations of motion for the effective nuclear fields $B_N^{L,R}$ and analyze the stable states of nuclear polarization given by $dB_N^{L,R}/dt = 0$. (vi) We use a Fokker-Planck equation to give a qualitative analysis of fluctuations of nuclear polarization and switching rates between the stable states.

5.4 Results

The evolution equation for B_N^L thus found reads

$$\frac{dB_N^L}{dt} = -\Gamma_1 B_{\text{ov}} P(\theta_{L,R}) - \left\{ \frac{1}{\tau_n} + \Gamma_2 R(\theta_{L,R}) \right\} B_N^L, \quad (5.2)$$

and the equation for B_N^R is obtained by permutation of L and R . The field B_{ov} is the Overhauser field of full polarization, $B_{\text{ov}} \approx 5$ T for GaAs. The functions P and R are dimensionless functions giving the functional dependence of the resonant nuclear spin pumping (P) and resonantly enhanced nuclear spin relaxation (R) on the mixing angles and on $\Gamma_s/\xi\Gamma_r$, and have a maximum ~ 1 . While R is roughly Lorentzian-shaped, the function P is zero far from resonance $\theta \rightarrow \{0, \pi\}$,

reaches maximum at $|f| \simeq \tilde{B}$, and falls off to zero again at the resonance $\theta = \pi/2$. This resonant dip is due to the vanishing of electron spin polarization at the saturated resonance. In Eq. (5.2), the terms proportional to $-B_N$ give nuclear spin relaxation: the first term presents the usual τ_n while the second term gives a resonant enhancement owing to spin exchange with electrons. Nuclear spin pumping is given by $\Gamma_1 B_{\text{ov}} P$ (~ 50 mT/s, much faster than the sweep rate in Fig. 5.2a), with a *sign opposite* to that following from the Overhauser reasoning: spin exchange under conditions of electron transport is mostly due to electrons polarized along the direction of the external field. The shape of a typical pumping curve is shown in Fig. 5.3.

We are now also able to understand the extended interval of hysteresis: ESR response can be observed as long as there exist stable solutions of $dB_N/dt = 0$ close to resonance. Eq. (5.2) determines the interval of hysteresis as $B_{\text{res}} \lesssim B_0 < B_{\text{res}} + |B_N^{\text{max}}|$, where the maximal nuclear field is $B_N^{\text{max}} = -B_{\text{ov}}\Gamma_1/(\Gamma_2 + \tau_n^{-1})$. Using the parameters as estimated above we find that $\Gamma_2\tau_n \sim 10$.

It is the two-peak shape of the pumping curve that is responsible for the multiple stable states of nuclear polarization, even at the edge of the hysteresis interval. If $B_0 \approx B_{\text{res}}$ (Fig. 5.3, green curve), there are four stable states for the double dot system. This is represented in Fig. 5.4a, where the circles indicate the

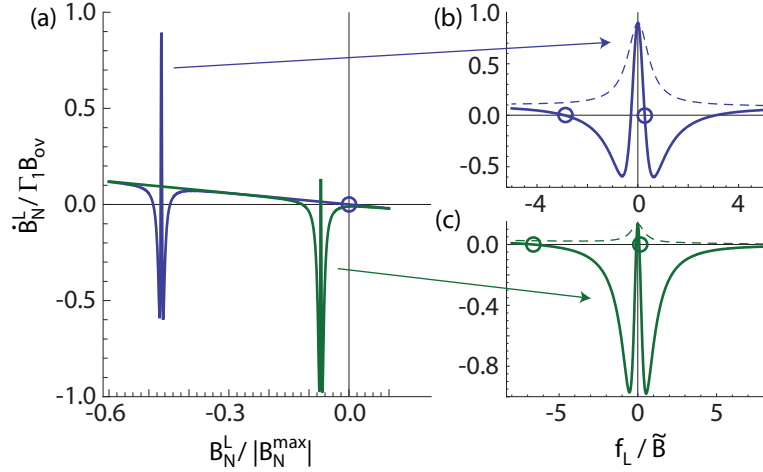


Figure 5.3: (a) Time-derivative dB_N^L/dt at the edge of the hysteresis interval $B_0 \approx B_{\text{res}}$ (green) and in the middle of the interval $B_0 \approx B_{\text{res}} + 0.5 |B_N^{\text{max}}|$ (blue). (b,c) Close-up at resonance. The curves consist of the usual relaxation (linear slope) which is resonantly enhanced (dashed lines), and spin pumping that adds a two-peak shape near the resonance. The circles indicate the stable states of nuclear polarization. We used $\Gamma_1/\Gamma_2 = 0.043$, $\Gamma_2\tau_n = 5$, $\theta_R = 0$, $\xi\Gamma_r/\Gamma_s = 0.75$, and assumed equally strong coupling \tilde{A}_k of all nuclei to the electron.

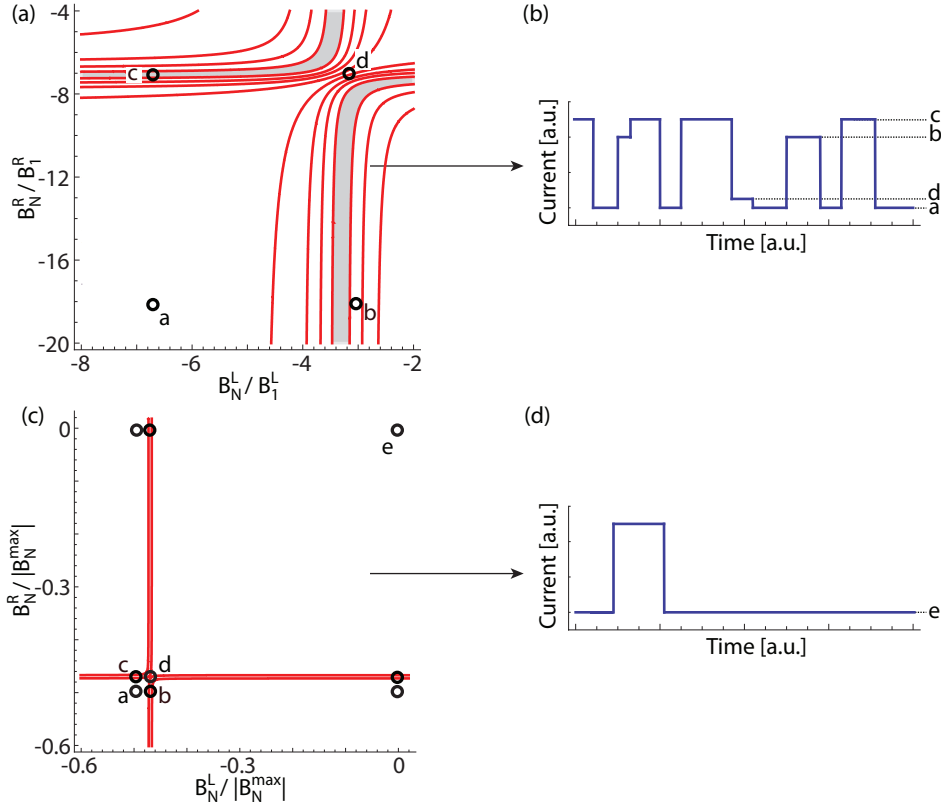


Figure 5.4: Stable polarizations in the plane (B_N^L, B_N^R) , for the cases (a) $B_0 - B_{\text{res}} \sim B_1$ and (d) $B_0 - B_{\text{res}} \sim 0.5 |B_N^{\max}|$. A contour plot of the current is included, the gray shade indicating the region with highest current. Switching between the stable points gives rise to RTS as presented in (b) and (c). A qualitative difference is that the point e in (d) is ‘isolated’, i.e. having switched to e , the system will never switch back. In (a) an asymmetry in $\tilde{B}_{L,R}$ and $N_{L,R}$ is included, resulting in four different current levels for $a-d$, whereas (d) is plotted assuming a symmetric double dot. Note the different scales at the axes in (a) and (d). The same plots (a) and (d) can be found in Section 5.6.5 where we included the local nuclear spin dynamics as a vector field.

stable points in the plane (B_N^L, B_N^R) . It is now clear how, even close to $B_0 = B_{\text{res}}$, the system can have *four stable states* with different current. A rough estimate for the duration of the switching between those states is the typical distance ($\sim B_1$) over the local speed of the spin dynamics ($\sim \Gamma_1 B_{\text{ov}}$), giving $\sim 10^{-2}$ s, which explains the *fast switching*. A typical time trace in this case will look like Fig. 5.4b, which is to be compared with Fig. 5.2b.

When increasing B_0 , both dots will develop a separate third unpolarized stable state (Fig. 5.3, blue curve), giving as many as nine stable points, as presented in Fig. 5.4d. At higher fields the unpolarized state (labeled e) will become isolated

from the other stable states: if the system switches to e , it will never switch back (see Fig. 5.4c). This also has been observed in experiment (see Chapter 6). When subsequently sweeping back from high to low field, the barrier for switching back from e to a high-current state is again gradually lowered. When the typical switching time becomes comparable to the time scale of the sweep, one can expect the current to switch to a high value (Fig. 5.2a, lower panel).

From Eq. (5.2) we construct a two dimensional Fokker-Planck equation to study the stochastic properties of the polarizations in more detail. Importantly, due to the accelerated dynamics, the fluctuations around all polarized states are suppressed as $\langle(\Delta B_N)^2\rangle/\Omega^2 \approx (B_1/|B_N^{\max}|)$, $\Omega^2 \equiv (A_k/g\mu_B)^2 N$ being the field variance in the unpolarized state. Using Kramers' method [75] we derive an expression for the switching rates between the stable states. All rates have the exponential dependence $\Gamma_{\text{sw}} \propto \exp\{-\alpha B_1 |B_N^{\max}|/\Omega^2\}$, where α is a numerical factor: the rates are suppressed exponentially with a power $\sim B_1^2/\langle(\Delta B_N)^2\rangle \gg 1$. This exponential dependence explains the large RTS time scale as well as the strong variation with Δ_{LR} in Fig. 5.2. We calculated the exponent explicitly for Γ_{sw} from a to d in Fig. 5.4d. We used $\Gamma_2\tau_n = 10$, $\Gamma_s/\xi\Gamma_r = \frac{16}{15}$, and $B_0 - B_{\text{res}} = 0.5 |B_N^{\max}|$ and found that $\alpha \approx 0.72$.

5.5 Conclusion

To conclude, we have observed multiple nuclear polarization states and locking of the ESR condition over a large range of magnetic fields in a double quantum dot under ESR. We presented a theoretical model that captures the existence of these phenomena and their unusual features as fast switching and a 'wrong' sign of DNSP. We acknowledge useful discussions with M. Laforest. This work was supported by the Dutch Foundation for Fundamental Research on Matter.

5.6 Appendix

5.6.1 Sample

The experimental data presented are obtained with the same sample as used in reference [34]. A device with the same gate pattern as used in the experiment is shown in Fig. 5.5a. The two coupled semiconductor quantum dots are defined by surface gates (Fig. 5.5a) on top of a two-dimensional electron gas (2DEG). The oscillating magnetic field that drives the spin transitions is generated by applying a radio-frequency (RF) signal generated by a Rohde & Schwarz SMR40

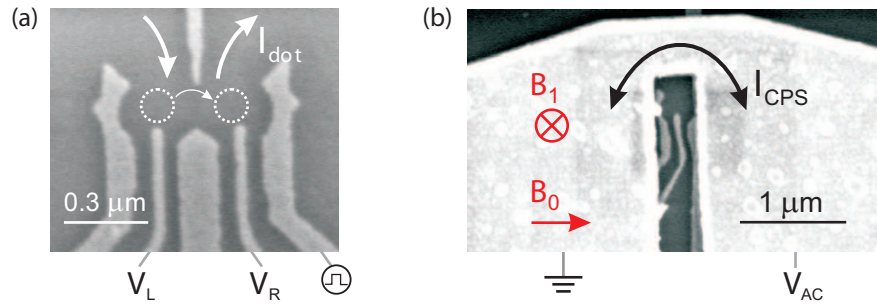


Figure 5.5: ESR device. (a) Scanning electron microscope (SEM) image of a device with the same gate pattern as used in the experiment. The Ti/Au gates are deposited on top of a GaAs/AlGaAs heterostructure containing a two-dimensional electron gas 90 nm below the surface. White arrows indicate current flow through the two coupled dots (dotted circles). The directions of the external magnetic field and the ac magnetic field are indicated. (b) SEM image of a device similar to the one used in the experiment. The termination of the coplanar stripline is visible on top of the gates. The gold stripline has a thickness of 400 nm and is designed to have a 50Ω characteristic impedance, Z_0 , up to the shorted termination. It is separated from the gate electrodes by a 100-nm-thick dielectric (Calixerene).

source to an on-chip coplanar stripline (CPS) which is terminated in a narrow wire, positioned near the dots and separated from the surface gates by a 100-nm-thick dielectric (Fig. 5.5b). The current through the wire generates an oscillating magnetic field B_1 at the dots, perpendicular to the static external field B_0 and slightly stronger in the left dot than in the right dot.

The GaAs/AlGaAs heterostructure from which the samples were made was purchased from Sumitomo Electric. The 2DEG has a mobility of $185 \times 10^3 \text{ cm}^2/\text{Vs}$ at 77 K, and an electron density of $4\text{-}5 \times 10^{11} \text{ cm}^{-2}$, measured at 30 mK with a different device than used in the experiment.

Background charge fluctuations made the quantum dot behavior excessively irregular. The charge stability of the dot was improved considerably in two ways. First, the gates were biased by +0.5 V relative to the 2DEG during the device cool-down. Next, after the device had reached base temperature, the reference of the voltage sources and I/V converter (connected to the gates and the 2DEG) were biased by +2 V. This is equivalent to a -2 V bias of both branches of the CPS, which therefore (like a gate) reduces the 2DEG density under the CPS.

The measurements were performed in a Oxford Instruments Kelvinox 400 HA dilution refrigerator operating at a base temperature of 35-40 mK.

5.6.2 Measurements

In both traces in Fig. 5.2a, the nuclear bath is unpolarized at the onset of electron spin resonance. In the case of the upper panel, B_0 is swept just before the measurement from 300 mT to -20 mT in about 40 s. During this sweep the nuclear field relaxes (typical relaxation time $\tau_n \sim 10$ s) or is even actively depolarized. Residual polarization would be indicated by a shift of the zero field peak and the onset of ESR response to a nominal non-resonant magnetic field, which is both not observed. In the case of the lower panel the magnetic field is swept from low to high magnetic field (to 300 mT) just before recording the trace. In this case there could be polarization still present at the beginning of the trace, however in that case that polarization relaxes much faster than the sweep rate of 60 mT/min, such that when reaching the resonant field the nuclear spin bath is equilibrated.

5.6.3 Candidate mechanisms

Here we describe how we identify the dominating process of hyperfine induced nuclear spin flips. The ‘flip-flop’ terms $\hat{S}^\pm \hat{I}_k^\mp$ in the hyperfine Hamiltonian are responsible for the exchange of spin between the electron and the nuclei. However, as the nuclear Zeeman splitting is 3 or 4 orders smaller than the electron splitting [24], the states coupled by $\hat{S}^\pm \hat{I}_k^\mp$ are roughly $g\mu_B B_0$ apart in energy. Therefore, spin exchange is only allowed in a second-order process in which some other mechanism supplies or absorbs the excess Zeeman energy.

This energy difference may (i) be dissipated by an environment (see Chapter 4), or (ii) be given to an electron tunneling out of the dot. In case (i) the environment, at sufficiently low temperatures, can only absorb energy, so that the electron Zeeman energy can only be reduced. This results in the same sign of DNSP as with the usual Overhauser effect [63]. In case (ii), owing to a voltage bias much larger than the Zeeman energy, the change of energy in the course of a spin-flip can be of either sign. In this case, a preferential direction of DNSP will be determined by some other spin asymmetry of the system. Such an asymmetry may arise from either (ii.a) a difference in spin-flip rates for different spin directions (e.g. due to different overlap between initial and final states), or (ii.b) different populations of the states with different spin directions (e.g. due to internal relaxation processes or differing decay rates).

Apart from these three mechanisms, there are two more options to choose between: as mentioned above, the a.c. electrical component of the exciting field B_1 moves the electrons in the dots with respect to the nuclei, and this we account

for by introducing a time-dependent component in the hyperfine coupling. The time-dependent and time-independent couplings will give rise to different flip rates, so this gives us in total six candidate mechanisms.

Let us first decide on the relative contributions of the time-dependent and time-independent hyperfine couplings, A_k and \tilde{A}_k . We compare the strength of second order transition rates, in both cases proportional to the coupling amplitude square and inversely proportional to the energy square of the virtual state. While for the time-independent coupling this energy is the electron Zeeman energy $E_Z \equiv g\mu_B B_0$, it is a much smaller energy for the resonant time-dependent coupling, involving the a.c. resonant magnetic field $E_{\text{rf}} \equiv g\mu_B B_1$. Therefore we have to compare the factors $(A_k/E_Z)^2$ and $(\tilde{A}_k/E_{\text{rf}})^2$. We estimate that for our conditions $\tilde{A}_k/A_k \simeq 0.1$ and $E_{\text{rf}}/E_Z = B_1/B_0 \simeq 0.01$, and conclude that the time-dependent coupling dominates.

To decide upon the other three options mentioned above, we have to compare the spin exchange rates involving electron tunneling, characterized by the broad-

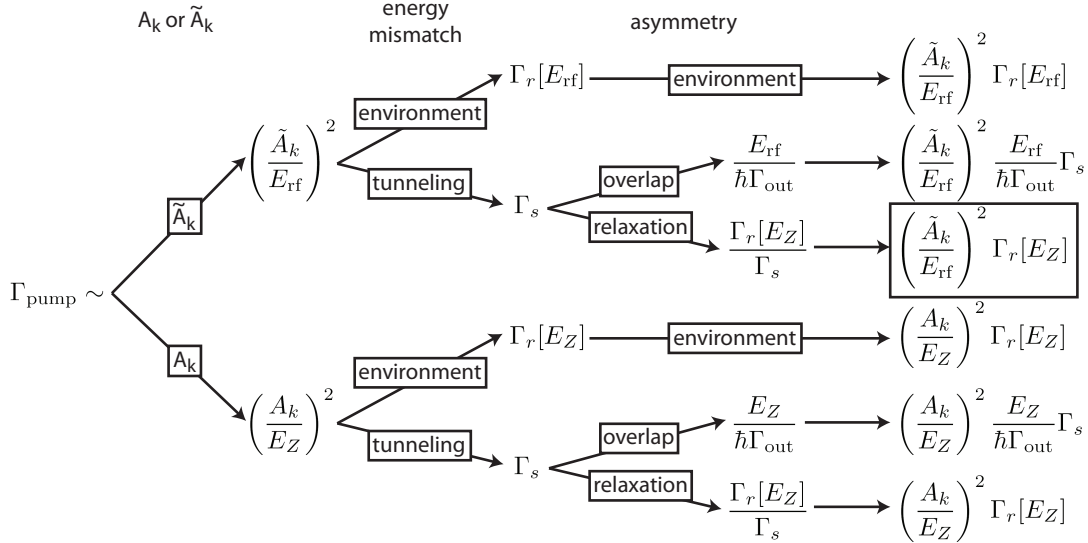


Figure 5.6: Overview of all mechanisms considered and the corresponding estimates for the nuclear spin pumping rate. The two key ingredients for spin pumping are dissipation of the energy mismatch and an asymmetry in spin giving a preferred direction for nuclear spin flips. Furthermore, we considered both the effect of \tilde{A}_k and A_k , i.e. time-dependent and time-independent hyperfine coupling. We conclude that, under the present experimental conditions, the dominant mechanism involves time-dependent hyperfine coupling, energy dissipation by electron transport and internal spin relaxation causing an asymmetry in the populations of the electron spin states.

ening of the (0, 2) singlet $\hbar\Gamma_{\text{out}}$ and the typical decay rate of the (1, 1) singlet $\Gamma_s \simeq t^2/\Gamma_{\text{out}}$, and internal spin relaxation within the dots, characterized by a rate $\Gamma_r[\varepsilon]$, ε being the energy dissipated. For mechanism (i) we find the scale $(\tilde{A}_k/E_{\text{rf}})^2\Gamma_r[E_{\text{rf}}]$, i.e. spin relaxation dissipates the remaining energy difference $\sim E_{\text{rf}}$. In case (ii) the energy is dissipated during tunneling, which takes place with a rate $\sim \Gamma_s$, giving a scale for the nuclear spin flip rate of $(\tilde{A}_k/E_{\text{rf}})^2\Gamma_s$. This rate however is symmetric in spin direction, so to find a preferred direction of DNSP we need to include an asymmetry: (ii.a) The states are split by $\sim E_{\text{rf}}$, so decay to the broadened (0, 2) singlet introduces a relative difference of $\sim E_{\text{rf}}/\hbar\Gamma_{\text{out}}$ in the rates, setting the scale of the DNSP rate $\sim \tilde{A}_k^2\Gamma_s/E_{\text{rf}}\hbar\Gamma_{\text{out}}$. (ii.b) Internal spin relaxation competes with tunneling processes, causing an asymmetry in the population probabilities of the states of $\sim \Gamma_r[E_Z]/\Gamma_s$ resulting in $(\tilde{A}_k/E_{\text{rf}})^2\Gamma_r[E_Z]$ for DNSP. In Fig. 5.6 we give a schematic representation of these considerations. We show all mechanisms investigated and give the corresponding estimates of the scale of nuclear spin pumping.

We estimate $\tilde{A}_k \sim 10^{-11}$ eV, $E_{\text{rf}} \sim 10^{-8}$ eV, $\Gamma_s \sim 10$ MHz, $\hbar\Gamma_{\text{out}} \sim 10^{-4}$ eV and $\Gamma_r[E_Z] \sim 100 \times \Gamma_r[E_{\text{rf}}] \sim 1$ MHz, resulting in the estimates for the scales of DNSP rate (i) 10^{-2} Hz, (ii.a) 10^{-4} Hz, and (ii.b) 1 Hz. Based on this argument we conclude that mechanism (ii.b) dominates: electric field assisted hyperfine flip-flops involve the absorption and emission of photons with energy $\hbar\omega$. Close to resonance this effectively reduces the energy mismatch of the states involved in a flip-flop from $g\mu_B B_0$ to the energy scale of the ESR driving $g\mu_B B_1$. Since this energy mismatch is too small to result in a significant nuclear spin pumping rate based on a standard Overhauser argument, another spin asymmetry is needed. Internal electron spin relaxation provides this asymmetry: it causes the electron spin ground state to be (slightly) more populated than the excited state. This difference in populations combined with photon assisted hyperfine flip-flops (which do not have a preferred direction) results in DNSP parallel to the spin of the electron ground state.

5.6.4 Theory

Here we will elaborate further on the six steps of the theoretical consideration as sketched in Section 5.3.

(i) The Hamiltonian for the electron spin operators $\hat{\mathbf{S}}_{L,R}$ in the rotating wave approximation reads

$$\hat{H} = -\hbar f_L \hat{S}_L^z - \hbar f_R \hat{S}_R^z + \frac{\hbar}{2} \left(\tilde{B}_L \hat{S}_L^x + \tilde{B}_R \hat{S}_R^x \right), \quad (5.3)$$

$L(R)$ referring to the left(right) dot. The rotating wave approximation is justified

by \tilde{B} , $|f| \ll \omega$. The eigenstates of \hat{H} form the basis $\{|+\rangle_L, |-\rangle_L\} \otimes \{|+\rangle_R, |-\rangle_R\}$, with $|+\rangle = \cos\theta|\uparrow\rangle + \sin\theta|\downarrow\rangle$ and $|-\rangle = \sin\theta|\uparrow\rangle - \cos\theta|\downarrow\rangle$, where the mixing angle is $\theta_{L,R} = \frac{1}{2} \arctan\{\tilde{B}_{L,R}/2f_{L,R}\}$.

(ii) The master equation includes the decay and relaxation rates, and is justified if \tilde{B} by far exceeds these rates [93]. The rates depend on the wave functions of the states involved. Any basis state $|n\rangle \in \{|++\rangle, |+-\rangle, |-+\rangle, |--\rangle\}$ decays via the (0,2) singlet to (0,1) with a rate $\Gamma_s^n = |\langle S|n\rangle|^2 \Gamma_s$, with $|S\rangle$ being (1,1) singlet. Such a decay process is followed by a charge transfer in the left junction $(0,1) \rightarrow |m\rangle$, whereby all four basis states $|m\rangle$ are re-initialized with equal rates $\Gamma_s/4$. Internal relaxation processes are due to coupling to an environment and involve energy dissipation of $\pm E_Z$ (see Chapter 4). We believe that the environment are mainly the electrons in the leads. Their temperature is typically large, $\xi \equiv k_B T/E_Z \simeq 5 \gg 1$, so we need to consider both emission and absorption rates. They read $\Gamma_{\text{abs}} = n_B(E_Z)\Gamma_r[E_Z]$ and $\Gamma_{\text{em}} = \Gamma_{\text{abs}} + \Gamma_r[E_Z]$, with $n_B(\varepsilon)$ being the Bose distribution and $\Gamma_r[E_Z]$ being the emission rate at zero temperature. In the high-temperature limit we find the transition rates $\Gamma_r^{n \rightarrow m} \approx \{\xi - \sum_{L,R} |\langle m|\hat{S}_{L,R}^-|n\rangle|^2\}\Gamma_r[E_Z]$. We are now able to construct a master equation

$$0 = -\Gamma_s^n p_n + \frac{1}{4} \sum_m \Gamma_s^m p_m + \sum_m \{\Gamma_r^{m \rightarrow n} p_m - \Gamma_r^{n \rightarrow m} p_n\}, \quad (5.4)$$

and solve it for the quasi-stationary populations p_n . These populations gain, via the rates Γ_s^n and $\Gamma_r^{n \rightarrow m}$, a resonant dependence on $f_{L,R}$ on the scale $f \simeq \tilde{B}$ and therefore also depend on the nuclear polarizations $B_N^{L,R}$. From the populations p_n we can calculate the current through the double dot as $I_{\text{dot}} = e\Gamma_s \sum_n |\langle S|n\rangle|^2 p_n$.

(iii-v) The rates of electron-nuclear spin exchange are calculated using second order perturbation theory. The positive and negative spin flip rates *per nucleus* in the left(right) dot read²

$$\Gamma_{\pm, L(R)}^{(1)} = \frac{1}{16} \tilde{A}_k^2 \Gamma_s \sum_{n,m} \left| \frac{\langle S|m\rangle \langle m|\hat{S}_{L(R)}^\mp|n\rangle}{E_n - E_m} \right|^2 p_n. \quad (5.5)$$

Non-zero diagonal matrix elements such as $\langle ++|\hat{S}^\pm|++\rangle$, will give rise to very small denominators in (5.5), of the order of the nuclear Zeeman energy. Therefore, we have to investigate the contribution of these, possibly dominating, terms in another way. We write the second order perturbation in the hyperfine Hamiltonian,

$$\frac{d\rho}{dt} = - \int_0^t \left[\hat{H}'_L(t) + \hat{H}'_R(t), \left[\hat{H}'_L(t') + \hat{H}'_R(t'), \rho \right] \right] dt', \quad (5.6)$$

²In this expression we assume for simplicity nuclei with spin 1/2. In GaAs $I = 3/2$, which gives rise to an extra numerical prefactor in the later results.

where the perturbation is $\hat{H}'_{L(R)}(t) = \frac{1}{4} \sum_k \tilde{A}_k \{ \hat{S}_{L(R)}^+(t) \hat{I}_{k,L(R)}^-(t) + \hat{S}_{L(R)}^-(t) \hat{I}_{k,L(R)}^+(t) \}$. After separating the time scales of the electronic and nuclear spin dynamics, assuming that we can separate the electronic and nuclear part of the density matrix as $\rho = \rho_{\text{el}} \otimes \rho_{\text{nuc}}$, and tracing over the electron part of the density matrix, we find that we can write for the time-evolution of the nuclear field in one of the dots

$$\frac{dB_N}{dt} = \frac{\tilde{A}_k^2}{8\hbar^2} \left\{ \frac{5}{3} (\chi^{xy} - \chi^{yx}) B_{\text{ov}} - (R^{xx} + R^{yy}) B_N \right\}, \quad (5.7)$$

$\chi^{ab} = -i \int^t \langle \hat{S}^a(t) \hat{S}^b(t') - \hat{S}^b(t') \hat{S}^a(t) \rangle dt'$ and $R^{ab} = \int^t \langle \hat{S}^a(t) \hat{S}^b(t') + \hat{S}^b(t') \hat{S}^a(t) \rangle dt'$, i.e. the susceptibility and zero-frequency fluctuations of the electron spin in the dot under consideration. In Eq. (5.7) we left out the contributions proportional to the polarization in the x - and y -direction while they are averaged out to zero. We focus on the contributions of the diagonal matrix elements and find that $\chi^{xy} - \chi^{yx} = 0$ and $R^{xx} + R^{yy}$ is only non-zero close to resonance, resulting in a resonant enhancement of nuclear spin relaxation.

We can combine Eqs (5.5) and (5.7) in an evolution equation for $B_N^{L,R}$

$$\frac{dB_N^L}{dt} = -\Gamma_1 B_{\text{ov}} P(\theta_{L,R}) - \left\{ \frac{1}{\tau_n} + \Gamma_2 R(\theta_{L,R}) \right\} B_N^L, \quad (5.8)$$

where we added a term describing diffusive spin relaxation $\propto 1/\tau_n$. The equation for B_N^R is obtained by permutation of L and R . The scales $\Gamma_{1,2}$ are the same as defined above, i.e. $\Gamma_1 = \frac{5}{3} (\tilde{A}_k/8\hbar\tilde{B})^2 (\Gamma_s/\xi)$ and $\Gamma_2 \simeq \tilde{A}_k^2 / (64\hbar^2 \xi \Gamma_r)$, and the functions P and R read

$$\begin{aligned} P(\theta_{L,R}) &= \frac{32\alpha(1+4\alpha) \cos\theta_L \cos\theta_R \cos(\theta_L - \theta_R) \sin^2\theta_L}{16\alpha(1+4\alpha) + \sin^2(\theta_L - \theta_R)} \\ &\quad + \frac{4\alpha\{1+8\alpha + \cos^2(\theta_L - \theta_R)\} \sin^2 2\theta_L}{16\alpha(1+4\alpha) + \sin^2(\theta_L - \theta_R)} \\ R(\theta_{L,R}) &= \frac{16\alpha \sin^2\theta_L}{1+16\alpha} \cdot \frac{\cos^2(\theta_L - \theta_R) + 1 + 8\alpha(3+16\alpha)}{\sin^2(\theta_L - \theta_R) + 16\alpha(1+4\alpha)}, \end{aligned} \quad (5.9)$$

where α is the dimensionless variable $\alpha \equiv \xi \Gamma_r [E_Z] / \Gamma_s$. For this representation of P we used the high temperature limit, i.e. $\xi \gg 1$ and assumed for simplicity all electron-nuclear spin couplings \tilde{A}_k equal.

(vi) We also investigated both the switching rates between the different stable states, and the small fluctuations near these states. To estimate the fluctuations, we use a two-dimensional Fokker-Planck equation for the distribution function of the nuclear fields $\mathcal{P}(B_N^L, B_N^R)$, where $-1 \leq B_N^{L,R} / B_{\text{ov}} \leq 1$. To derive the equation, we regard the nuclear dynamics in both dots as a random walk on a discrete set of spin values $n = \frac{1}{2}(N_\uparrow - N_\downarrow)$, where $N_{\uparrow(\downarrow)}$ is the number of nuclei with spin

up(down). The DNSP rate Γ_1 only causes transitions from n to $n + 1$, while the spin relaxation rates Γ_2 and $1/\tau_n$ cause transitions in both directions with a rate $(1/2\tau_n + \Gamma_2/2)N_{\uparrow,\downarrow} \gg \Gamma_1 N$, with $N \equiv N_{\uparrow} + N_{\downarrow}$. We go to the continuous limit, justified by the large number of nuclei per dot ($N \sim 10^6$) to obtain [75]

$$\begin{aligned} \frac{\partial \mathcal{P}(B_N^L, B_N^R, t)}{\partial t} = & \frac{\partial}{\partial B_N^L} \left\{ -\mathcal{P} \frac{dB_N^L}{dt} + \frac{2B_{\text{ov}}^2}{N} \frac{\partial}{\partial B_N^L} \mathcal{P} \left(\frac{1}{2\tau_n} + \Gamma_2 \right) \right\} \\ & + \frac{\partial}{\partial B_N^R} \left\{ -\mathcal{P} \frac{dB_N^R}{dt} + \frac{2B_{\text{ov}}^2}{N} \frac{\partial}{\partial B_N^R} \mathcal{P} \left(\frac{1}{2\tau_n} + \Gamma_2 \right) \right\} \end{aligned} \quad (5.10)$$

From the steady state solution of (5.10) we evaluate the small fluctuations of the nuclear fields around the stable states. For any unpolarized dot we find $\langle (\Delta B_N)^2 \rangle = A_k^2 N \equiv \Omega^2$, i.e. the fluctuations are not affected by ESR. If one or both of the dots are polarized, then we can express the resulting nuclear field fluctuations in the polarized dot in terms of the maximally reachable field as $\langle (\Delta B_N)^2 \rangle \approx (B_1/|B_N^{\text{max}}|)\Omega^2$, i.e. the fluctuations are suppressed by a factor $B_1/|B_N^{\text{max}}|$.

5.6.5 More detailed results

Here we will present three plots in addition to Fig. 5.4. The plots in this section are generated using the same parameters as in Fig. 5.4, but supply some extra details which were omitted from Fig. 5.4 for reasons of clarity: here we include vector field plots of the time-derivatives $\{\dot{B}_N^L, \dot{B}_N^R\}$ in the plane (B_N^L, B_N^R) . Starting from a specific nuclear field configuration (B_N^L, B_N^R) , following the arrows shows the evolution in time of the nuclear fields. We added the current through the system I_{dot} as color background, this gives a more quantitative picture of the current levels in the different stable points.

As mentioned above, the current through the double dot can be calculated from the quasi-stationary populations p_n as $I_{\text{dot}} = e\Gamma_s \sum_n |\langle S|n \rangle|^2 p_n$, and is a function of $f_{L,R}/\tilde{B}_{L,R}$ (and therefore of the nuclear polarizations in the two dots), the temperature ξ and the ratio $\Gamma_r[E_Z]/\Gamma_s$. In Fig. 5.7 we plotted I_{dot} close to the point where both dots are on resonance, i.e. where $f_L = f_R = 0$. The function has the structure of two crossing Lorentzians, with a suppression at the resonant point $f_L = f_R = 0$. In all current plots in this section, we subtracted the leakage current far away from resonance: it is a measure for the spin relaxation rate $\Gamma_r[E_Z]$.

In Fig. 5.8 we replotted Fig. 5.4a, and added $\{\dot{B}_N^L, \dot{B}_N^R\}$ as vector field and the current I_{dot} as color background. In this case $B_0 - B_{\text{res}} \sim B_1$, i.e. the detuning of B_0 and ω is relatively small. In the whole plane we distinguish four stable

points: two with low and two with high current. As can be seen from the close ups in Figs 5.8b and c, the two values of high current can differ with ca. 15 %. The asymmetry in $\tilde{B}_{L,R}$ and $N_{L,R}$ is implemented by using $\Gamma_1^L/\Gamma_1^R = 0.097$ and $\Gamma_2^L/\Gamma_2^R = 0.44$. This corresponds to a difference in a.c. magnetic fields $B_1^{L,R}$ of $\sim 50\%$ and a difference in effective numbers of nuclei of $\sim 30\%$.

In Fig. 5.9 we present the same plot as in Fig. 5.4d, again with the vector field of time evolution and the current added. Here $B_0 \approx B_{\text{res}} + 0.5 |B_N^{\text{max}}|$, i.e. the system is in the middle of the hysteresis interval and we assume a symmetric double dot, i.e. equal parameters for both dots. In the whole plane nine stable points can be distinguished. In four of those points the current through the double dot is relatively high. The unpolarized point $B_N^L = B_N^R = 0$ is so far away from the other stable states that, as soon as the system switches to the unpolarized state, it will stay there forever.

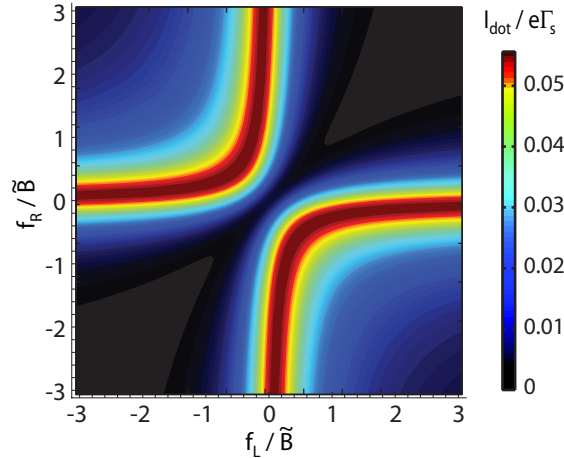


Figure 5.7: The current through the double quantum dot I_{dot} as a function of f_L and f_R . We find high current when only one of the two dots is on resonance and low current in the rest of the plane. To generate this plot we used $\xi = 5$ and $\Gamma_s = 20\Gamma_r[E_Z]$ and we subtracted the leakage current far away from both resonances.

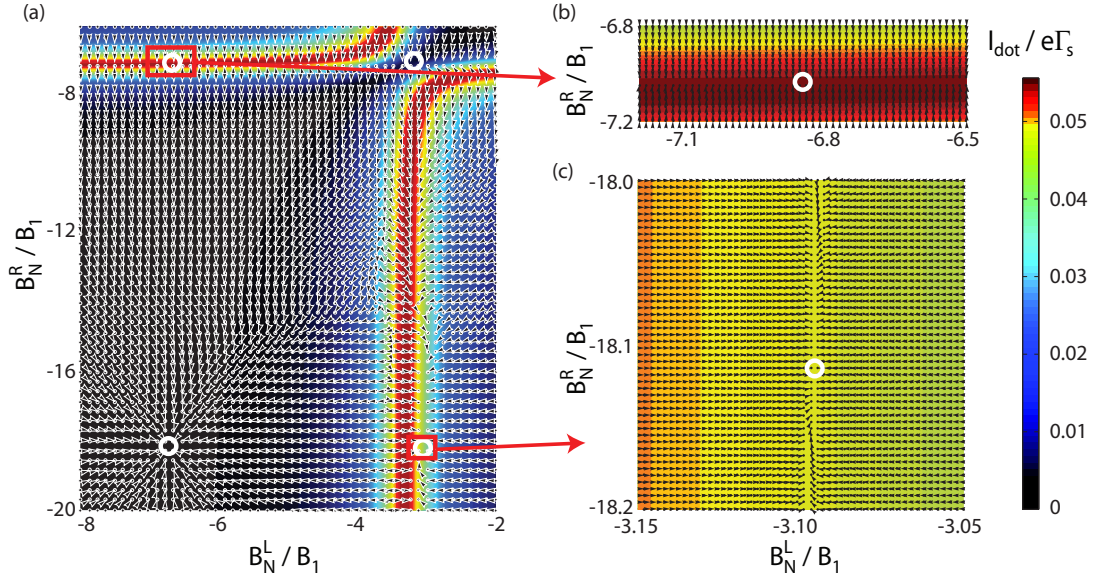


Figure 5.8: On the edge of the hysteresis interval, $B_0 - B_{\text{res}} \sim B_1$, assuming an asymmetric double dot (Fig. 5.4a). Here we add vector plots of $\{\dot{B}_N^L, \dot{B}_N^R\}$ in the plane (B_N^L, B_N^R) and the current I_{dot} as color background. The circles indicate the stable points of nuclear polarization. (a) Overview of the whole region where stable points are expected: four stable points can be distinguished. (b,c) Close ups around the two stable points with high current (corresponding respectively to points *c* and *b* in Fig. 5.4a). From the background colors we can see that the difference in current is $\sim 15\%$. To generate these plots we used for both dots $\xi\Gamma_r[E_Z]/\Gamma_s = 0.25$. In the left dot $\Gamma_1/\Gamma_2 = 3.6 \cdot 10^{-3}$, $\Gamma_2\tau_n = 9.04$, and $B_0 - \omega = 3.3 B_1^L$, and in the right dot $\Gamma_1/\Gamma_2 = 16 \cdot 10^{-3}$, $\Gamma_2\tau_n = 20.3$, and $B_0 - \omega = 7.1 B_1^R$.

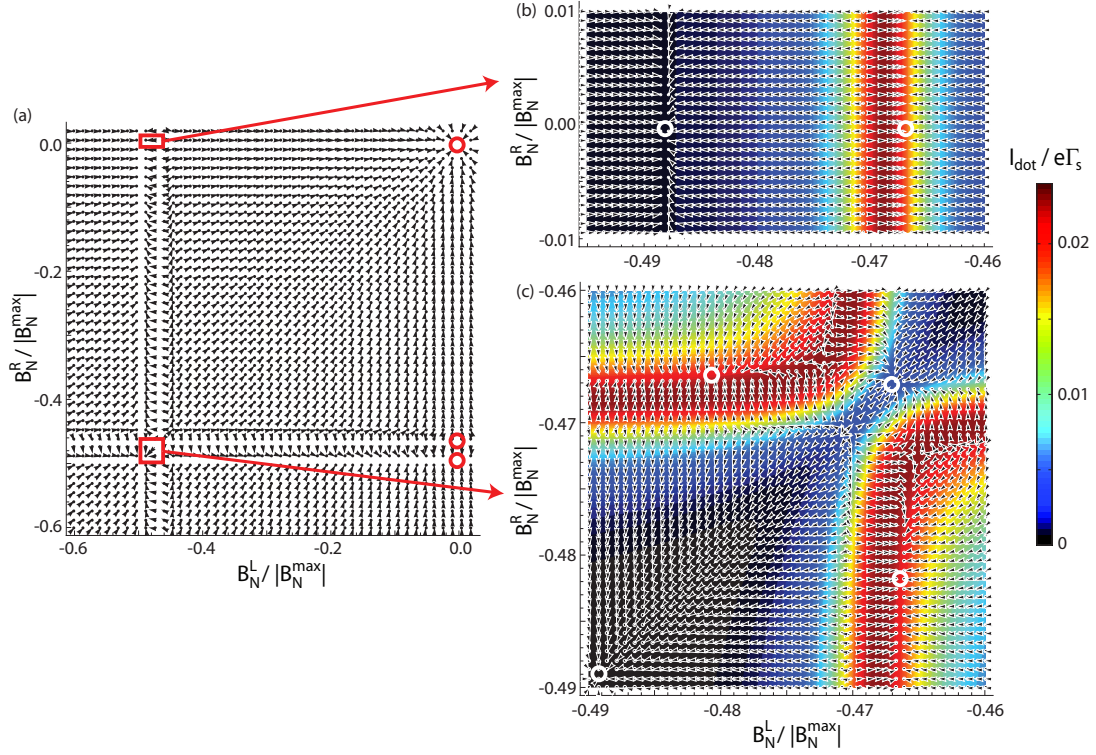


Figure 5.9: In the middle of the hysteresis interval, $B_0 \approx B_{\text{res}} + 0.5 |B_N^{\text{max}}|$, assuming a symmetric double dot (Fig. 5.4d). Again we show vector plots of $\{\dot{B}_N^L, \dot{B}_N^R\}$ in the plane (B_N^L, B_N^R) . (a) Overview of the whole plane, where the circles indicate the stable points of nuclear polarization. Owing to the double-peak structure of the pumping curve, the left(right) dot has three stable points along the line $B_N^{R(L)} = 0$, i.e. where the right(left) dot is unpolarized. (b) Close up of the region where the right dot is unpolarized and the left dot is close to resonance. One of the stable points in this region corresponds to a high current through the system, the other to low current. (c) Close up of the region where both dots are close to resonance. Four additional stable points can be distinguished, two of which correspond to low current and two to high current. To generate these plots, we used $\xi\Gamma_r[E_Z]/\Gamma_s = 0.75$, $\Gamma_1/\Gamma_2 = 21 \cdot 10^{-3}$, $\Gamma_2\tau_n = 5$, and $B_0 - \omega = 0.47 B_N^{\text{max}}$.

Chapter 6

Locking electron spins into magnetic resonance by electron-nuclear feedback

Quantum information processing requires accurate coherent control of quantum mechanical two-level systems but is hampered by their coupling to an uncontrolled environment. For electron spins in III-V quantum dots, the random environment is mostly given by the nuclear spins in the quantum dot host material; they collectively act on the electron spin through the hyperfine interaction, much like a random magnetic field. Here we show that the same hyperfine interaction can be harnessed such that partial control of the normally uncontrolled environment becomes possible. In particular, we observe that the electron spin resonance frequency remains locked to the frequency of an applied microwave magnetic field, even when the external magnetic field or the excitation frequency are changed. The nuclear field thereby adjusts itself such that the electron spin resonance condition remains satisfied. General theoretical arguments indicate that this spin resonance locking is accompanied by a significant reduction of the randomness in the nuclear field.¹

¹This chapter has been accepted for publication in Nature Physics.

6.1 Introduction

Individual electron spins in semiconductor quantum dots are attractive for applications in quantum information processing, as demonstrated by the considerable progress that has been made towards this goal [24]. Nearly all experiments in this direction have been realized in III-V materials where all isotopes carry nuclear spin. In thermodynamic equilibrium, the nuclear spins in the quantum dot host material are randomly oriented, even at dilution refrigerator temperatures and in magnetic fields of a few Tesla. An electron spin confined in the quantum dot interacts via the hyperfine coupling with $N \sim 10^6$ nuclear spins and as a result experiences a random nuclear field B_N . This random nuclear field is sampled from a distribution with a root mean square width $\propto IA/g\mu_B\sqrt{N}$, where g is the electron g -factor, μ_B the Bohr magneton, I the nuclear spin and A the hyperfine coupling constant ($IA \approx 135 \mu\text{eV}$ in GaAs). Measurements typically give a width of ~ 1 mT. As a result, we lose track of the phase of a freely evolving electron spin within a time T_2^* of a few tens of nanoseconds [77, 56, 36, 94, 78]. Similarly, when the spin evolves under an oscillating driving field, the nuclear field leads to a random offset in the resonance condition which has a comparable amplitude to presently achievable driving fields. This results in poorly controlled spin rotations [34].

It is therefore of great importance to develop the ability to control and manipulate the nuclear field with great precision. In particular, it would be highly desirable to set the nuclear field to a narrow distribution of values at the start of every experiment [95, 58, 96, 97]. This would immediately reduce the rapid dephasing, and the electron spin would lose phase coherence only from the slow subsequent evolution of the nuclear field, giving a predicted spin coherence time of $1 - 10 \mu\text{s}$ [98, 42]. Such narrowing has been achieved in an ensemble of self-assembled quantum dots by synchronizing the precessing spins with a series of laser pulses [99]. Also, the spread of the difference in nuclear fields in two neighboring quantum dots was reduced via a gate voltage controlled pumping cycle, giving a 70-fold increase in the T_2^* for states in the two-electron $m_z = 0$ subspace [69].

Here we exploit electron-nuclear feedback in order to control and manipulate the nuclear fields in two coupled quantum dots during continuous wave (CW) driving of the electron spins in the dots. We observe that each nuclear field adjusts itself such that the electron spin in the corresponding quantum dot remains in resonance with a fixed driving frequency, even when we sweep the external magnetic field away from the nominal resonance condition. Similarly, the electron spin resonance frequency remains locked to the excitation frequency when the excitation frequency is swept back and forth. These distinctive features set

our observations apart from the many previous observations of dynamic nuclear spin polarization in quantum dots, both in transport [33, 37, 100, 101, 102] and optical measurements [67, 103, 104]. We investigate the origin of this feedback by studying its dependence on the amplitudes of the applied *ac* magnetic and electric fields and on the sweep rates. Furthermore, we show theoretically that the spin resonance locking must be accompanied by a narrowing of the nuclear field distribution, in the present experiment by more than a factor of 10.

6.2 ESR detection scheme

The measurements are performed on an electrostatically defined double quantum dot tuned to the Pauli spin blockade regime [91], with effectively one excess electron on each dot (the actual electron number is small but unknown). We measure the *dc* current through the double quantum dot device, which depends on the spin states of the electrons residing on the dots. When the two electrons have parallel spins, the electron flow through the dots is blocked. When one of the spins is flipped, the spin blockade is lifted and electrons flow through the two dots until the system returns to a state with parallel spins on the two dots. As previously demonstrated [34], it is possible to flip the electron spins via magnetic resonance, by *ac* excitation of an on-chip wire which generates an oscillating magnetic field at the dots: when the excitation frequency, f , matches the electron spin resonance (ESR) frequency, $|g|\mu_B B_0/h$, a finite current flows through the device. Here h is Planck's constant, and B_0 the external magnetic field. In addition, current can flow at zero magnetic field, where the electron spins can flip-flop with the nuclear spins in the substrate [37]. We use this zero-field feature to determine and adjust for small magnetic field offsets present in our setup. The zero-field peak and the ESR response are seen in current measurements under CW excitation with increasing excitation frequency at fixed magnetic fields (Fig. 6.1a), similar to the data published in Ref. [34], and taken on the same device but in a different cooldown.

6.3 Locking to the spin resonance condition

Surprisingly, when we reverse the sweep direction, a distinctly different behavior is observed over a wide range of dot settings (see Section 6.9.1 for details of the tuning parameters). Current starts flowing when the driving frequency hits the spin resonance frequency but *remains* high even as the frequency is swept well below the nominal resonance condition (Fig. 6.1b). The fact that the current

remains high implies that the electron spin is still on resonance with the excitation frequency, and that an effective field, B_{eff} , counteracts the external magnetic field B_0 : $hf = |g|\mu_B(B_0 + B_{\text{eff}})$. From the fact that the current is strongly reduced when we simultaneously excite any of the three nuclear spin species in the substrate (data not shown), we conclude that this effective field is created by dynamical nuclear spin polarization, i.e. $B_{\text{eff}} = B_N$. This nuclear field builds up exactly at the right rate in order to keep the electron spin in resonance with the changing driving frequency, which implies there is a built-in electron-nuclear feedback mechanism.

Similar dragging of the resonance is observed when sweeping the magnetic field for a fixed excitation frequency. In Fig. 6.2a we show typical data obtained from measurements where the magnetic field is swept from -33 mT to 97 mT (right vertical axis) in about 25 seconds. We first see the zero-field peak, as expected, and next the current jumps up around $B_0 = 67$ mT, which is slightly below the nominal resonance condition ($f = 400$ MHz, $|g| = 0.36$). The current remains high as the field is swept further to 97 mT, which is well outside the ESR linewidth in the absence of feedback (see Fig. 6.4b). Similar to the case of the frequency sweeps, a nuclear field builds up exactly in such a way as to maintain the ESR frequency locked to the excitation frequency. When we subsequently

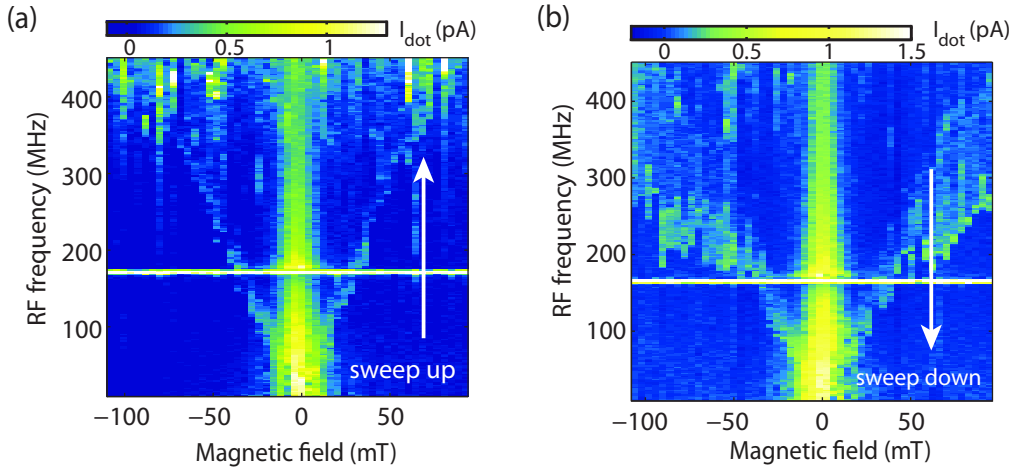


Figure 6.1: Electron spin resonance locking during frequency sweeps. (a) Current through the double dot (colorscale) subject to CW magnetic excitation, when sweeping the frequency up at fixed magnetic fields. The bright fork indicates the position of the ESR condition. (b) Similar to (a) but sweeping the frequency down. The ESR frequency remains locked to the excitation frequency when the excitation frequency is swept past the nominal resonance condition. The feature at 180 MHz is due to a resonance in the transmission line in our dilution refrigerator.

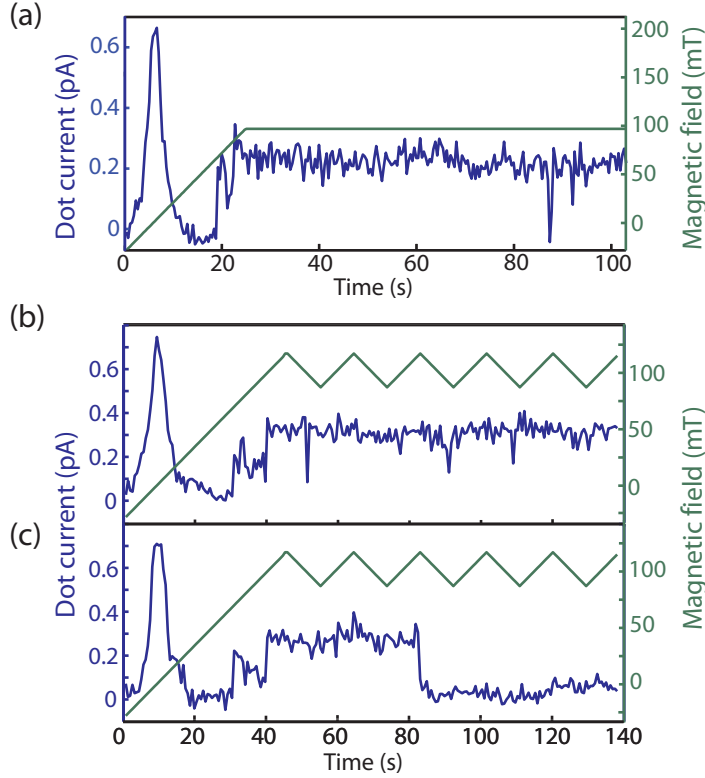


Figure 6.2: Electron spin resonance locking during magnetic field sweeps. (a) Current through the double dot as a function of time, while the magnetic field is first ramped up (right axis) and subsequently held fixed, under CW excitation ($f = 400$ MHz). (b-c) Two current traces similar to (a), but after the magnetic field is ramped up, it is repeatedly swept down and back up over a 30 mT range (right axis). After the ESR condition is first met, the electron spin remains locked into magnetic resonance for up to two minutes, even though the resonance condition is shifted back and forth.

keep the field fixed at 97 mT, we observe that the electron spin can remain locked into magnetic resonance for well over a minute.

It is even possible to drag the nuclear field back and forth under fixed-frequency excitation. In Figs. 6.2b and 6.2c, B_0 is ramped up from -33 mT to 117 mT, and is subsequently swept back and forth between 117 mT and 87 mT in a triangular pattern. The current again jumps up as we sweep through resonance and subsequently remains high independent of the sweep direction, implying that after the system is locked on resonance the sign of dB_0/dt (df/dt) does not matter as long as the condition $B_0 > B^{res} = hf/g\mu_B$ ($f < f^{res} = g\mu_B B_0/h$) remains fulfilled. In Fig. 6.2c the resonance is lost after approximately 1 minute, whereas in Fig. 6.2b the spin remains locked on resonance during the entire experiment.

6.4 Locking characteristics

These remarkable observations of spin resonance locking due to electron-nuclear feedback are characterized by a number of common features. First, the current jumps up abruptly, in many cases in less than a few 100 ms, at a field value that varies over 10-30 mT around the nominal resonance condition (see the green circles in Fig. 6.4 below). This is a further indication that the system is actively pulled into resonance – without feedback a current peak with smooth flanks and a width of a few mT is expected [105]. Second, the resonance dragging generally occurs only for fields larger than the nominal resonant field, or for frequencies lower than the nominal resonance frequency. This is opposite to the case of the usual Overhauser effect, as discussed further below. Third, the initial current jump is usually followed by a second current jump, before the current drops back to zero. A possible explanation for this double step is that the first current plateau corresponds to a situation where both dots are on-resonance, and that only one dot remains on resonance after the second jump (see Section 6.9.4 for a discussion of the current levels). When the resonance is lost in this last dot too, the current returns to zero.

This interpretation of the double current step is supported by pump-probe measurements shown in Fig. 6.3. Starting from the second current plateau with $B_0 = 80$ mT and $f = 276$ MHz, we switch off the CW excitation and probe the position of the ESR frequency as the nuclear field returns to equilibrium (we use short bursts for probing in order to minimize feedback during the probe phase). We see that the ESR frequency returns to its nominal value, slightly above 400 MHz, within 20 seconds, corresponding to the relaxation time of the local nuclear spin polarization (white dashed line). This signal must originate from a dot that is still locked into magnetic resonance at the end of the pump phase. In addition, we see a response at the nominal resonance frequency already from the start of the probe phase (red dashed line). Presumably, this signal arises from the other dot, where the resonance was lost during the pump phase and the nuclear field has (nearly) relaxed by the time the probe phase starts.

6.5 Dependence on sweep and excitation parameters

In order to better understand the locking mechanism, we study how far the nuclear spin polarization can be dragged by performing magnetic field sweeps as a function of the applied microwave power, the microwave frequency and the magnetic field

sweep rate. Specifically, we repeatedly ramp the magnetic field from -28 mT upwards and record (i) the field at which the current jumps up (circle in Fig. 6.4a), (ii) the field where the current jumps to a still higher value (diamond), and (iii) the field where the current drops back to zero (cross). The resulting data points are shown as scatter plots in Figs 6.4c-e, using the same symbols.

The first current jump always occurs as the nominal resonant field (in the absence of feedback) is first approached. The second jump and the current drop occur at fields that increase with driving amplitude over the range that we could explore (for still stronger driving, spin blockade was lifted by photon assisted tunneling so that we lost sensitivity to spin flips). For the highest powers accessible in the experiment, the electron spin is maintained on resonance over a magnetic field range of a few 100 mT. As the power is reduced, the locking effect vanishes. Furthermore, the field that can be reached before the resonance is lost, increases

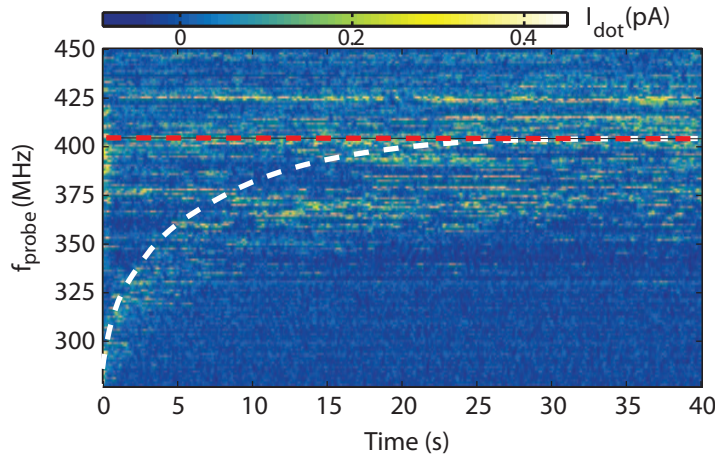


Figure 6.3: Pump-probe measurement of the relaxation of the nuclear spin polarization. At a fixed magnetic field of $B_0 = 80$ mT, we apply CW excitation ($P = -13$ dBm) sweeping the frequency from 500 MHz to 276 MHz at 43 MHz/s, and dragging the nuclear field along (pump phase). Next we turn off the CW excitation and record the current as a function of time while applying 140 ns microwave bursts every $2 \mu\text{s}$ at frequency f_{probe} (vertical axis) throughout a 40 s probe phase. As the nuclear spin polarization relaxes, the resonance condition $|g| \mu_B (B_0 + B_N(t)) = hf_{\text{probe}}$ will be fulfilled at some point in time at which the current sets on again. Varying f_{probe} reveals then the nuclear spin relaxation as indicated by the white dashed line (guide to the eye) marking the onset of the current, where the probe pulses have had the least effect on the nuclear polarization. Even though the excitation is applied only in bursts, the electron spin nevertheless remains locked into resonance in some cases, stalling the nuclear spin relaxation. The red dashed line marks an additional signal at the nominal resonance frequency already present from the start of the probe phase.

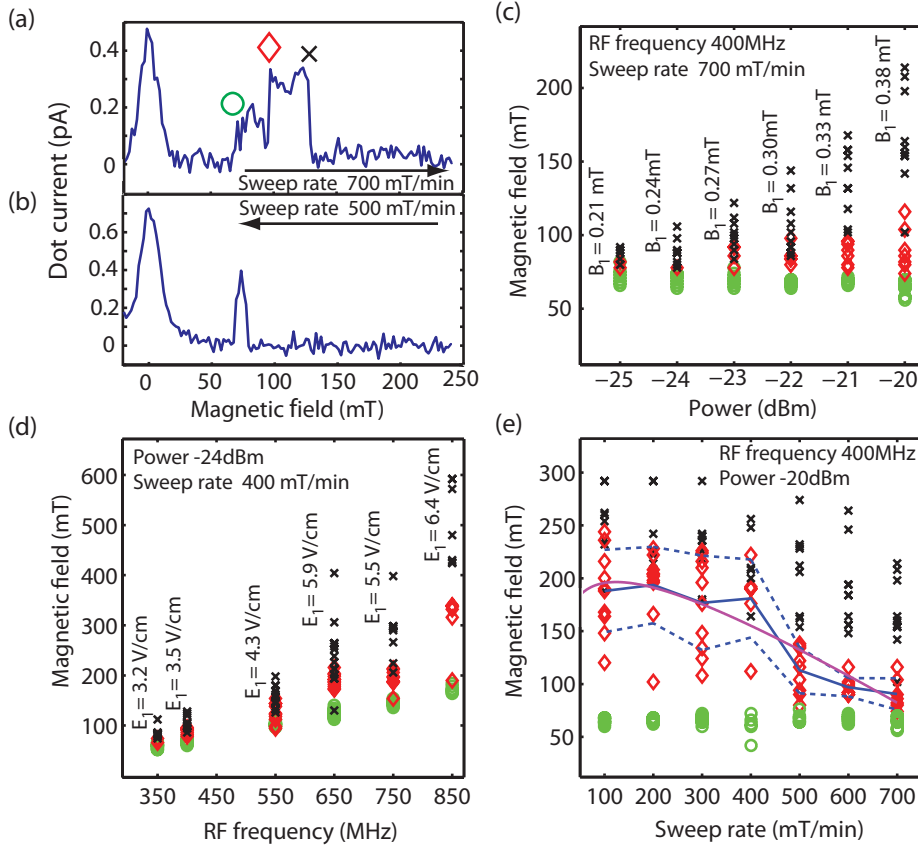


Figure 6.4: ESR locking dependence on excitation power, frequency and sweep rate. (a) Current through the double dot as the magnetic field is swept up ($f = 400$ MHz). (b) Similar to (a) but now B_0 is swept down. No dragging effects are observed; the narrow peak gives the position of the nominal resonant field. (c) Scatter plot of the switching fields as indicated by the symbols in (a) as a function of the power applied to the on-chip wire, obtained from multiple sweeps as in (a). The corresponding resonant magnetic field amplitude B_1 at the dot is given as well. (d) Scatter plot similar to (c), as a function of f . The electric field amplitude E_1 estimated from photon assisted tunneling generally increases with f , and is shown in the figure. (e) Scatter plot similar to (c) as a function of magnetic field sweep rate. Blue lines: average and standard deviation of the magnetic fields where the second current jump is observed. Purple curve: fit of these average values with a theoretical model (see Section 6.9.3). We note that there is no build-up of B_N in the limit of zero sweep rate, so the predicted switching field first increases with sweep rate, before decreasing.

with excitation frequency. Earlier measurements on the same sample showed that along with the ac magnetic field an ac electric field is generated whose amplitude for a fixed power (and magnetic field amplitude) increases roughly linearly with the excitation frequency [34]. The dependence on driving frequency can there-

fore also be interpreted as stronger locking for higher electric field amplitudes. Finally, we see that for higher magnetic field sweep rates the resonance is lost at lower fields.

6.6 A phenomenological model

A few basic considerations give insight into the mechanism behind these observations. To describe the nuclear spin dynamics we construct a phenomenological model directly from the experimental data. For clarity we discuss the nuclear spin dynamics in one of the dots; the results for two dots are qualitatively similar (see Chapter 5) and the fact that the tunnel coupling is small (smaller than the typical nuclear field in equilibrium) justifies considering the electron spins as independent. First we describe in general terms a mechanism which explains the observed locking and the dragging of the nuclear polarization, and afterwards we turn to the origin of this mechanism.

The nuclear spin polarization x in the dot is felt as an effective magnetic field by the electron spin: $IAx = g\mu_B B_N$ (x is defined as dimensionless $-1 \leq x \leq 1$; in our experiments, $|x| \ll 1$). In the absence of any excitation, the polarization naturally relaxes to zero on a characteristic time scale τ_n , due to nuclear spin diffusion. However, the nuclear spin dynamics will be altered by hyperfine-mediated electron-nuclear flip-flops when the electron spins are brought out of equilibrium [33, 37, 100]. In the spin blockade regime at finite B_0 , such non-equilibrium dynamics is induced when the electron spins are resonantly excited by an external microwave magnetic or electric field. This occurs when the nuclear polarization is close to x^{res} with $IAx^{\text{res}} = g\mu_B B_N^{\text{res}} = |g|\mu_B B_0 - hf$ such that the electron spin is in resonance with the excitation. Regardless of the relevant microscopic processes, we thus expect in very general terms a polarization-dependent pump rate Γ_p , which is non-zero only close to the resonance condition. The dynamics of the polarization in the dot is then described by

$$\frac{dx}{dt} = \Gamma_p(x - x^{\text{res}}) - \frac{1}{\tau_n}x, \quad (6.1)$$

where Γ_p peaks when its argument $(x - x^{\text{res}})$ is 0. Fig. 6.5 qualitatively visualizes Eq. (6.1) in the form of a pumping curve for three different values of x^{res} , where we have (for now arbitrarily) chosen the resonant contribution to be positive. From the figure we can see that stable points of nuclear polarization occur when dx/dt crosses zero with a negative slope: if x is higher (lower) than the stable polarization x_0 , dx/dt is negative (positive) and x gets pushed back to x_0 . Due to nuclear spin relaxation there is almost always a stable point at $x = 0$. Depending

on the particular shape of Γ_p , hence on the specific experimental regime, there can be one or more additional stable points [93] (and see Chapters 4 and 5).

We now interpret the field sweep experiments within this simple picture. First, given that the current remains high in field sweeps, a stable point must exist close to resonance, in agreement with our expectation of a resonant peak in Γ_p . Next, since dragging is generally observed only for $x > 0$, Γ_p must be positive, as in Fig. 6.5. Finally, from the maximum nuclear field B_N^{\max} that can be achieved by dragging, we can estimate the height of Γ_p : when the maximum of the pumping peak falls below zero, i.e. when nuclear spin relaxation exceeds the resonant pumping, the stable point at $x > 0$ disappears and B_N relaxes to zero (Fig. 6.5, red curve).

During actual field sweeps, the resonance is lost at fields below B_N^{\max} : since a dynamic equilibrium is reached when $dx/dt = |g|\mu_B\dot{B}_0/IA$ instead of $dx/dt = 0$, the stable operating point moves up the pumping curve (see Fig. 6.5) and disappears when the sweep rate exceeds the maximum of the pumping peak. In practice we will lose the resonance even earlier, because intrinsic nuclear field fluctuations can drive the nuclear field across the maximum. We model the average switching field taking into account such fluctuations by assuming an exponential dependence of the switching rate on the ‘barrier height’. The result is illustrated in Fig. 6.4e. This combined picture captures very well the experimental observation that for higher sweep rates the resonance is more easily lost, but not at exactly the same field every time.

We next turn to the nature of the extrinsic pumping process, Γ_p . First,

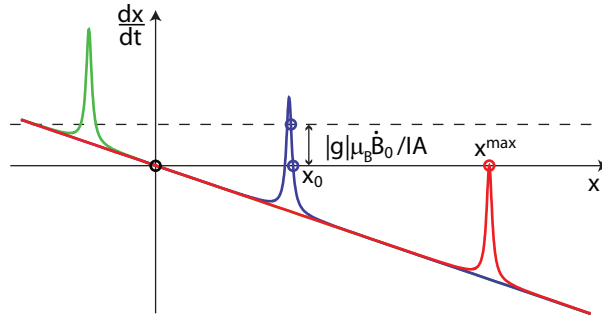


Figure 6.5: Nuclear spin pumping curves. The nuclear spin polarization rate for one dot (dx/dt) is shown as a function of its polarization x for three different values of x^{res} (the green, blue and red curve). The overall negative slope is due to nuclear spin relaxation and the resonant peak is due to the external driving. Circles indicate stable points in nuclear spin polarization and are found whenever the curve crosses the x -axis with a negative slope. During a field (or frequency) sweep, a dynamic equilibrium is reached where $dx/dt = |g|\mu_B\dot{B}_0/IA$.

the stable points in the experiment generally occur for $x > 0$, i.e. the nuclear field points against the external magnetic field. This is opposite to the usual Overhauser effect, where electron spins are excited by magnetic resonance and relax back from \downarrow to \uparrow by flip-flopping with the nuclear spins, thereby creating a nuclear polarization in the direction of the electron spin excited state. The observed ‘reverse’ pumping is possible when there is an excess of \uparrow electrons, which are excited to \downarrow by resonant electric fields, whereby the nuclear spins absorb the angular momentum [93, 59]. Spin relaxation in general creates an excess of \uparrow electrons, which favors reverse pumping. In our experiment, we believe the dominating electron spin relaxation process to be spin-exchange with the leads due to photon assisted tunneling (estimated to be 10 – 100 kHz). Second, the locking effect gets stronger, hence Γ_p becomes larger, not only with stronger driving in general (Fig. 6.4c), but also with stronger electric excitation by itself (higher f , Fig. 6.4d). Based on these observations, we suggest that electric-field assisted electron-nuclear flip-flops combined with electron spin relaxation are mainly responsible for the resonant pumping (see Chapter 5).

6.7 Implications for electron spin dephasing

Finally, we analyze theoretically the implications of our observations for the width of the nuclear field distribution. We define $\Gamma_{\pm}(x)$ as the total positive and negative nuclear spin flip rates that result from the intrinsic relaxation and resonant response combined, so $dx/dt = \frac{2}{N}(\Gamma_+ - \Gamma_-)$, where N denotes the total number of nuclei. We also define $\gamma(x)$ as the total rate of nuclear spin flips, $\gamma = \frac{2}{N}(\Gamma_+ + \Gamma_-)$. Using the fact that the pumping curve exhibits a resonant peak at $|x_0| \ll 1$, we can then approximate the variance of the nuclear polarization distribution around x_0 as (see Section 6.9.2)

$$\sigma^2 \approx \frac{1}{N} \frac{\gamma(x_0)}{\left(-\frac{\partial}{\partial x} \frac{dx}{dt}\right) \Big|_{x_0}}. \quad (6.2)$$

The numerator is the local diffusion rate, and the denominator is the restoring force – the steeper the slope of dx/dt , the stronger the restoring force. When labeling the number of nuclei with spin up (down) by $N_{+(-)}$ we get for the case without pumping $\Gamma_{\pm} = N_{\mp}/2\tau_n$, so Eq. 6.2 gives us the usual result $\sigma^2 = 1/N$. (Note that we assume here for simplicity nuclear spin $I = 1/2$. For higher values of spin, e.g. $I = 3/2$ as in GaAs, the results do not change qualitatively.) For a stable point $x_0 > 0$ near resonance, we take as a rough estimate for the local slope the maximum of Γ_p divided by its width. This gives $\sigma^2 \approx B_1/NB_N^{\max}$ (see Section 6.9.2). Since B_N^{\max} was several 100 mT with $B_1 < 1$ mT, these arguments

imply that the nuclear field distribution was narrowed by more than a factor of 10. Future experiments will aim at a quantitative study of the impact of this narrowing on the electron spin dephasing time via Ramsey-style experiments.

Narrowing of the nuclear field distribution would greatly enhance our level of control of the electron spin dynamics. Furthermore, the observed locking effect allows us to accurately set the spin resonance frequency of an electron in a quantum dot to a value determined only by the externally controlled excitation frequency. Finally, our measurements suggest that we can selectively control the ESR frequency in one of the dots, which could be exploited for independent addressing of electron spins in quantum dots that are less than 100 nm apart.

6.8 Acknowledgments

We thank F. R. Braakman, P. C. de Groot, R. Hanson, M. Laforest, L. R. Schreiber, G. A. Steele and S.-C. Wang for help and discussions, and R. Schouten, A. van der Enden, R. G. Roeleveld and P. van Oossanen for technical support. This work is supported by the ‘Stichting voor Fundamenteel Onderzoek der Materie’ and the ‘Nederlandse Organisatie voor Wetenschappelijk Onderzoek’.

6.9 Appendix

6.9.1 Tuning the double dot

The conditions for observing a pronounced electron-nuclear feedback are as follows. Qualitatively, the interdot tunnel coupling and the tunnel coupling to the outgoing lead are increased compared to the regime of Ref. [34]. Furthermore, the potentials of the double dot are tuned such that the interdot transition occurs without energy loss: at low power, the configuration of the dot potentials is such that electrons can tunnel elastically from the left to the right dot when spin blockade is lifted. Thereby, the interdot transition is made from the $(1, 1)$ singlet to the $(0, 2)$ singlet, where (m, n) represent the effective electron numbers on the two dots. This working point cannot be used at strong driving, since the electric field component of the excitation causes photon assisted tunneling to the $(0, 2)$ triplet, thereby lifting spin blockade irrespective of the spin states of the two electrons. Instead, the double dot must be tuned such that the $(0, 2)$ singlet electrochemical potential is higher than that of the $(1, 1)$ singlet. This is nominally in the Coulomb blockade regime, but photon-assisted tunneling now provides the missing energy in order to make the transition from the $(1, 1)$ to the $(0, 2)$ singlet.

6.9.2 Suppression of fluctuations

In this section we derive an estimate for the typical magnitude of nuclear field fluctuations around a stable point close to resonance. For the sake of argument we show here the derivation for a *single* quantum dot, although a similar argument holds for a double dot setup and the results are qualitatively similar as well. In the double dot case, a *two dimensional* Fokker-Planck equation must be considered, where stable points correspond to zeros of $\{\partial_t x_1, \partial_t x_2\}$ in the plane (x_1, x_2) .

We consider all possible configurations of the nuclear spin system in the dot as discrete points, labeled n , defining $n \equiv \frac{1}{2}(N_+ - N_-)$, where $N_{+(-)}$ denotes the number of nuclei with spin up(down).² This results in $N \equiv N_+ + N_-$ possible values for n , ranging from $-N/2$ to $N/2$. To investigate the stochastic properties we derive a Fokker-Planck equation for the probability distribution function $\mathcal{P}(n)$, starting from a simple master equation

$$\frac{\partial \mathcal{P}(n)}{\partial t} = -\mathcal{P}(n)[\Gamma_+(n) + \Gamma_-(n)] + \mathcal{P}(n-1)\Gamma_+(n-1) + \mathcal{P}(n+1)\Gamma_-(n+1). \quad (6.3)$$

In this equation $\mathcal{P}(n)$ gives the chance of finding the system in state n , and $\Gamma_{\pm}(n)$ is the rate at which the spin bath flips from the configuration n to $n \pm 1$. We go over to the continuous limit, justified by the large number of nuclei $N \sim 10^6$ [75], and expand all functions around n up to second order. We find

$$\frac{\partial \mathcal{P}}{\partial t} = \frac{\partial}{\partial n} \left\{ (\Gamma_- - \Gamma_+) \mathcal{P} + \frac{1}{2} \frac{\partial}{\partial n} (\Gamma_- + \Gamma_+) \mathcal{P} \right\}, \quad (6.4)$$

a Fokker-Planck equation where all rates Γ_{\pm} are still functions of n . Due to the large number of nuclei, the spin flip rates Γ_{\pm} do not change on their full scale when increasing n by only ± 1 (the features of Γ_{\pm} occur on the scale of the width of the resonance ~ 1 mT, whereas changing n by ± 1 corresponds to $IA/N \sim 5$ μ T). This implies that $|\partial_n \Gamma_{\pm}| \ll \Gamma_{\pm}$, which allows us to neglect one of the cross terms resulting from the last term in (6.4).

In the resulting continuity equation, the right-hand side corresponds to the derivative of a probability flux. In equilibrium this probability flux must vanish, which enables us to write down a general equilibrium solution of (6.4). In terms of the bath polarization $x \equiv 2n/N$ this solution reads

$$\mathcal{P}(x) = \exp \left\{ \int^x N \frac{\Gamma_+ - \Gamma_-}{\Gamma_+ + \Gamma_-} dx' \right\}. \quad (6.5)$$

²We assume here for simplicity nuclear spin $I = 1/2$. For higher values of spin, e.g. $I = 3/2$ as in GaAs, the results do not change qualitatively.

Maxima and minima of this distribution are found at the zeros of the derivative of the exponent. Suppose the point x_0 is one of these solutions corresponding to a maximum of $\mathcal{P}(x)$ (i.e. the second derivative in the point x_0 is negative). We then expand the exponent of $\mathcal{P}(x)$ up to second order around the maximum, giving a Gaussian approximation for $\mathcal{P}(x)$,

$$\begin{aligned} \mathcal{P}(x) &\approx \exp \left\{ \int^{x_0} N \frac{\Gamma_+ - \Gamma_-}{\Gamma_+ + \Gamma_-} dx' + \frac{N}{2} \frac{\partial}{\partial x} \frac{\Gamma_+ - \Gamma_-}{\Gamma_+ + \Gamma_-} \Big|_{x_0} (x - x_0)^2 \right\} \\ &= \mathcal{P}(x_0) \exp \left\{ - \frac{(x - x_0)^2}{2\sigma^2} \right\}, \end{aligned} \quad (6.6)$$

where σ gives the width of the distribution. So we find that

$$\sigma^2 = \frac{1}{N} \left(- \frac{\partial}{\partial x} \frac{\Gamma_+ - \Gamma_-}{\Gamma_+ + \Gamma_-} \Big|_{x_0} \right)^{-1} = \frac{1}{N} \frac{\Gamma_+ + \Gamma_-}{\frac{\partial}{\partial x} (\Gamma_- - \Gamma_+) \Big|_{x_0}}, \quad (6.7)$$

where we used that $(\Gamma_+ - \Gamma_-)|_{x_0} = 0$. We now only still want to translate this expression in terms of the ‘pumping curve’. We use the relation $dx/dt = (2/N)(\Gamma_+ - \Gamma_-)$ and define $\gamma(x) = (2/N)(\Gamma_+ + \Gamma_-)$. In the limit of small polarizations, i.e. $|x| \ll 1$, we can write

$$\frac{dx}{dt} = L(x) - \gamma(x)x. \quad (6.8)$$

In this notation the effect of Γ_p is separated into two parts: (i) a polarization-dependent net spin pumping contribution, $L(x)$, and (ii) a polarization-dependent contribution to the relaxation, which together with the intrinsic relaxation rate $1/\tau_n$ is written as $\gamma(x)$. One can rewrite equation (6.7) in terms of dx/dt and $\gamma(x)$ using the relations given above. This gives us finally the expression

$$\sigma^2 \approx \frac{1}{N} \frac{\gamma(x_0)}{\left(- \frac{\partial}{\partial x} \frac{dx}{dt} \right) \Big|_{x_0}}. \quad (6.9)$$

To get an idea of the magnitude of this variance, we approximate the derivative of the pumping curve at the stable point as roughly the height of $L(x)$ over the width (see Fig. 6.4), i.e. $-\partial_x(dx/dt)|_{x_0} \approx L^{\max}/\tilde{x}$, where \tilde{x} is the width of $L(x)$. From equation (6.8) we see that we can write for the absolute maximum of achievable polarization $x^{\max} = L^{\max}/\gamma(x^{\max})$. Combining these two expressions and using that $\gamma(x^{\max}) \sim \gamma(x_0)$, we find the order of magnitude of the variance σ^2 to be

$$\sigma^2 \sim \frac{1}{N} \frac{\tilde{x}}{x^{\max}}. \quad (6.10)$$

In terms of the effective nuclear field B_N , this variance reads

$$\sigma_{B_N}^2 \sim \Omega^2 \frac{B_1}{|B_N^{\max}|}, \quad (6.11)$$

where $\Omega \equiv IA/g\mu_B\sqrt{N}$ are the diffusive fluctuations around the unpolarized state, and B_1 is the scale of the width of the pumping term L , in our case given by the strength of the microwave driving field.

6.9.3 Statistics of switching

Here we explain how we calculated the purple curve in Fig. 6.4e. We suggest that the second current jump (red diamonds in the Figure) corresponds to the resonance being lost in one of the two dots. This occurs when the effective barrier between the polarized and unpolarized states becomes small enough for a typical nuclear field fluctuation to overcome. If we assume a simple linear decrease of this effective barrier for increasing B_N and include the effect of the finite sweep rate \dot{B}_0 , we find the polarization-dependent switching rate

$$\Gamma_{\text{sw}}(B_N) = \Gamma_0 \exp \left\{ \gamma \left(\frac{B_N}{B_N^{\max}} + \frac{\dot{B}_0}{\dot{B}_0^{\max}} \right) \right\}, \quad (6.12)$$

where \dot{B}_0^{\max} is the maximal sweep rate to observe any locking at all. From this expression we can derive the standard deviation in B_N where the second jump is observed, σ_{sw} , and the average switching field $\langle B_N^{\text{sw}} \rangle$. Explicitly, we find

$$\sigma_{\text{sw}} = \frac{B_N^{\max}}{\gamma} \quad \text{and} \quad \langle B_N^{\text{sw}} \rangle = \sigma_{\text{sw}} \ln \frac{\dot{B}_0^{\max}}{\sigma_{\text{sw}} \Gamma_0} + \sigma_{\text{sw}} \ln \frac{\dot{B}_0}{\dot{B}_0^{\max}} - B_N^{\max} \frac{\dot{B}_0}{\dot{B}_0^{\max}}. \quad (6.13)$$

We analyzed the set of red diamonds in Fig. 6.4e. From (6.13) we expect σ_{sw} to be constant in first approximation, which is indeed observed for lower sweep rates (100-400 mT/min). The decrease of σ_{sw} for sweep rates above 400 mT/min could be a consequence of the average switching field lying too close to the resonance condition. Therefore we averaged the standard deviation over the first four values to find $\sigma_{\text{sw}} = 39$ mT. Using this value for the standard deviation, we fitted equation (6.13) to the data in Fig. 6.4e. This resulted in the fitting parameters $B_N^{\max} = 289.6$ mT, $\dot{B}_0^{\max} = 920.7$ mT/min and $\gamma = 6.946 \cdot 10^{-4} \text{ s}^{-1}$, giving a sample correlation coefficient of $R = 0.948$. The resulting fitting curve is plotted in purple in Fig. 6.4e. Another way to estimate B_N^{\max} and \dot{B}_0^{\max} is to extrapolate the set of red diamonds in Fig. 6.4e to the two axes. In this way one finds the estimates $B_N^{\max} \approx 300$ mT and $\dot{B}_0^{\max} \approx 900$ mT/min, both in reasonable agreement with the results of the fit.

6.9.4 Analysis of ESR current levels

Next to the *position* of the current jumps, we also analyzed the *height* of the current plateaus between the jumps as function of driving amplitude. For different microwave powers we repeatedly swept the external magnetic field from low to high with a sweep speed of $\dot{B}_0 = 400$ mT/min, keeping the driving frequency fixed at $f = 400$ MHz. For each trace we averaged the current of the first plateau and the current of the second plateau, and we determined the height of the zero-field peak. The result is plotted in Figure 6.6 as a scatter plot for the different microwave powers. We clearly observe that in all traces the highest current was measured in the zero-field peak, and that the second plateau exhibited higher current than the first. As to the dependence of the current levels on driving power, we see that (i) the height of the zero-field peak tends to decrease with increasing excitation power and (ii) the height of the ESR current plateaus seems nearly constant. As we attribute the observed double step feature to dragging of the nuclear field, first in two and then only in one dot, we here give some general considerations concerning the current levels during resonant electron transport in double quantum dot ESR experiments.

Let us first consider the limit of strong microwave driving with a saturated ESR, i.e. $g\mu_B B_1/h$ much larger than all relaxation and decay rates. If *both* dots are exactly on resonance, the driving causes the electrons to evolve entirely within the triplet subspace [34], i.e. in the cycle $|T_+\rangle \rightarrow \frac{1}{2} \{|T_+\rangle + \sqrt{2}|T_0\rangle + |T_-\rangle\} \rightarrow |T_-\rangle \rightarrow \frac{1}{2} \{|T_+\rangle - \sqrt{2}|T_0\rangle + |T_-\rangle\} \rightarrow |T_+\rangle$. As all three (1, 1) triplet states are Pauli spin blockaded, current can only flow to the extent there is relaxation from the triplets to the singlet. If only *one* of the two dots is on resonance, the system will evolve due to driving in the cycle $|T_\pm\rangle \rightarrow \frac{1}{\sqrt{2}} \{|T_0\rangle \pm |S\rangle\} \rightarrow |T_\pm\rangle$, where in the course of every cycle the state $\frac{1}{\sqrt{2}} \{|T_0\rangle \pm |S\rangle\}$ can decay via the (0, 2) singlet to the outgoing lead, giving rise to a current. Therefore, we expect in this limit of strong driving to observe the highest current when only one dot is on resonance. Since the resonance is saturated in the strong driving regime, we expect to first approximation no dependence of the current on microwave power.

In the limit of very weak driving, with $g\mu_B B_1/h$ much smaller than the relevant rates, one would expect quite the opposite. In this case the system spends most time in a Pauli spin blockaded state. The blockade can be lifted by spin relaxation in one of the two dots or by a spin flip in either of the dots caused by the driving field B_1 . In this limit we therefore expect increasing current with increasing driving power, and furthermore that current will be highest when both dots are on resonance, simply because more spin flips take place.

During a field or frequency sweep, it is in principle possible that a nuclear

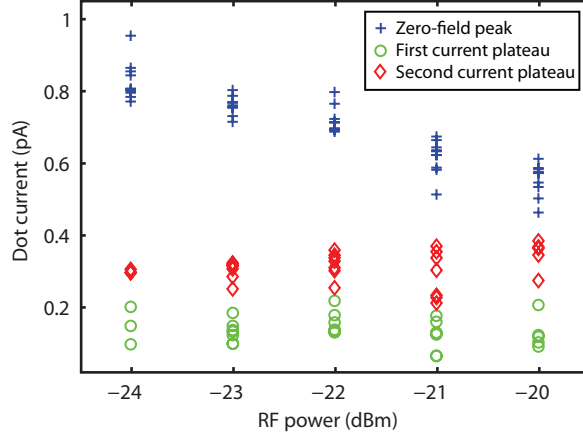


Figure 6.6: Current levels of the zero-field peak and the two plateaus. An offset is subtracted from all current levels given by the average current between the tail of zero-field peak and the ESR resonance. The height of the zero-field peak is determined by averaging 3 points around the position of its maximum, which is determined by first averaging 10 consecutive measurements and determining the maximum current in the averaged trace. The current levels of the first plateau are obtained by averaging individual traces between the magnetic field values where the first step occurs (indicated by green circles in Fig. 6.4a) and the field where the second step occurs or the field value where the current drops to zero, if that occurs before the second step (red diamonds and black crosses in Fig. 6.4a). We require these magnetic field intervals to be longer than 10 measurement points (corresponding to 20 mT) in order not to be omitted. The height of the second plateau is determined in a similar way but now by averaging between the magnetic field values where the second step occurs and the field where the current drops to zero. The resulting heights of the zero-field peak, first and second current plateaus are represented here by respectively blue crosses, green circles and red diamonds for different excitation powers.

field builds up in only one dot when the nominal ESR condition is first reached, subsequently locking the dot to the ESR condition. However, it is very unlikely that a nuclear field would build up in the other dot at a later time, when the ESR frequency in that dot is very far away from the driving frequency. A much more likely scenario is that a nuclear field builds up in both dots when the ESR condition is first reached (first plateau, low current), and that at the second current jump, the polarization in one dot relaxes to zero and only the other dot polarizes further (second plateau, high current). This would suggest that our experiments were performed in the regime of strong driving.

However, there is an issue which does not fit in this simple picture. The decrease of the zero-field peak height for increasing power suggests that the electric field component of the excitation smears out the current peak in gate voltage

space due to photon-assisted tunneling (at high frequencies, discrete sidebands are visible, at low frequencies, the sidebands overlap). This could account for the decrease of the zero-field current, but should presumably affect the ESR current levels in the same way since the ESR transition is saturated at strong driving. However, experimentally, the current levels at the two ESR plateaus are roughly independent of power, rather than decreasing with power. This point remains at present unresolved.

In order to develop a coherent picture of electron transport at zero-field and at spin resonance, a more systematic and detailed study of the dependence of the current levels on driving power and on the tuning of the double dot (tunnel coupling, detuning) is needed. This is quite involved, since the behavior of even the zero-field peak varies widely with tuning parameters.

6.9.5 Pump-probe measurements

Fig. 6.7 shows the full dataset for the pump-probe measurements presented in Fig. 6.3, now including the pump phase ($t < 0$). The pump-phase data and accompanying discussion was left out from Fig. 6.3 for brevity. We note that the signal in the pump phase is much stronger than the signal in the probe phase, since during the pump phase a strong (-13 dBm) continuous microwave excitation is applied, whereas during the probe phase, the excitation is applied only in bursts with a duty cycle of less than 10%. Even though the excitation is applied only in bursts, the electron spin sometimes remains locked into resonance during the probe phase as well, stalling the nuclear spin relaxation.

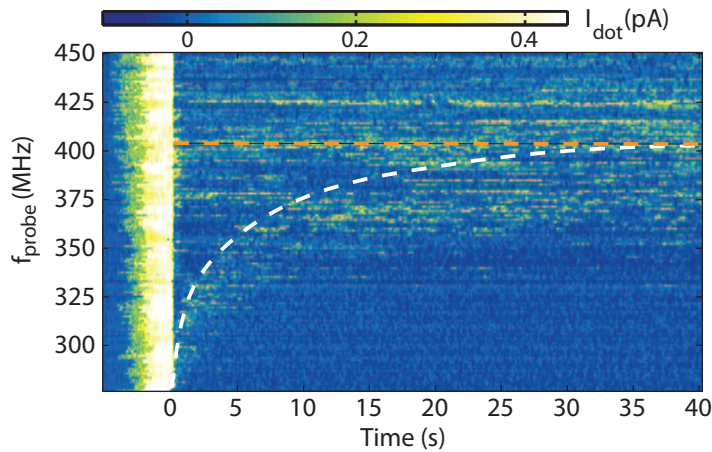


Figure 6.7: Pump-probe measurement of the relaxation of the nuclear spin polarization. At a fixed magnetic field of $B_0 = 80$ mT, we apply CW excitation ($P = -13$ dBm) sweeping the frequency from 500 MHz to 276 MHz at 43 MHz/s, and dragging the nuclear field along (pump phase). Next we turn off the CW excitation and apply 140 ns microwave bursts every $2 \mu\text{s}$ at frequency f_{probe} throughout a 40 s probe phase. This pump-probe cycle is repeated for different probe frequencies, $277 \text{ MHz} \leq f_{\text{probe}} \leq 450 \text{ MHz}$ (see vertical axis). The horizontal axis indicates the time t into the probe phase; the data for $t < 0$ correspond to the pump phase. In the pump phase, the current (plotted in colorscale) jumps up twice, reaching the highest current plateau (traces where the resonance is lost by the end of the pump phase are left out). When the frequency is switched to f_{probe} at $t = 0$, the current drops to zero since the excitation is now off-resonance. As the nuclear spin polarization relaxes, the resonance condition $|g| \mu_B (B_0 + B_N(t)) = hf_{\text{probe}}$ will be fulfilled at some point in time at which the current sets on again. Varying f_{probe} reveals then the nuclear spin relaxation as indicated by the white dashed line (guide to the eye) marking the onset of the current, where the probe pulses have had the least effect on the nuclear polarization. The orange dashed line marks an additional signal at the nominal resonance frequency already present from the start of the probe phase.

Chapter 7

Pauli spin blockade in the presence of strong spin-orbit coupling

We study electron transport in a double quantum dot in the Pauli spin blockade regime, in the presence of strong spin-orbit coupling. The effect of spin-orbit coupling is incorporated into a modified interdot tunnel coupling. We elucidate the role of the external magnetic field, the nuclear fields in the dots, and spin relaxation. We find qualitative agreement with experimental observations, and we propose a way to extend the range of magnetic fields in which blockade can be observed.¹

¹This chapter has been published in Physical Review B **80**, 041301(R) (2009).

7.1 Introduction

Blockade phenomena, whereby strong interactions between single particles affect the global transport or excitation properties of a system, are widely used to control and detect quantum states of single particles. In single electron transistors, the electrostatic interaction between electrons can block the current flow [106], thereby enabling precise control over the number of charges on the transistor [107]. In semiconductor quantum dots, the Pauli exclusion principle can lead to a spin-selective blockade [91], which has proven to be a powerful tool for read-out of the spin degree of freedom of single electrons [34, 35, 36, 37, 38].

In this spin blockade regime, a double quantum dot is tuned such that current involves the transport cycle $(0, 1) \rightarrow (1, 1) \rightarrow (0, 2) \rightarrow (0, 1)$, (n, m) denoting a charge state with $n(m)$ excess electrons in the left(right) dot (see Fig. 7.1(a)). Since the only accessible $(0, 2)$ state is a spin singlet, the current is blocked as soon as the system enters a $(1, 1)$ triplet state (Fig. 7.1(b)): transport is then due to spin relaxation processes, possibly including interaction with the nuclear fields [80]. This blockade has been used in GaAs quantum dots to detect coherent rotations of single electron spins [34, 35], coherent rotations of two-electron spin

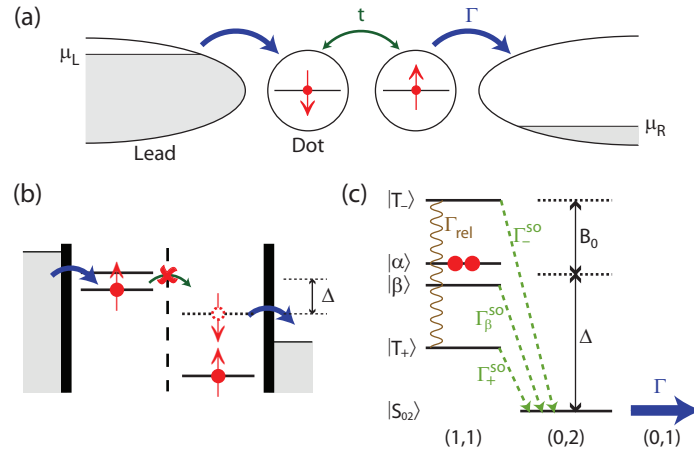


Figure 7.1: Double quantum dot in the Pauli spin blockade regime. (a) The double dot is coupled to two leads. Due to a voltage bias, electrons can only run from the left to the right lead. (b) Energy diagram assuming *spin-conserving* interdot coupling. The only accessible $(0, 2)$ state is a spin singlet: all $(1, 1)$ triplet states are not coupled to the $(0, 2)$ state and the current is blocked. (c) Energy levels and transition rates assuming *non-spin-conserving* interdot coupling. We consider the ‘high’-field limit and neglect the effects of the nuclear fields. Then three of the four $(1, 1)$ states can decay, leaving only one spin-blockaded state $|\alpha\rangle$. Isotropic spin relaxation $\sim \Gamma_{\text{rel}}$ causes transitions between all $(1, 1)$ states.

states [36], and mixing of two-electron spin states due to hyperfine interaction with nuclear spins [38, 37].

Motivated by a possibly large increase of efficiency of magnetic and electric control over the spin states [108, 109], also quantum dots in host materials with a relatively large g -factor and strong spin-orbit interaction are being investigated. Very recently, Pauli spin blockade has been demonstrated in a double quantum dot defined by top gates along an InAs nanowire [110, 111]. However, as compared to GaAs, spin blockade in InAs nanowire quantum dots seems to be destroyed by the strong spin-orbit coupling: significant spin blockade has been only observed at very small external magnetic fields ($\lesssim 10$ mT [110]). An important question is whether there exists a way to extend this interval of magnetic fields. To answer that question, one first has to understand the physical mechanism behind the lifting of the blockade.

In this Chapter we study Pauli spin blockade in the presence of strong spin-orbit mixing. We show that the only way spin-orbit coupling interferes with electron transport through a double dot is by introducing non-spin-conserving tunneling elements between the dots. This yields coupling of the $(1, 1)$ triplet states to the outgoing $(0, 2)$ singlet, thereby lifting the spin blockade. However, for sufficiently small external magnetic fields this does not happen. If the $(1, 1)$ states are not split apart by a large Zeeman energy, they will rearrange to one coupled, decaying state and three blocked states. When the external field B_0 is increased, it couples the blocked states to the decaying state. As soon as this field induced decay grows larger than the other escape rates (i.e. $B_0^2\Gamma/t^2 > \Gamma_{\text{rel}}$, where Γ is the decay rate of the $(0, 2)$ singlet, t the strength of the tunnel coupling, and Γ_{rel} the spin relaxation rate²) the blockade is lifted. Therefore, the current exhibits a dip at small fields.

The presence of two random nuclear fields in the dots (of typical magnitude $K \sim 1$ mT) complicates matters since it adds another dimension to the parameter space. We distinguish two cases: if the nuclear fields are small compared to t^2/Γ , they just provide an alternative way to escape spin blockade, which may compete with spin relaxation. There is still a dip at small magnetic fields, and the current and width of the dip are determined by the maximum of Γ_{rel} and $K^2\Gamma/t^2$. In the second case, $K \gg t^2/\Gamma$, the current may exhibit either a peak or a dip, depending on the strength and orientation of the spin-orbit mixing. If there is a peak in this regime, the cross-over from dip to peak takes place at $K \sim t^2/\Gamma$.

²Throughout this Chapter we present energies and magnetic fields in terms of frequencies. This corresponds to setting $\hbar = g\mu_B = 1$.

7.2 Model and approach

Let us now turn to our model. We describe the relative detuning of the $(1, 1)$ states and the $(0, 2)$ states by the Hamiltonian $\hat{H}_e = -\Delta |S_{02}\rangle \langle S_{02}|$, where $|S_{02}\rangle$ denotes the $(0, 2)$ spin singlet state. The energies of the four $(1, 1)$ states are further split by the magnetic fields acting on the electron spins, $\hat{H}_m = B_0(\hat{S}_L^z + \hat{S}_R^z) + \vec{K}_L \cdot \hat{\vec{S}}_L + \vec{K}_R \cdot \hat{\vec{S}}_R$, where $\hat{\vec{S}}_{L(R)}$ is the electron spin operator in the left(right) dot (for InAs nanostructures $g \sim 7$ [112]). We chose the z -axis along \vec{B}_0 , and included two randomly oriented effective nuclear fields $\vec{K}_{L,R}$ resulting from the hyperfine coupling of the electron spin in each dot to N nuclear spins (in InAs quantum dots $N \sim 10^5$ (see Ref. [112]), yielding a typical magnitude $K \propto 1/\sqrt{N} \sim 0.6 \mu\text{eV}$). We treat the nuclear fields classically, disregarding feedback of the electron spin dynamics which could lead to dynamical nuclear spin polarization (see also Chapter 5).

Let us now analyze the possible effects of spin-orbit coupling. (i) It can mix up the spin and orbital structure of the electron states. The resulting states will remain Kramers doublets, thus giving no qualitative difference with respect to the common spin up and down doublets. (ii) The mixing also renormalizes the g -factor that defines the splitting of the doublets in a magnetic field. This, however, is not seen provided we measure B_0 in units of energy. (iii) The coupling also can facilitate spin relaxation [47], but this is no qualitative change either. Some of these aspects have been investigated in [113, 114].

The only place where strong spin-orbit interaction leads to a qualitative change, is in the coupling between the dots. (i) The interdot tunnel coupling provides a finite overlap of states *differing* in index of the Kramers doublet (in further discussion we refer to this index as to ‘spin’), effectively introducing non-‘spin’-conserving tunneling elements. (ii) The mutual Coulomb interaction between electrons in different dots introduces an effective spin-spin coupling scaling with B_0^2 (see Ref. [108, 115]). Both these mechanisms influence the electron spin dynamics in the system and could be responsible for lifting of the spin blockade. However, when all energy scales investigated are much smaller than the typical orbital energy splitting E_{orb} in the dots, the effect of the tunnel coupling dominates that of the Coulomb interaction [108, 115]. Since most lifting effects were observed at $B_0 \sim 10 \text{ mT} \ll E_{\text{orb}}$, we are working in this regime and therefore focus on the spin-orbit modified tunnel coupling.

The most general non-spin-conserving tunneling Hamiltonian for two doublet electrons in a left and right state reads $\hat{H}_t = \sum_{\alpha,\beta} \left\{ t_{\alpha\beta}^L \hat{a}_{L\alpha}^\dagger \hat{a}_{R\beta} + t_{\alpha\beta}^R \hat{a}_{R\alpha}^\dagger \hat{a}_{L\beta} \right\}$, α, β being the spin indices, $\hat{a}_{L(R)}^\dagger$ and $\hat{a}_{L(R)}$ the electron creation and annihilation oper-

ators in the left(right) state, and $t^{L,R}$ coupling matrices. We impose conditions of hermiticity and time-reversibility on \hat{H}_t and concentrate on the matrix elements between the (1, 1) states and $|S_{02}\rangle$ in our double dot setup. In the convenient basis of orthonormal unpolarized triplet states $|T_{x,y}\rangle \equiv i^{1/2\mp 1/2}\{|T_{-}\rangle \mp |T_{+}\rangle\}/\sqrt{2}$, $|T_z\rangle \equiv |T_0\rangle$, and the (1, 1) singlet $|S\rangle$, this Hamiltonian reads

$$\hat{H}_t = i\vec{t} \cdot |\vec{T}\rangle \langle S_{02}| + t_0 |S\rangle \langle S_{02}| + \text{h.c.}, \quad (7.1)$$

with $|\vec{T}\rangle \equiv \{|T_x\rangle, |T_y\rangle, |T_z\rangle\}$. The model therefore adds a 3-vector of new coupling parameters, $\vec{t} = \{t_x, t_y, t_z\}$, to the usual spin-conserving t_0 , the vector being a ‘real’ vector with respect to coordinate transformations. The degree of spin state mixing by spin-orbit interaction, and therefore the typical ratio $|\vec{t}|/t_0$, is estimated as $E_{\text{so}}/E_{\text{orb}}$, E_{so} being the energy scale of the matrix elements in the spin-orbit interaction Hamiltonian. We assume that $E_{\text{so}} \gtrsim E_{\text{orb}}$ (which is believed to be the case in InAs structures), and then all four coupling parameters are generally of the same order of magnitude $t_{0,x,y,z} \sim t$. As the structure of the localized electron wave functions is very much dependent on the nanostructure design and its inevitable imperfections, the direction of \vec{t} is hard to predict: we consider arbitrary directions.

We describe the electron dynamics with an evolution equation for the density matrix [80]. Next to the Hamiltonian terms, we complement the equation with (i) the rates $\sim \Gamma$ describing the decay of $|S_{02}\rangle$ and the refill to a (1, 1) state, and (ii) a small electron spin relaxation rate $\Gamma_{\text{rel}} \ll \Gamma$. The full evolution of the electron density matrix then can be written as

$$\frac{d\hat{\rho}}{dt} = -i[\hat{H}_e + \hat{H}_m + \hat{H}_t, \hat{\rho}] + \mathbf{\Gamma}\hat{\rho} + \mathbf{\Gamma}_{\text{rel}}\hat{\rho}. \quad (7.2)$$

Experimentally, the temperature exceeds the Zeeman energy [110], allowing us to assume isotropic spin relaxation: each (1, 1) state will transit to any of the other (1, 1) states with a rate $\Gamma_{\text{rel}}/3$. Explicitly, we use $\mathbf{\Gamma}_{\text{rel}}\hat{\rho} = -\Gamma_{\text{rel}}\hat{\rho} + \frac{1}{6}\Gamma_{\text{rel}}\sum_{\alpha,d}\hat{\sigma}_d^\alpha\hat{\rho}\hat{\sigma}_d^\alpha$, $\hat{\sigma}_{L(R)}^\alpha$ being the Pauli matrices in the left(right) dot.

Motivated by experimental work, we assume that the decay rate Γ of $|S_{02}\rangle$ is by far the largest frequency scale in (7.2), i.e. $\Gamma \gg B_0, K, t, \Gamma_{\text{rel}}$ (in principle Γ can be comparable with the detuning Δ). Under this assumption, we separate the time scales and derive the effective evolution equation for the density matrix in the (1, 1) subspace

$$\frac{d\hat{\rho}}{dt} = -i[\hat{H}_m + \hat{H}'_t, \hat{\rho}] - \mathbf{G}^{\text{out}}\hat{\rho} + \mathbf{G}^{\text{in}}\hat{\rho} + \mathbf{\Gamma}_{\text{rel}}\hat{\rho}. \quad (7.3)$$

The decay and refill terms are now incorporated into

$$\begin{aligned} G_{kl,mn}^{\text{out}} &= 2\{\delta_{km}T_{n2}T_{2l} + \delta_{ln}T_{k2}T_{2m}\}\Gamma/(\Gamma^2 + 4\Delta^2) \\ G_{kl,mn}^{\text{in}} &= \delta_{kl}T_{n2}T_{2m}\Gamma/(\Gamma^2 + 4\Delta^2), \end{aligned} \quad (7.4)$$

where $T_{a2} \equiv \langle a | \hat{H}_t | S_{02} \rangle$. The coupling between the dots gives also rise to an exchange Hamiltonian $(H'_t)_{ij} = 4T_{i2}T_{2j}\Delta/(\Gamma^2 + 4\Delta^2)$, with $H'_t \sim G^{\text{out}}$ provided $\Gamma \sim \Delta$. This anisotropic exchange interaction has been investigated in detail in Ref. [116]. The diagonal elements of \mathbf{G}^{out} give us the decay rates: If we consider $|T_{\pm}\rangle$ and $|T_0\rangle$, the three triplet states split by an external magnetic field, we find $\Gamma_{\pm}^{\text{so}} \equiv G_{\pm\pm,\pm\pm}^{\text{out}} = 2\Gamma(t_x^2 + t_y^2)/(\Gamma^2 + 4\Delta^2)$ and $\Gamma_0^{\text{so}} \equiv G_{00,00}^{\text{out}} = 4\Gamma t_z^2/(\Gamma^2 + 4\Delta^2)$, all of which are $\sim \Gamma^{\text{so}} \sim t^2/\Gamma$.

Let us neglect for a moment the nuclear fields, and focus on zero detuning, $\Delta = 0$. This allows us to grasp qualitatively the peculiarities of the spin blockade lifting, determined by competition between the Hamiltonian ($\sim B_0$) and dissipative terms ($\sim t^2/\Gamma, \Gamma_{\text{rel}}$) in Eq. 7.3.

At sufficiently large fields, the basis states $|T_0\rangle$ and $|S\rangle$ are aligned in energy. The spin-orbit modulated tunnel coupling then sets the difference between these states, which is best seen in a basis that mixes the states, $|\alpha\rangle \equiv \{t_0 |T_0\rangle + it_z |S\rangle\}/\sqrt{t_0^2 + t_z^2}$ and $|\beta\rangle \equiv \{it_z |T_0\rangle + t_0 |S\rangle\}/\sqrt{t_0^2 + t_z^2}$. Now $|\alpha\rangle$ is a blocked state, i.e. $G_{\alpha\alpha,\alpha\alpha}^{\text{out}} = 0$, while $|\beta\rangle$ decays with an effective rate $\Gamma_{\beta}^{\text{so}} \equiv G_{\beta\beta,\beta\beta}^{\text{out}} = 4\Gamma(t_0^2 + t_z^2)/(\Gamma^2 + 4\Delta^2)$. In Fig. 7.1(c) we give the energy levels of the five states and all transition rates in the limit of ‘large’ external fields. It is clear that the system will spend most time in the state $|\alpha\rangle$. The current is determined by the spin-relaxation decay rate of this state to any unblocked state, $3\Gamma_{\text{rel}}/3 = \Gamma_{\text{rel}}$. Let us note that if n_b states out of n states are blocked, such a decay produces on average n/n_b electrons tunneling to the outgoing lead before the system is recaptured in a blocked state. Therefore, the current is $I/e = 4\Gamma_{\text{rel}}$.

This picture holds until the decay rates of the three non-blocked states become comparable with Γ_{rel} , which takes place at $B_0 \sim \sqrt{\Gamma^{\text{so}}\Gamma_{\text{rel}}}$. To understand this, let us start with considering the opposite limit, $B_0 \ll \sqrt{\Gamma^{\text{so}}\Gamma_{\text{rel}}}$. In this case all four $(1, 1)$ states are almost aligned in energy, and the instructive basis to work in is the one spanned by a single decaying state $|m\rangle \equiv \{it \cdot \vec{T} + t_0 |S\rangle\}/\sqrt{|\vec{t}|^2 + t_0^2}$, and three orthonormal states $|1\rangle$, $|2\rangle$ and $|3\rangle$ that are not coupled to $|S_{02}\rangle$. At $B_0 = 0$ three of the four states are blocked, and spin relaxation to the unblocked state proceeds with a rate $\Gamma_{\text{rel}}/3$. A relaxation process produces on average $n/n_b = 4/3$ electron transfers, so that the total current is reduced by a factor of 9 in comparison with the ‘high’-field case, $I/e = \frac{4}{9}\Gamma_{\text{rel}}$. This factor of 9 agrees remarkably well with experimental observations (see Fig. 2b in Ref. [110]).

We now add a finite external field B_0 to this picture. Since \vec{t} is generally not parallel to B_0 , the external field will split the states $|1\rangle$, $|2\rangle$ and $|3\rangle$ in energy and mix two of them with the decaying state $|m\rangle$. This mixing results in an effective decay rate $\sim B_0^2/\Gamma^{\text{so}}$, which may compete with the spin relaxation rate Γ_{rel} . At

$B_0 \sim \sqrt{\Gamma^{\text{so}}\Gamma_{\text{rel}}}$, we cross over to the ‘high’-field regime described above, where only one blocked state is left. Therefore, the current exhibits a dip (suppression by a factor 9) around zero field with a width estimated as $\sqrt{\Gamma^{\text{so}}\Gamma_{\text{rel}}}$ (Fig. 7.2).

Let us now include the effects of the nuclear fields $\vec{K}_{L,R}$ on a qualitative level. If the fields are small compared to the scale t^2/Γ , their only relevant effect is to mix the states described above. This mixing creates a new possibility for decay of the blocked states, characterized by a rate $\Gamma_N \sim K^2/\Gamma^{\text{so}}$. This rate may compete with spin relaxation $\sim \Gamma_{\text{rel}}$, and could cause the current to scale with Γ_N and the width of the dip with K . In the opposite limit, $K \gg t^2/\Gamma$, the nuclear fields dominate the energy scales and separation of the (1,1) states at $B_0 \lesssim K$. Then, generally all four states are coupled to $|S_{02}\rangle$ on equal footing and the spin blockade is lifted. Qualitatively, this situation is similar to that without spin-orbit interaction (see Eqs 10-12 in [80]). *Without* spin-orbit interaction, an increase of magnetic field leads to blocking of two triplet states, resulting in a current peak at zero field. *With* spin-orbit interaction, $t_{x,y}$ still couple the split-off triplets to the decaying state. Depending on the strength and orientation of \vec{t} , the current in the limit of ‘high’ fields can be either smaller or larger than that at $B_0 = 0$, so we expect either peak or dip. If it is a peak, the transition from peak to dip is expected at $K \sim \Gamma^{\text{so}}$, that is, at $t \sim \sqrt{K\Gamma}$. Indeed, such a transition has been observed upon varying the magnitude of the tunnel coupling (Fig. 2 in Ref. [110]). If we assume that $K \sim 1.5$ mT and associate the level broadening observed (~ 100 μeV) with Γ , we estimate $t \sim 8$ μeV , which agrees with the range of coupling energies mentioned in [110].

7.3 Results

Let us now support the qualitative arguments given above with explicit analytical and numerical solutions. The current through the double dot is evaluated as $I/e = \rho_{22}\Gamma$, ρ_{22} being the steady-state probability to be in $|S_{02}\rangle$, as obtained from solving Eq. 7.2. We give an analytical solution for $\Delta = 0$, neglecting the nuclear fields, and expressing the answer in terms of the dimensionless parameter $\vec{t}/t_0 = \vec{\eta}$. Under these assumptions, we find

$$I = I_{\text{max}} \left(1 - \frac{8}{9} \frac{B_c^2}{B^2 + B_c^2} \right), \quad (7.5)$$

with $B_c = 2\sqrt{2}(1 + |\vec{\eta}|^2)(\eta_x^2 + \eta_y^2)^{-1/2}t_0\sqrt{\Gamma_{\text{rel}}/\Gamma}$ and $I_{\text{max}} = 4e\Gamma_{\text{rel}}$. The current exhibits a Lorentzian-shaped dip (see Fig. 7.2, compare with Fig. 2b in Ref. [110]). The width B_c and the limits at low and ‘high’ fields agree with the qualitative estimations given above.

To include the effect of the two nuclear fields, we compute steady-state solutions of (7.2) and average over many configurations of $\vec{K}_{L,R}$ [80]. In Fig. 7.3 we present the resulting current versus magnetic field and detuning for three different regimes. To produce the plots we turned to concrete values of the parameters, setting $\Gamma = 0.1$ meV, $\Gamma_{\text{rel}} = 1$ MHz, $\vec{\eta} = 0.25 \times \{1, 1, 1\}$. We averaged over 5000 configurations of $\vec{K}_{L,R}$, randomly sampled from a normal distribution with a r.m.s. of $0.4 \mu\text{eV}$.

In Fig. 7.3(a) and (b) we assumed large tunnel coupling, $t_0^2/\Gamma = 6 \mu\text{eV}$ so that $K\Gamma/t_0^2 = 0.07$ is small. In (a) we plot the current at $\Delta = 0$, while in (b) we plot it versus detuning for different fixed B_0 . We observe in (a) a Lorentzian-like dip in the current at $B_0 = 0$. While it looks similar to the plots in Fig. 7.2, the width is determined by the nuclear fields since $K \gg \Gamma_{\text{rel}}$. The curve can be accurately fit with the Lorentzian (7.5), giving $B_c = 7.4 K$ and $I_{\text{max}} = 0.62 K^2\Gamma/t_0$. Fig. 7.3(b) illustrates the unusual broadening of the resonant peak with respect to its natural width determined by Γ . The width in this case scales as $\sim t_0^2/K$ and is determined by competition of Γ^{so} and Γ_N . These plots qualitatively agree with data presented in Fig. 2b in Ref. [110]. In Fig. 7.3(c) and (d) we present the same plots, for smaller tunnel coupling, $t_0^2/\Gamma = 0.2 \mu\text{eV} = 0.5 K$. We included in plot (c) the curves for two random nuclear field configurations: it is clear that the current strongly depends on $\vec{K}_{L,R}$, which agrees with our expectation that in the regime $\Gamma_{\text{rel}} < \Gamma_N$ the current $I \propto \Gamma_N \propto K^2$. Remarkably, averaging over many configurations smooths the sharp features at small B_0 (c.f. [80]). Plots (d) exhibit no broadening with respect to Γ , in correspondence with Fig. 2a of Ref. [110]. In Fig. 7.3(e) and (f) we again made the same plots for yet smaller tunnel coupling, $t_0^2/\Gamma = 2 \text{ neV} \ll K$. Since the nuclear fields now dominate the splitting of the (1, 1) states, we see a peak comparable to the one in Fig. 4 of Ref. [80] surmounting a finite background current due to spin-orbit decay of the split-off triplets.

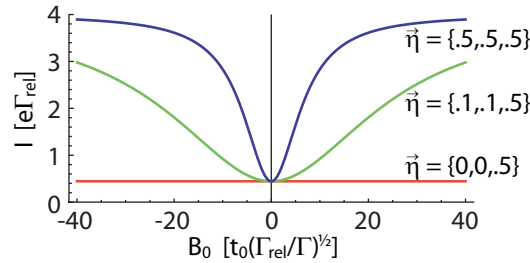


Figure 7.2: Current as a function of B_0 , at $\Delta = 0$, and neglecting the nuclear fields. Around zero field a dip is observed, its width depends on the magnitude and orientation of $\vec{\eta}$.

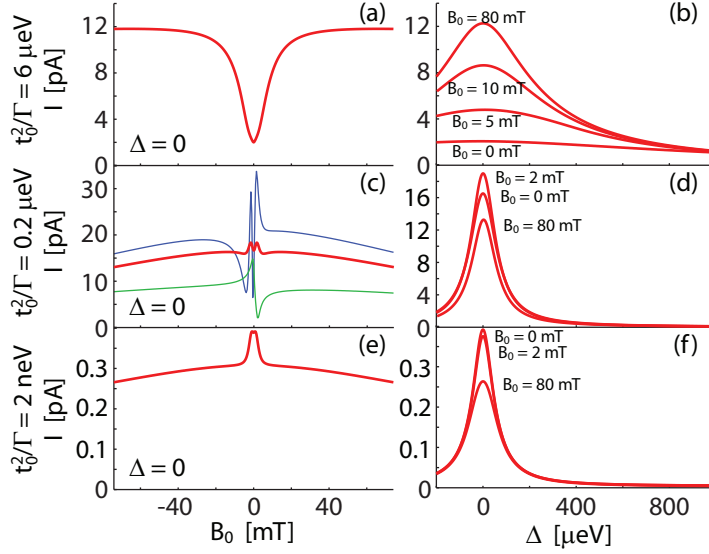


Figure 7.3: The current $I = e\rho_{22}\Gamma$ for (a,b) large, (c,d) intermediate, and (e,f) small tunnel coupling. The dip observed around zero field (a) disappears when $t_0^2/\Gamma \sim K$ (c) and evolves into a peak for even smaller tunnel coupling (e).

We expect our results to hold for any quantum dot system with strong spin-orbit interaction. Indeed, recent experiments on quantum dots in carbon nanotubes in the spin blockade regime [117] display the very same specific features, as e.g. a zero-field dip in the current.

Now that we understand the origin of the lifting of spin blockade, we also propose a way to extend the blockade region. If one would have a freely rotatable magnet as source of the field B_0 , one would observe a large increase in width of the blockade region as soon as \vec{B}_0 and \vec{t} are parallel. One can understand this as follows. If \vec{t} effectively points along the z -direction, t_x and t_y and thus Γ_{\pm}^{so} are zero: the states $|T_{\pm}\rangle$ are blocked (see Fig. 7.2). As $|T_{\pm}\rangle$ are eigenstates of the field B_0 , this blockade could persist up to arbitrarily high fields. Since $|T_0\rangle$ and $|S\rangle$ are rotated into $|\alpha\rangle$ and $|\beta\rangle$, current will then scale in general with the anti-parallel component of spin instead of only the spin singlet.

7.4 Conclusion

To conclude, we presented a model to study electron transport in the Pauli spin blockade regime in the presence of strong spin-orbit interaction. It reproduces all features observed in experiment, such as lifting of the spin blockade at high external fields or at low interdot tunnel coupling. We explain the mechanisms involved and identify all relevant energy scales. We also propose a simple way to

extend the region of spin blockade.

We acknowledge fruitful discussions with A. Pfund, S. Nadj-Perge, S. Frolov, and K. Ensslin. This work is part of the research program of the Stichting FOM.

Chapter 8

Nuclear spin effect in a metallic spin valve

We study electronic transport through a ferromagnet normal-metal ferromagnet system and we investigate the effect of hyperfine interaction between electrons and nuclei in the normal-metal part. A switching of the magnetization directions of the ferromagnets causes nuclear spins to precess. We show that the effect of this precession on the current through the system is large enough to be observed in experiment.¹

¹This chapter has been published in Physical Review Letters **97**, 146602 (2006).

8.1 Introduction

In recent years considerable theoretical and experimental work is aimed at the controlled manipulation of electron spin in nanoscale solid state systems, a field commonly referred to as *spintronics* [6]. The main motivations for this research are applications in conventional computer hardware [118] as well as the futuristic possibility of *quantum computation* [119], using single electron spins as information carrying units (*qubits*). For both purposes, understanding the mechanisms of spin polarization, relaxation, and dephasing in solid state systems is crucial.

The branch of metallic spintronics has quickly evolved after the discovery of the giant magnetoresistance (GMR) in hybrid ferromagnetic normal metal structures [4, 5]. Theoretical and experimental studies on magnetic multilayers have not only revealed interesting physics, but also already led to several applications in magnetoelectronic devices. Magnetic recording read heads based on the GMR were first developed some ten years ago [120], but nowadays can be found in nearly all hard disk drives.

In the context of quantum computation, semiconductor quantum dots are regarded as promising candidates for storing electron spin based qubits [20]. Recent progress in quantum manipulation of single spins [36] has overcome the effects of various spin relaxation processes in these devices. The unavoidable hyperfine interaction between electron and nuclear spin presently attracts much attention. It has been identified as the main source of spin relaxation in high-purity samples at low temperatures [56, 121] and can even govern the electron transport in double dots [37]. At present, hyperfine interaction is seen as the main obstacle to demonstrate quantum computation with electron spins in solid state devices.

In many other fields, for instance nuclear magnetic resonance (NMR) experiments, hyperfine interactions play a central role already for decades. The Overhauser effect [63] is a common way to increase the degree of nuclear polarization in metals enhancing NMR peaks. In semiconductors, optical orientation techniques [122] are used to polarize the nuclear system. In the context of *metallic* devices, hyperfine interaction has been thought to be too weak to influence charge transport directly, and it has been regarded merely as an extra source of spin relaxation [6].

8.2 Overview

In this Chapter, we predict a clearly observable hyperfine effect on electron transport in a *metallic* device. Thereby we demonstrate that hyperfine interactions may be important and possibly even dominant also for metallic spintronic devices.

We consider electronic transport through a ferromagnet normal-metal ferromagnet multilayer. This so-called *spin valve* is the basic magnetoelectronic device and the core component of all GMR based read heads. By changing the magnetization directions of the two ferromagnetic leads, one alters the total resistance of the device as well as the degree and direction of electronic polarization in the normal metal part in the presence of a current.

Although the spin and particle transport properties of spin valves are well investigated and understood [72], effects of hyperfine interaction in magnetic multilayers have been hardly studied at all. One may think that these effects are negligible owing to the small value of the hyperfine interaction constant $A \simeq 10^{-6}$ eV in metals. We show, however, that electron spins accumulating in the normal metal part can build up a significant polarization of nuclear spins. The direction of this polarization is determined by the magnetizations of the leads. If the magnetizations are suddenly changed, this affects the electronic spin distribution in the normal metal part immediately (at a time scale $\tau_e \simeq 10^{-11}$ s). The nuclear spin polarization reacts on a much longer time scale and will start to precess slowly around its new equilibrium direction. In this paper we are mainly interested in the feedback of the nuclear polarization on the electronic system. We show that due to such feedback the precession manifests itself as oscillations in the net current through the device. The amplitude of these oscillations is estimated as A/E_{th} . Here E_{th} is the Thouless energy characterizing the typical electron dwell time in the valve. The estimation is valid provided this time is shorter than the spin relaxation time τ_{sf} , which sets an upper bound for the effect, $A\tau_{sf}/\hbar$. For typical parameters, the relative magnitude of the current oscillations can be of the order $10^{-4} \sim 10^{-5}$, which is clearly large enough to be measured in experiments.

8.3 Model

We model our system as a small metallic island connected to two ferromagnetic leads (Fig. 8.1). We assume the island to be smaller than the spin diffusion length l_{sf} and the time an electron spends in the island much smaller than τ_{sf} , which allows us to disregard spin-orbit relaxation mechanisms in the island. We also assume that the resistance of the junctions by far exceeds the resistance of the island itself. In this case, we can describe the electronic states in the island with a single coordinate-independent distribution function $f(E, t)$.

The two ferromagnetic leads are modeled as large reservoirs in local equilibrium, with magnetizations in arbitrary directions \vec{m}_L and \vec{m}_R . Assuming for

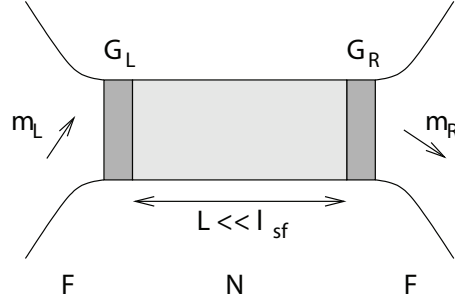


Figure 8.1: A schematic picture of the system considered. A small metallic island is connected to two large ferromagnetic reservoirs with magnetizations \vec{m}_L and \vec{m}_R . The contacts are characterized by conductances G_L and G_R , which consist of spin-dependent parts G^\uparrow and G^\downarrow , and a mixing conductance $G^{\uparrow\downarrow}$. The length of the normal metal part is significantly smaller than the spin diffusion length.

simplicity $T = 0$, we approximate the electronic distribution function in the leads as $f_{L(R)}(E) = \theta(\mu_{L(R)} - E)$. The difference in chemical potentials is due to the bias voltage applied $eV_b = \mu_L - \mu_R$. We can disregard temperature provided $eV_b \gg k_B T$.

In our model, the electron spin polarization is mainly determined by the balance of spin-polarized currents flowing into and out of the ferromagnetic leads. However, a significant correction to this balance comes from hyperfine coupling between the electron and nuclear spins. The resulting change of the polarization affects the net electric current in the device. So we will first derive an expression for hyperfine induced polarization of electrons and nuclei, and then we combine the result with the known expressions for spin transport through spin valves.

The Hamiltonian we use to describe the electronic and nuclear states in the island consists of an electronic part and a part describing the hyperfine interactions,

$$\begin{aligned}
 \hat{H} &= \hat{H}_{el} + \hat{H}_{hf} \\
 \hat{H}_{el} &= \sum_k \epsilon_k \left(\hat{a}_{k\uparrow}^\dagger \hat{a}_{k\uparrow} + \hat{a}_{k\downarrow}^\dagger \hat{a}_{k\downarrow} \right) \\
 \hat{H}_{hf} &= \sum_n A_n \hat{S}_n(t) \cdot \hat{\Psi}^\dagger(\vec{r}_n) \frac{1}{2} \vec{\sigma} \hat{\Psi}(\vec{r}_n),
 \end{aligned} \tag{8.1}$$

where $\hat{a}_{k\alpha}^{(\dagger)}$ are electron annihilation (creation) operators for spin up and down ($\alpha = \uparrow, \downarrow$). We expressed the usual hyperfine contact Hamiltonian in electronic field operators, defined as $\hat{\Psi}(\vec{r}) = \Omega^{-1/2} \sum_{k,\alpha} \hat{a}_{k\alpha} e^{ik\vec{r}}$, where Ω is the volume of the island. A_n is the hyperfine coupling coefficient between an electron and the

nucleus at position \vec{r}_n , the vectors \hat{S}_n are the nuclear spin operators and $\vec{\sigma}$ the Pauli spin matrices.

8.4 Approach

We apply a second order perturbation expansion to find an expression for the time dependence of the electronic distribution function $f(k, t) = \langle \hat{a}_{k\alpha}^\dagger(t) \hat{a}_{k\beta}(t) \rangle$

$$\frac{df(k, t)}{dt} \approx \left\langle \frac{i}{\hbar} [\hat{H}(t), \hat{a}_{k\alpha}^\dagger \hat{a}_{k\beta}] \right\rangle - \left\langle \int_{-\infty}^t \frac{dt'}{\hbar^2} [\hat{H}(t), [\hat{H}(t'), \hat{a}_{k\alpha}^\dagger \hat{a}_{k\beta}]] \right\rangle, \quad (8.2)$$

where the indices α and β now span a 2×2 spin space. We see that the expansion can be completely expressed in the commuting operators \hat{S}_n and $\hat{a}^{(\dagger)}$.

Using Wick's theorem, we write the terms with four and six creation and annihilation operators as products of pairs, which then again can be interpreted as distribution functions $f(E, t)$. Further, we assume that the electrons are distributed homogeneously on the island and approximate $A_n = A/n_0$, A being the hyperfine coupling energy of the material and n_0 the density of nuclei with non-zero spin [123]. We find up to the second order

$$\begin{aligned} \left(\frac{d\vec{f}_s}{dt} \right)_{hf} &= \frac{A}{\hbar} \langle \vec{S}(t) \rangle \times \vec{f}_s(t) - \frac{1}{\tau_{hf}} \left[\frac{1}{2} - \vec{f}_s(t) \cdot \langle \vec{S}(t) \rangle \right] \vec{f}_s(t) \\ &+ \frac{1}{\tau_{hf}} f_p(t) [1 - f_p(t)] \langle \vec{S}(t) \rangle, \end{aligned} \quad (8.3)$$

where we used the notation $f = f_p \mathbb{1} + \vec{f}_s \cdot \vec{\sigma}$, i.e. we split f in a particle and spin part. Nuclear spin enters here as the average polarization $\langle \vec{S}(t) \rangle$. The first-order term describes the precession of electron spin in the field of the nuclei and disappears if electron and nuclear polarizations are aligned. The second-order terms are all proportional to the hyperfine relaxation time defined as $\tau_{hf} = \hbar n_0 / \pi A^2 \nu$, ν being the density of states at the Fermi energy. Since hyperfine interaction affects the electron spin only, the contribution to the time derivative of f_p is zero.

This contribution is not the main one in the balance in the spin valve. Mainly, it is determined by electron transfers through the spin-active junctions. To describe this, we use the approach of [72] that is valid for non-collinear magnetiza-

tions. This yields

$$\begin{aligned} \left(\frac{d\vec{f}_s}{dt}\right)_{sv} = & \vec{B}_e \times \vec{f}_s(t) - \frac{1}{\tau_e} \vec{f}_s(t) + \frac{1}{\tau_e} \left\{ \alpha_L [1 - f_p(t)] + \beta_L \vec{m}_L \cdot \vec{f}_s(t) \right\} \vec{m}_L \\ & + \frac{1}{\tau_e} \left\{ \alpha_R [-f_p(t)] + \beta_R \vec{m}_R \cdot \vec{f}_s(t) \right\} \vec{m}_R. \end{aligned} \quad (8.4)$$

Following [72], we describe each spin-active junction with four conductances, G^\uparrow , G^\downarrow and $G^{\uparrow\downarrow} = (G^{\downarrow\uparrow})^*$. (If the junction is not spin-active, $G^\uparrow = G^\downarrow = G^{\uparrow\downarrow} = G^{\downarrow\uparrow} = G$). The electron spin is subject to an effective field

$$\vec{B}_e = -\frac{1}{\tau_e} \frac{\text{Im}(G_L^{\uparrow\downarrow})\vec{m}_L + \text{Im}(G_R^{\uparrow\downarrow})\vec{m}_R}{\text{Re}(G_L^{\uparrow\downarrow} + G_R^{\uparrow\downarrow})},$$

and we introduce dimensionless parameters characterizing the spin activity of the junctions

$$\begin{aligned} \alpha_{L(R)} &= \frac{G_{L(R)}^\uparrow - G_{L(R)}^\downarrow}{2\text{Re}(G_L^{\uparrow\downarrow} + G_R^{\uparrow\downarrow})}, & P_{L(R)} &= \frac{G_{L(R)}^\uparrow - G_{L(R)}^\downarrow}{G_{L(R)}^\uparrow + G_{L(R)}^\downarrow} \\ \beta_{L(R)} &= \frac{2\text{Re}(G_{L(R)}^{\uparrow\downarrow}) - G_{L(R)}^\uparrow - G_{L(R)}^\downarrow}{2\text{Re}(G_L^{\uparrow\downarrow} + G_R^{\uparrow\downarrow})}. \end{aligned}$$

The order of magnitude of (8.4) is estimated as $1/\tau_e$, τ_e being a typical electron dwell time in the island, $\tau_e = e^2\nu\Omega/2\text{Re}(G_L^{\uparrow\downarrow} + G_R^{\uparrow\downarrow})$.

Since by the essence of the spin valve, the spin balance affects the particle current through the device, the time derivative of f_p is non-zero now,

$$\frac{df_p}{dt} = \frac{1}{\tau_e} \left\{ \frac{\alpha_L}{P_L} [1 - f_p(t)] - \frac{\alpha_R}{P_R} f_p(t) - (\alpha_L \vec{m}_L + \alpha_R \vec{m}_R) \cdot \vec{f}_s(t) \right\}. \quad (8.5)$$

We also need an equation for the time dependence of the nuclear spin polarization. One can obtain it from a perturbation expansion similar to (8.2) or directly inherit it from the fact that hyperfine interaction conserves the total spin of electrons and nuclei

$$n_0 \left(\frac{d\langle \vec{S} \rangle}{dt} \right)_{hf} = -\nu e V_b \left(\frac{d\vec{f}_s}{dt} \right)_{hf}. \quad (8.6)$$

We see from this that the relaxation time of nuclear spins $\tau_d \simeq \tau_{hf} n_0 / \nu e V_b$. We assume that no other relaxation mechanism provides a shorter relaxation time.

Let us now estimate and compare the time scales involved. For the nuclear system, the precession frequency $\omega = A\nu e V_b |\vec{f}_s| / \hbar n_0$ and the relaxation time

$\tau_d \simeq \hbar n_0^2 / \pi A^2 \nu^2 e V_b$. Typical values for A range from 10^{-7} eV for weak coupling to 10^{-4} eV (e.g. in GaAs [123]); we chose $A = 5 \times 10^{-6}$ eV. We take typical solid-state parameters to estimate $n_0 = 2.9 \times 10^{29} \text{ m}^{-3}$ and $\nu = 1.3 \times 10^{47} \text{ J}^{-1} \text{ m}^{-3}$. For an applied bias voltage of $V_b = 10 \text{ mV}$, this results in a precession frequency $\omega \sim 10^5 \text{ Hz}$ and a nuclear relaxation time $\tau_d \sim 0.5 \text{ s}$. For the electronic system, the spin relaxation rate consists of two terms $\propto 1/\tau_e$ and $\propto 1/\tau_{hf}$. We set the conductance of the F/N-interfaces to $G \sim 3 \Omega^{-1}$ [124]. If we choose dimensions of the metal island of $0.1 \times 0.1 \times 5 \mu\text{m}^3$, we find $\tau_e \sim 10^{-11} \text{ s}$. This corresponds to a Thouless energy $E_{th} = \hbar/\tau_e \simeq 0.06 \text{ meV}$. The estimation for the hyperfine relaxation time reads $\tau_{hf} \sim 10^{-4} \text{ s}$.

We conclude that on the time scale of all nuclear processes, \vec{f}_s and f_p instantly adjust themselves to current values of voltage, magnetization, and importantly, nuclear spin polarization. Their values are determined from the spin balance,

$$\left(\frac{d\vec{f}_s}{dt} \right)_{hf} + \left(\frac{d\vec{f}_s}{dt} \right)_{sv} = 0 \quad \text{and} \quad \frac{df_p}{dt} = 0. \quad (8.7)$$

As to nuclear polarization at constant voltage and magnetization, it is of the order of 1 owing to a sort of Overhauser effect produced by non-equilibrium electrons passing the island. Indeed, it follows from Eq. 8.6 that the stationary $2\langle \vec{S} \rangle = \vec{f}_s / [f_p(1 - f_p) + |\vec{f}_s|^2]$. We see that $\langle \vec{S} \rangle$ and \vec{f}_s are parallel under stationary conditions. This is disappointing since this will not result in any precession.

The essential ingredient of our proposal is to change in time the magnetization(s) of the leads. Let us consider the effect of sudden change of the magnetization in one of the leads at $t = 0$. The electrons will find their new distribution, characterized by \vec{f}_{new} , on a timescale of τ_e . As we see from (8.6), the nuclear spin system will start to precess around \vec{f}_{new} with the frequency estimated. The precessing polarization will contribute to the effective field \vec{B}_e , $\vec{B}_e \rightarrow \vec{B}_e + A\langle \vec{S}(t) \rangle / \hbar$ in (8.7). This will result in a small correction to \vec{f}_{new} , $\vec{f}^{(1)}$, which is visible in the net current through the junction, due to its oscillating nature. A simple expression for this correction is obtained in the limit of weakly polarizing junctions ($\alpha_{L,R}, \beta_{L,R} \ll 1$),

$$\vec{f}^{(1)}(t) = \frac{A\tau_e}{\hbar} \langle \vec{S}(t) \rangle \times \vec{f}_{new} \quad \propto \quad A/E_{th}, \quad (8.8)$$

while a more general expression is obtained by solving (8.7) up to first order in A . The oscillatory part of the resulting current is given by

$$\tilde{I}(t) = V_b \frac{e^2 \nu \Omega}{2\tau_e} [P_R \vec{m}_R - P_L \vec{m}_L] \cdot \vec{f}^{(1)}(t). \quad (8.9)$$

The time dependence of nuclear polarization is still governed by Eq. 8.6.

Combining Eqs 8.8 and 8.9, we find that the time-dependent current follows the behavior of $\langle \vec{S}(t) \rangle$ and therefore exhibits oscillations with frequency ω that are damped at the long time scale τ_d . The amplitude of these oscillations ΔI in the limit of small α and β reads

$$\frac{|\Delta I|}{\langle I \rangle} \approx \frac{A\tau_e}{\hbar} |\langle \vec{S}_{old} \rangle \times \vec{f}_{new}| |P_R \vec{m}_R^\perp - P_L \vec{m}_L^\perp|, \quad (8.10)$$

again proportional to A/E_{th} . In this equation $\langle \vec{S}_{old} \rangle$ refers to the nuclear polarization before switching the magnetizations and $\vec{m}_{L(R)}^\perp$ is the part of $\vec{m}_{L(R)}$ perpendicular to \vec{f}_{new} . This relation makes it straightforward that one needs non-collinear magnetizations to observe any effect.

In the same limit, the damping time and precession frequency are given by

$$\tau_d = \tau_{hf} \frac{n_0}{\nu e V_b} \{ \xi + \xi^{-1} + 2 \}, \quad (8.11)$$

and

$$\omega = \frac{A \nu e V_b}{\hbar n_0} \frac{|P_R \vec{m}_R^\perp - P_L \vec{m}_L^\perp|}{\xi + \xi^{-1} + 2}. \quad (8.12)$$

where $\xi = G_L/G_R$ characterizes the asymmetry of the conductance of the contacts.

In Fig. 8.2a we plotted a numerical solution for the current $\tilde{I}(t)/\langle I \rangle$ and in 8.2b the dependence of ω and τ_d on the asymmetry in conductance of the contacts. For 8.2a we made use of equations (8.6) and (8.7), and inserted realistic $\alpha_{L,R}$ and $\beta_{L,R}$. For the parameters used, the estimate (8.10) of the amplitude is 4.4×10^{-5} . Eqs (8.11) and (8.12) give $\tau_d = 0.63$ s and $\omega = 1.0 \times 10^5$ Hz, in agreement with the plot. Typical currents through spin valves of these dimensions using a bias voltage of 10 mV range between 10 and 100 mA. Oscillations of the order of 10^{-5} - 10^{-4} should be clearly visible in experiment. The unavoidable shot noise due to the discrete nature of the electrons crossing the junctions will not prevent even an accurate single-shot measurement, since the measurement time can be of the order of τ_d . An estimate using $(\delta I)^2 \simeq 2eI/\tau_d$ gives a relative error of 10^{-8} - 10^{-9} , at least three orders smaller than the oscillations.

So far we have assumed precisely uniform electron distributions. In a realistic situation however, the finite resistance of the island results in a voltage drop over the island, thus causing spatial variation of f_0 and \vec{f}_s . Importantly, this gives variations in the precession frequency $\omega \propto A|\vec{f}_s|/\hbar$. Such variation $\Delta\omega$ over the length of the island will contribute to an apparent relaxation of the spin

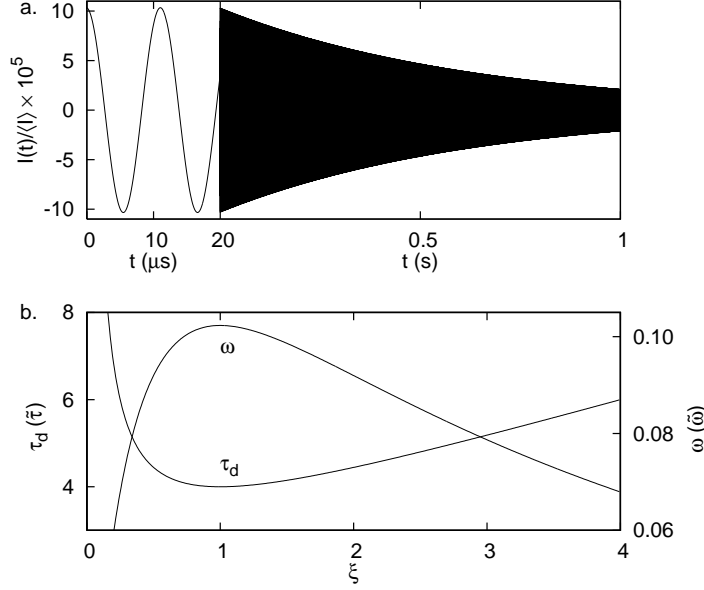


Figure 8.2: (a) Numerical calculation of the relative current fluctuations as a function of time. For $t > 20 \mu\text{s}$ the t -axis is compressed. We used the parameters chosen in the text and further we took for both contacts $\alpha = 0.128$, $\beta = 0.115$ and $P = 0.333$. The magnetizations switch at $t = 0$ from $m_L = (0, 0, 1)$, $m_R = (0, 0, -1)$ to $m_L = (0, 1, 0)$, $m_R = (0, 0, -1)$. (b) The dependence of the relaxation time and the frequency of the fluctuations on the asymmetry ξ in the conductances, where $\tilde{\tau} = \hbar n_0 / \pi A^2 \nu^2 e V_b$ and $\tilde{\omega} = A \nu e V_b / \hbar n_0$.

polarization, since precession in different points of the island occurs with a slightly different frequency. This effect adds a term $1/\tau^* = \Delta\omega$ to the damping rate $1/\tau_d$. Assuming a simple linear voltage drop over the normal metal part, we find $1/\tau^* = (G_{\text{junc}}/G_{\text{isl}})\omega_0$, i.e. the ratio of the total conductance of the spin valve and the conductance of the metal island times the average oscillation frequency ω_0 . Although the effect can reduce the apparent relaxation time, provided $(\Delta\omega)\tau_d \gg 1$, it will not influence the time-dependent current just after $t = 0$.

8.5 Conclusion

In conclusion, we have shown how hyperfine-induced nuclear precession in the normal metal part of a spin valve can be made experimentally visible. The precession should give a clear signature in the form of small oscillations in the net current through the valve after sudden change of the magnetizations of the leads.

We found a coupled set of equations describing the nuclear and electron spin dynamics resulting from a second order perturbation expansion in the hyperfine contact Hamiltonian. We presented a numerical solution for the net current and derived an estimate for the amplitude of the oscillations. We found that the relative amplitude of these oscillations is sufficiently big to be observable.

The authors acknowledge financial support from FOM and useful discussions with G. E. W. Bauer.

Bibliography

- [1] R. A. Webb, S. Washburn, C. P. Umbach, and R. B. Laibowitz, “Observation of h/e Aharonov-Bohm oscillations in normal-metal rings,” *Phys. Rev. Lett.*, vol. 54, pp. 2696–2699, Jun 1985.
- [2] Y. K. Kato, R. C. Myers, A. C. Gossard, and D. D. Awschalom, “Observation of the spin Hall effect in semiconductors,” *Science*, vol. 306, no. 5703, pp. 1910–1913, 2004.
- [3] H. Ohno, “Making nonmagnetic semiconductors ferromagnetic,” *Science*, vol. 281, no. 5379, pp. 951–956, 1998.
- [4] M. N. Baibich, J. M. Broto, A. Fert, F. N. Van Dau, F. Petroff, P. Etienne, G. Creuzet, A. Friederich, and J. Chazelas, “Giant magnetoresistance of (001)Fe/(001)Cr magnetic superlattices,” *Phys. Rev. Lett.*, vol. 61, pp. 2472–2475, Nov 1988.
- [5] G. Binasch, P. Grünberg, F. Saurenbach, and W. Zinn, “Enhanced magnetoresistance in layered magnetic structures with antiferromagnetic interlayer exchange,” *Phys. Rev. B*, vol. 39, pp. 4828–4830, Mar 1989.
- [6] I. Zutíć, J. Fabian, and S. Das Sarma, “Spintronics: Fundamentals and applications,” *Rev. Mod. Phys.*, vol. 76, no. 2, pp. 323–410, 2004.
- [7] R. P. Feynman, *The Feynman Lectures on Computation*. Perseus Publishing, 2000.
- [8] C. H. Bennett, G. Brassard, C. Crépeau, R. Jozsa, A. Peres, and W. K. Wootters, “Teleporting an unknown quantum state via dual classical and Einstein-Podolsky-Rosen channels,” *Phys. Rev. Lett.*, vol. 70, pp. 1895–1899, Mar 1993.
- [9] A. K. Ekert, “Quantum cryptography based on Bell’s theorem,” *Phys. Rev. Lett.*, vol. 67, pp. 661–663, Aug 1991.

-
- [10] P. W. Shor, “Algorithms for quantum computation: Discrete logarithms and factoring,” in *Proceedings of 35th Annual Symposium on Foundations of Computer Science*, IEEE Press, 1994.
- [11] D. Deutsch, “Quantum theory, the Church-Turing principle and the universal quantum computer,” *Proc. Roy. Soc. London A*, vol. 400, no. 1818, pp. 97–117, 1985.
- [12] S. Lloyd, “Universal Quantum Simulators,” *Science*, vol. 273, no. 5278, pp. 1073–1078, 1996.
- [13] L. K. Grover, “Quantum mechanics helps in searching for a needle in a haystack,” *Phys. Rev. Lett.*, vol. 79, pp. 325–328, Jul 1997.
- [14] P. W. Shor, “Fault-tolerant quantum computation,” in *Proceedings of 37th Annual Symposium on Foundations of Computer Science*, IEEE Press, 1996.
- [15] D. Aharonov and M. Ben-Or, “Fault-tolerant quantum computation with constant error rate,” *SIAM Journal on Computing*, vol. 38, no. 4, pp. 1207–1282, 2008.
- [16] G. K. Brennen, C. M. Caves, P. S. Jessen, and I. H. Deutsch, “Quantum logic gates in optical lattices,” *Phys. Rev. Lett.*, vol. 82, pp. 1060–1063, Feb 1999.
- [17] J. I. Cirac and P. Zoller, “Quantum computations with cold trapped ions,” *Phys. Rev. Lett.*, vol. 74, pp. 4091–4094, May 1995.
- [18] I. L. Chuang, N. Gershenfeld, and M. Kubinec, “Experimental implementation of fast quantum searching,” *Phys. Rev. Lett.*, vol. 80, pp. 3408–3411, Apr 1998.
- [19] J. E. Mooij, T. P. Orlando, L. Levitov, L. Tian, C. H. van der Wal, and S. Lloyd, “Josephson persistent-current qubit,” *Science*, vol. 285, no. 5430, pp. 1036–1039, 1999.
- [20] D. Loss and D. P. DiVincenzo, “Quantum computation with quantum dots,” *Phys. Rev. A*, vol. 57, pp. 120–126, Jan 1998.
- [21] R. Vrijen, E. Yablonovitch, K. Wang, H. W. Jiang, A. Balandin, V. Roychowdhury, T. Mor, and D. DiVincenzo, “Electron-spin-resonance transistors for quantum computing in silicon-germanium heterostructures,” *Phys. Rev. A*, vol. 62, p. 012306, Jun 2000.

- [22] F. Jelezko, T. Gaebel, I. Popa, A. Gruber, and J. Wrachtrup, "Observation of coherent oscillations in a single electron spin," *Phys. Rev. Lett.*, vol. 92, p. 076401, Feb 2004.
- [23] L. M. K. Vandersypen, M. Steffen, G. Breyta, C. S. Yannoni, M. H. Sherwood, and I. L. Chuang, "Experimental realization of Shor's quantum factoring algorithm using nuclear magnetic resonance," *Nature*, vol. 414, p. 883, 2001.
- [24] R. Hanson, L. P. Kouwenhoven, J. R. Petta, S. Tarucha, and L. M. K. Vandersypen, "Spins in few-electron quantum dots," *Rev. Mod. Phys.*, vol. 79, no. 4, p. 1217, 2007.
- [25] D. L. Klein, P. L. McEuen, J. E. B. Katari, R. Roth, and A. P. Alivisatos, "An approach to electrical studies of single nanocrystals," *Appl. Phys. Lett.*, vol. 68, no. 18, pp. 2574–2576, 1996.
- [26] L. P. Kouwenhoven, C. M. Marcus, P. L. McEuen, S. Tarucha, R. M. Westervelt, and N. S. Wingreen, *Mesoscopic Electron Transport, Vol. 345 of NATO Advanced Studies Institute, Series E: Applied Sciences*, p. 16. Kluwer Academic, Dordrecht, 1997.
- [27] M. T. Bjork, C. Thelander, A. E. Hansen, L. E. Jensen, M. W. Larsson, L. R. Wallenberg, and L. Samuelson, "Few-electron quantum dots in nanowires," *Nano Letters*, vol. 4, no. 9, pp. 1621–1625, 2004.
- [28] S. M. Reimann and M. Manninen, "Electronic structure of quantum dots," *Rev. Mod. Phys.*, vol. 74, pp. 1283–1342, Nov 2002.
- [29] W. G. van der Wiel, S. De Franceschi, J. M. Elzerman, T. Fujisawa, S. Tarucha, and L. P. Kouwenhoven, "Electron transport through double quantum dots," *Rev. Mod. Phys.*, vol. 75, pp. 1–22, Dec 2002.
- [30] L. P. Kouwenhoven, D. G. Austing, and S. Tarucha, "Few-electron quantum dots," *Rep. Prog. Phys.*, vol. 64, pp. 701–737, 2001.
- [31] D. H. Cobden and J. Nygård, "Shell filling in closed single-wall carbon nanotube quantum dots," *Phys. Rev. Lett.*, vol. 89, p. 046803, Jul 2002.
- [32] N. Mason, M. J. Biercuk, and C. M. Marcus, "Local gate control of a carbon nanotube double quantum dot," *Science*, vol. 303, no. 5658, pp. 655–658, 2004.

- [33] K. Ono and S. Tarucha, “Nuclear-spin-induced oscillatory current in spin-blockaded quantum dots,” *Phys. Rev. Lett.*, vol. 92, p. 256803, Jun 2004.
- [34] F. H. L. Koppens, C. Buizert, K. J. Tielrooij, I. T. Vink, K. C. Nowack, T. Meunier, L. P. Kouwenhoven, and L. M. K. Vandersypen, “Driven coherent oscillations of a single electron spin in a quantum dot,” *Nature*, vol. 442, pp. 766–771, 2006.
- [35] K. C. Nowack, F. H. L. Koppens, Y. V. Nazarov, and L. M. K. Vandersypen, “Coherent control of a single electron spin with electric fields,” *Science*, vol. 318, no. 5855, pp. 1430–1433, 2007.
- [36] J. R. Petta, A. C. Johnson, J. M. Taylor, E. A. Laird, A. Yacoby, M. D. Lukin, C. M. Marcus, M. P. Hanson, and A. C. Gossard, “Coherent manipulation of coupled electron spins in semiconductor quantum dots,” *Science*, vol. 309, no. 5744, pp. 2180–2184, 2005.
- [37] F. H. L. Koppens, J. A. Folk, J. M. Elzerman, R. Hanson, L. H. W. van Beveren, I. T. Vink, H. P. Tranitz, W. Wegscheider, L. P. Kouwenhoven, and L. M. K. Vandersypen, “Control and detection of singlet-triplet mixing in a random nuclear field,” *Science*, vol. 309, no. 5739, pp. 1346–1350, 2005.
- [38] A. C. Johnson, J. R. Petta, J. M. Taylor, A. Yacoby, M. D. Lukin, C. M. Marcus, M. P. Hanson, and A. C. Gossard, “Triplet-singlet spin relaxation via nuclei in a double quantum dot,” *Nature*, vol. 435, pp. 925–928, 2005.
- [39] V. Cerletti, W. A. Coish, O. Gywat, and D. Loss, “Recipes for spin-based quantum computing,” *Nanotechnology*, vol. 16, no. 4, pp. R27–R49, 2005.
- [40] M. Atature, J. Dreiser, A. Badolato, A. Hogege, K. Karrai, and A. Imamoglu, “Quantum-dot spin-state preparation with near-unity fidelity,” *Science*, vol. 312, no. 5773, pp. 551–553, 2006.
- [41] R. Hanson, L. H. Willems van Beveren, I. T. Vink, J. M. Elzerman, W. J. M. Naber, F. H. L. Koppens, L. P. Kouwenhoven, and L. M. K. Vandersypen, “Single-shot readout of electron spin states in a quantum dot using spin-dependent tunnel rates,” *Phys. Rev. Lett.*, vol. 94, no. 19, p. 196802, 2005.
- [42] W. A. Coish and D. Loss, “Hyperfine interaction in a quantum dot: Non-markovian electron spin dynamics,” *Phys. Rev. B*, vol. 70, p. 195340, Nov 2004.

- [43] L. L. Foldy and S. A. Wouthuysen, “On the Dirac theory of spin 1/2 particles and its non-relativistic limit,” *Phys. Rev.*, vol. 78, pp. 29–36, Apr 1950.
- [44] C. G. Darwin, “The wave equations of the electron,” *Proc. Roy. Soc. London A*, vol. 118, no. 780, pp. 654–680, 1928.
- [45] G. Dresselhaus, “Spin-orbit coupling effects in zinc blende structures,” *Phys. Rev.*, vol. 100, pp. 580–586, Oct 1955.
- [46] E. I. Rashba, “Properties of semiconductors with an extremum loop. 1. Cyclotron and combinational resonance in a magnetic field perpendicular to the plane of the loop,” *Sov. Phys. Solid State*, vol. 2, pp. 1109–1122, 1960.
- [47] A. V. Khaetskii and Y. V. Nazarov, “Spin-flip transitions between Zeeman sublevels in semiconductor quantum dots,” *Phys. Rev. B*, vol. 64, p. 125316, Sep 2001.
- [48] S. Amasha, K. MacLean, I. P. Radu, D. M. Zumbühl, M. A. Kastner, M. P. Hanson, and A. C. Gossard, “Electrical control of spin relaxation in a quantum dot,” *Phys. Rev. Lett.*, vol. 100, no. 4, p. 046803, 2008.
- [49] F. Marquardt and V. A. Abalmassov, “Spin relaxation in a quantum dot due to nyquist noise,” *Phys. Rev. B*, vol. 71, no. 16, p. 165325, 2005.
- [50] M. Borhani, V. N. Golovach, and D. Loss, “Spin decay in a quantum dot coupled to a quantum point contact,” *Phys. Rev. B*, vol. 73, no. 15, p. 155311, 2006.
- [51] A. V. Khaetskii and Y. V. Nazarov, “Spin relaxation in semiconductor quantum dots,” *Phys. Rev. B*, vol. 61, pp. 12639–12642, May 2000.
- [52] N. W. Ashcroft and N. D. Mermin, *Solid State Physics*. Saunders, New York, 1974.
- [53] M. Kroutvar, Y. Ducommun, D. Heiss, M. Bichler, D. Schuh, G. Abstreiter, and J. J. Finley, “Optically programmable electron spin memory using semiconductor quantum dots,” *Nature*, vol. 432, p. 81, 2004.
- [54] D. Paget, G. Lampel, B. Sapoval, and V. I. Safarov, “Low field electron-nuclear spin coupling in gallium arsenide under optical pumping conditions,” *Phys. Rev. B*, vol. 15, pp. 5780–5796, Jun 1977.

- [55] W. A. Coish, D. Loss, E. A. Yuzbashyan, and B. L. Altshuler, “Quantum versus classical hyperfine-induced dynamics in a quantum dot,” *J. Appl. Phys.*, vol. 101, no. 8, p. 081715, 2007.
- [56] I. A. Merkulov, A. L. Efros, and M. Rosen, “Electron spin relaxation by nuclei in semiconductor quantum dots,” *Phys. Rev. B*, vol. 65, p. 205309, Apr 2002.
- [57] C. P. Slichter, *Principles of Magnetic Resonance*. Springer-Verlag, Berlin, 1990.
- [58] D. Klauser, W. A. Coish, and D. Loss, “Nuclear spin state narrowing via gate-controlled rabi oscillations in a double quantum dot,” *Phys. Rev. B*, vol. 73, no. 20, p. 205302, 2006.
- [59] E. A. Laird, C. Barthel, E. I. Rashba, C. M. Marcus, M. P. Hanson, and A. C. Gossard, “Hyperfine-mediated gate-driven electron spin resonance,” *Phys. Rev. Lett.*, vol. 99, no. 24, p. 246601, 2007.
- [60] A. Abragam, *The Principles of Nuclear Magnetism*. Clarendon, Oxford, 1961.
- [61] W. M. Witzel, R. de Sousa, and S. Das Sarma, “Quantum theory of spectral-diffusion-induced electron spin decoherence,” *Phys. Rev. B*, vol. 72, p. 161306, Oct 2005.
- [62] N. Shenvi, R. de Sousa, and K. B. Whaley, “Universal scaling of hyperfine-induced electron spin echo decay,” *Phys. Rev. B*, vol. 71, no. 22, p. 224411, 2005.
- [63] A. W. Overhauser, “Polarization of nuclei in metals,” *Phys. Rev.*, vol. 92, pp. 411–415, Oct 1953.
- [64] T. R. Carver and C. P. Slichter, “Experimental verification of the Overhauser nuclear polarization effect,” *Phys. Rev.*, vol. 102, pp. 975–980, May 1956.
- [65] M. Kroner, K. M. Weiss, B. Biedermann, S. Seidl, S. Manus, A. W. Holleitner, A. Badolato, P. M. Petroff, B. D. Gerardot, R. J. Warburton, and K. Karrai, “Optical detection of single-electron spin resonance in a quantum dot,” *Phys. Rev. Lett.*, vol. 100, no. 15, p. 156803, 2008.

- [66] A. Greilich, A. Shabaev, D. R. Yakovlev, A. L. Efros, I. A. Yugova, D. Reuter, A. D. Wieck, and M. Bayer, “Nuclei-induced frequency focusing of electron spin coherence,” *Science*, vol. 317, no. 5846, pp. 1896–1899, 2007.
- [67] A. I. Tartakovskii, T. Wright, A. Russell, V. I. Fal’ko, A. B. Van’kov, J. Skiba-Szymanska, I. Drouzas, R. S. Kolodka, M. S. Skolnick, P. W. Fry, A. Tahraoui, H.-Y. Liu, and M. Hopkinson, “Nuclear spin switch in semiconductor quantum dots,” *Phys. Rev. Lett.*, vol. 98, no. 2, p. 026806, 2007.
- [68] M. S. Rudner and L. S. Levitov, “Self-polarization and dynamical cooling of nuclear spins in double quantum dots,” *Phys. Rev. Lett.*, vol. 99, no. 3, p. 036602, 2007.
- [69] D. J. Reilly, J. M. Taylor, J. R. Petta, C. M. Marcus, M. P. Hanson, and A. C. Gossard, “Suppressing spin qubit dephasing by nuclear state preparation,” *Science*, vol. 321, no. 5890, pp. 817–821, 2008.
- [70] A. Brataas, G. E. Bauer, and P. J. Kelly, “Non-collinear magnetoelectronics,” *Phys. Rep.*, vol. 427, no. 4, pp. 157–255, 2006.
- [71] A. Brataas, Y. V. Nazarov, and G. E. W. Bauer, “Spin-transport in multi-terminal normal metal-ferromagnet systems with non-collinear magnetizations,” *Eur. Phys. J. B*, vol. 22, p. 99, 2001.
- [72] A. Brataas, Y. V. Nazarov, and G. E. W. Bauer, “Finite-element theory of transport in ferromagnet-normal metal systems,” *Phys. Rev. Lett.*, vol. 84, pp. 2481–2484, Mar 2000.
- [73] A. W. Overhauser, “Paramagnetic relaxation in metals,” *Phys. Rev.*, vol. 89, pp. 689–700, Feb 1953.
- [74] J. J. Sakurai, *Modern Quantum Mechanics*. Addison-Wesley, Reading MA, 1994.
- [75] N. G. van Kampen, *Stochastic Processes in Physics and Chemistry*. North-Holland, Amsterdam, 1990.
- [76] H. A. Kramers, “Brownian motion in a field of force and the diffusion model of chemical reactions,” *Physica*, vol. 7, pp. 284–304, 1940.

- [77] A. V. Khaetskii, D. Loss, and L. Glazman, “Electron spin decoherence in quantum dots due to interaction with nuclei,” *Phys. Rev. Lett.*, vol. 88, p. 186802, Apr 2002.
- [78] A. Greilich, D. R. Yakovlev, A. Shabaev, A. L. Efros, I. A. Yugova, R. Oulton, V. Stavarache, D. Reuter, A. Wieck, and M. Bayer, “Mode locking of electron spin coherences in singly charged quantum dots,” *Science*, vol. 313, no. 5785, pp. 341–345, 2006.
- [79] J. Iñarrea, G. Platero, and A. H. MacDonald, “Electronic transport through a double quantum dot in the spin-blockade regime: Theoretical models,” *Phys. Rev. B*, vol. 76, no. 8, p. 085329, 2007.
- [80] O. N. Jouravlev and Y. V. Nazarov, “Electron transport in a double quantum dot governed by a nuclear magnetic field,” *Phys. Rev. Lett.*, vol. 96, no. 17, p. 176804, 2006.
- [81] C. W. Lai, P. Maletinsky, A. Badolato, and A. Imamoglu, “Knight-field-enabled nuclear spin polarization in single quantum dots,” *Phys. Rev. Lett.*, vol. 96, no. 16, p. 167403, 2006.
- [82] J. M. Taylor, C. M. Marcus, and M. D. Lukin, “Long-lived memory for mesoscopic quantum bits,” *Phys. Rev. Lett.*, vol. 90, p. 206803, May 2003.
- [83] J. R. Petta, J. M. Taylor, A. C. Johnson, A. Yacoby, M. D. Lukin, C. M. Marcus, M. P. Hanson, and A. C. Gossard, “Dynamic nuclear polarization with single electron spins,” *Phys. Rev. Lett.*, vol. 100, no. 6, p. 067601, 2008.
- [84] J. Dreiser, M. Atatüre, C. Galland, T. Müller, A. Badolato, and A. Imamoglu, “Optical investigations of quantum dot spin dynamics as a function of external electric and magnetic fields,” *Phys. Rev. B*, vol. 77, no. 7, p. 075317, 2008.
- [85] S. I. Erlingsson and Y. V. Nazarov, “Hyperfine-mediated transitions between a zeeman split doublet in GaAs quantum dots: The role of the internal field,” *Phys. Rev. B*, vol. 66, p. 155327, Oct 2002.
- [86] A. Abragam, “Overhauser effect in nonmetals,” *Phys. Rev.*, vol. 98, pp. 1729–1735, Jun 1955.
- [87] D. Paget, “Optical detection of NMR in high-purity GaAs: Direct study of the relaxation of nuclei close to shallow donors,” *Phys. Rev. B*, vol. 25, pp. 4444–4451, Apr 1982.

- [88] M. Pioro-Ladrière, T. Obata, Y. Tokura, Y.-S. Shin, T. Kubo, K. Yoshida, T. Taniyama, and S. Tarucha, “Electrically driven single-electron spin resonance in a slanting Zeeman field,” *Nature Physics*, vol. 4, pp. 776–779, 2008.
- [89] P. Maletinsky, A. Badolato, and A. Imamoglu, “Dynamics of quantum dot nuclear spin polarization controlled by a single electron,” *Phys. Rev. Lett.*, vol. 99, no. 5, p. 056804, 2007.
- [90] V. L. Korenev, “Nuclear spin nanomagnet in an optically excited quantum dot,” *Phys. Rev. Lett.*, vol. 99, no. 25, p. 256405, 2007.
- [91] K. Ono, D. G. Austing, Y. Tokura, and S. Tarucha, “Current rectification by Pauli exclusion in a weakly coupled double quantum dot system,” *Science*, vol. 297, no. 5585, pp. 1313–1317, 2002.
- [92] A. C. Johnson, J. R. Petta, C. M. Marcus, M. P. Hanson, and A. C. Gossard, “Singlet-triplet spin blockade and charge sensing in a few-electron double quantum dot,” *Phys. Rev. B*, vol. 72, no. 16, p. 165308, 2005.
- [93] M. S. Rudner and L. S. Levitov, “Electrically driven reverse overhauser pumping of nuclear spins in quantum dots,” *Phys. Rev. Lett.*, vol. 99, no. 24, p. 246602, 2007.
- [94] F. H. L. Koppens, K. C. Nowack, and L. M. K. Vandersypen, “Spin echo of a single electron spin in a quantum dot,” *Phys. Rev. Lett.*, vol. 100, no. 23, p. 236802, 2008.
- [95] G. Burkard, D. Loss, and D. P. DiVincenzo, “Coupled quantum dots as quantum gates,” *Phys. Rev. B*, vol. 59, pp. 2070–2078, Jan 1999.
- [96] G. Giedke, J. M. Taylor, D. D’Alessandro, M. D. Lukin, and A. Imamoglu, “Quantum measurement of a mesoscopic spin ensemble,” *Phys. Rev. A*, vol. 74, no. 3, p. 032316, 2006.
- [97] D. Stepanenko, G. Burkard, G. Giedke, and A. Imamoglu, “Enhancement of electron spin coherence by optical preparation of nuclear spins,” *Phys. Rev. Lett.*, vol. 96, no. 13, p. 136401, 2006.
- [98] W. M. Witzel and S. Das Sarma, “Quantum theory for electron spin decoherence induced by nuclear spin dynamics in semiconductor quantum computer architectures: Spectral diffusion of localized electron spins in the

- nuclear solid-state environment,” *Phys. Rev. B*, vol. 74, no. 3, p. 035322, 2006.
- [99] A. Greilich, S. Spatzek, I. A. Yugova, I. A. Akimov, D. R. Yakovlev, A. L. Efros, D. Reuter, A. D. Wieck, and M. Bayer, “Collective single mode precession of electron spins in a quantum dot ensemble.” arXiv:0811.1783, 2008.
- [100] D. J. Reilly, J. M. Taylor, E. A. Laird, J. R. Petta, C. M. Marcus, M. P. Hanson, and A. C. Gossard, “Measurement of temporal correlations of the overhauser field in a double quantum dot,” *Phys. Rev. Lett.*, vol. 101, no. 23, p. 236803, 2008.
- [101] J. Baugh, Y. Kitamura, K. Ono, and S. Tarucha, “Large nuclear Overhauser fields detected in vertically coupled double quantum dots,” *Phys. Rev. Lett.*, vol. 99, no. 9, p. 096804, 2007.
- [102] S. Foletti, J. Martin, M. Dolev, D. Mahalu, V. Umansky, and A. Yacoby, “Dynamic nuclear polarization using a single pair of electrons.” arXiv:0801.3613, 2008.
- [103] P. Maletinsky, C. W. Lai, A. Badolato, and A. Imamoglu, “Nonlinear dynamics of quantum dot nuclear spins,” *Phys. Rev. B*, vol. 75, no. 3, p. 035409, 2007.
- [104] P.-F. Braun, B. Urbaszek, T. Amand, X. Marie, O. Krebs, B. Eble, A. Lemaitre, and P. Voisin, “Bistability of the nuclear polarization created through optical pumping in $\text{In}_{1-x}\text{Ga}_x\text{As}$ quantum dots,” *Phys. Rev. B*, vol. 74, no. 24, p. 245306, 2006.
- [105] F. H. L. Koppens, C. Buizert, I. T. Vink, K. C. Nowack, T. Meunier, L. P. Kouwenhoven, and L. M. K. Vandersypen, “Detection of single electron spin resonance in a double quantum dot,” *J. Appl. Phys.*, vol. 101, no. 8, p. 081706, 2007.
- [106] T. A. Fulton and G. J. Dolan, “Observation of single-electron charging effects in small tunnel junctions,” *Phys. Rev. Lett.*, vol. 59, pp. 109–112, Jul 1987.
- [107] R. C. Ashoori, H. L. Stormer, J. S. Weiner, L. N. Pfeiffer, S. J. Pearton, K. W. Baldwin, and K. W. West, “Single-electron capacitance spectroscopy of discrete quantum levels,” *Phys. Rev. Lett.*, vol. 68, pp. 3088–3091, May 1992.

- [108] C. Flindt, A. S. Sørensen, and K. Flensberg, “Spin-orbit mediated control of spin qubits,” *Phys. Rev. Lett.*, vol. 97, no. 24, p. 240501, 2006.
- [109] V. N. Golovach, M. Borhani, and D. Loss, “Electric-dipole-induced spin resonance in quantum dots,” *Phys. Rev. B*, vol. 74, no. 16, p. 165319, 2006.
- [110] A. Pfund, I. Shorubalko, K. Ensslin, and R. Leturcq, “Suppression of spin relaxation in an InAs nanowire double quantum dot,” *Phys. Rev. Lett.*, vol. 99, no. 3, p. 036801, 2007.
- [111] A. Pfund, I. Shorubalko, R. Leturcq, and K. Ensslin, “Pauli spin-blockade in an InAs nanowire double quantum dot,” *Physica E: Low-dimensional Systems and Nanostructures*, vol. 40, no. 5, pp. 1279 – 1281, 2008. 17th International Conference on Electronic Properties of Two-Dimensional Systems.
- [112] A. Pfund, I. Shorubalko, K. Ensslin, and R. Leturcq, “Spin-state mixing in InAs double quantum dots,” *Phys. Rev. B*, vol. 76, no. 16, p. 161308, 2007.
- [113] C. L. Romano, P. I. Tamborenea, and S. E. Ulloa, “Spin-orbit effects on two-electron states in nanowhisker double quantum dots.” arXiv:0801.1808, 2008.
- [114] H.-Y. Chen, V. Apalkov, and T. Chakraborty, “Spin-orbit effects on resonant tunneling conductance through a double-quantum-dot system,” *J. Phys.: Cond. Matt.*, vol. 20, no. 13, p. 135221 (7pp), 2008.
- [115] M. Trif, V. N. Golovach, and D. Loss, “Spin-spin coupling in electrostatically coupled quantum dots,” *Physical Review B (Condensed Matter and Materials Physics)*, vol. 75, no. 8, p. 085307, 2007.
- [116] K. V. Kavokin, “Anisotropic exchange interaction of localized conduction-band electrons in semiconductors,” *Phys. Rev. B*, vol. 64, p. 075305, Jul 2001.
- [117] H. O. H. Churchill, F. Kuemmeth, J. W. Harlow, A. J. Bestwick, E. I. Rashba, K. Flensberg, C. H. Stwertka, T. Taychatanapat, S. K. Watson, and C. M. Marcus, “Relaxation and dephasing in a two-electron ^{13}C nanotube double quantum dot,” *Phys. Rev. Lett.*, vol. 102, no. 16, p. 166802, 2009.
- [118] S. Parkin, X. Jiang, C. Kaiser, A. Panchula, K. Roche, and M. Samant, “Magnetically engineered spintronic sensors and memory,” *Proc. IEEE*, vol. 91, pp. 661–680, 2003.

-
- [119] D. D. Awschalom, D. Loss, and N. Samarth, eds., *Semiconductor Spintronics and Quantum Computation*. Springer-Verlag, Berlin, 2002.
- [120] S. S. P. Parkin, “Giant magnetoresistance in magnetic nanostructures,” in *Annual Review of Materials Science* **25** (B. W. Wessels, ed.), p. 357, Annual Review Inc., Palo Alto, CA, 1995.
- [121] S. I. Erlingsson, Y. V. Nazarov, and V. I. Fal’ko, “Nucleus-mediated spin-flip transitions in GaAs quantum dots,” *Phys. Rev. B*, vol. 64, p. 195306, Oct 2001.
- [122] F. Meier and B. P. Zakharchenya, eds., *Optical orientation*. Elsevier, Amsterdam, 1984.
- [123] J. Schliemann, A. Khaetskii, and D. Loss, “Electron spin dynamics in quantum dots and related nanostructures due to hyperfine interaction with nuclei,” *J. Phys.: Cond. Matt.*, vol. 15, pp. 1809–1833, December 2003.
- [124] K. Xia, P. J. Kelly, G. E. W. Bauer, A. Brataas, and I. Turek, “Spin torques in ferromagnetic/normal-metal structures,” *Phys. Rev. B*, vol. 65, p. 220401, May 2002.

Summary

In this thesis we investigate effects of interaction between electron spins and nuclear spins in two nanoscopic devices, the *quantum dot* and the *spin valve*.

A quantum dot is a small quantum well in which one can trap electrons. One of the proposed applications of quantum dots is the implementation of electron spin qubits. Since most of the environmental degrees of freedom couple only to the *charge* of an electron in a quantum dot, it was widely believed that its *spin* is very well isolated from the environment, and therefore could be used as a reliable qubit. In experiment however, it turned out that electron spin qubits in quantum dots are subject to rapid decoherence. All evidence points at the nuclear spins in the quantum dot host material as being the main problem: a million randomly fluctuating nuclear spins couple via the hyperfine interaction to the electron spin, and thereby act as a small but unknown effective magnetic field. This field introduces rapid electron spin dephasing and thus decoherence of the qubit. Hyperfine interaction however, works both ways: the electron spin, in turn, also affects the nuclear spins. Recently, several experiments showed clear signs of dynamical nuclear spin pumping driven by the electron spin dynamics in a quantum dot. It was realized that there might exist ways to harness this electron-nuclear spin interaction such that the fluctuations in the nuclear field become suppressed and, thereby, the electron spin coherence time improved.

In Chapter 4 of this thesis we investigate the coupled electron-nuclear spin dynamics in a single quantum dot under conditions of electron spin resonance. We show how the non-equilibrium electron spin dynamics can cause strong nuclear spin pumping. At small frequency mismatch the nuclear field detunes the resonance. Remarkably, at larger frequency mismatch its effect is opposite: the nuclear system is bistable, and in one of the stable states the field accurately tunes the electron spin splitting to resonance. In this state the nuclear field fluctuations are strongly suppressed and nuclear spin relaxation is accelerated.

Then, in Chapters 5 and 6, we turn to the same effect in a double quantum dot. We experimentally observe in the double dot under conditions of electron spin

resonance multiple stable states of nuclear polarization and nuclear self-tuning over a large range of fields, even when the external static magnetic field or the excitation frequency are changed back and forth. The nuclear field apparently adjusts itself such that the electron spin resonance condition remains satisfied. We explain these observations within an elaborated theoretical rate equation model for the polarization in each of the dots, in the limit of strong driving. This model also captures unusual features of the data, such as fast switching and a ‘wrong’ sign of polarization. The results reported enable applications of this polarization effect, including accurate manipulation and control of nuclear fields.

In Chapter 7 we present the first step of our analysis of similar effects which have been observed in quantum dots in materials with strong spin-orbit coupling. We study electron transport in such a system in the Pauli spin blockade regime. It had been experimentally observed that the presence of spin-orbit coupling drastically modifies the basic spin physics in the dots: when a small external magnetic field is applied the spin blockade is lifted. This is inconvenient since spin blockade is a useful tool for electron spin manipulation and read-out. In our model, we incorporate the effect of spin-orbit coupling into a modified interdot tunnel coupling. We finally elucidate the role of spin-orbit interaction, the external magnetic field, the nuclear fields, and spin relaxation in the basic transport properties of the system. We find qualitative agreement with experimental observations, and we propose a way to extend the range of magnetic fields in which blockade can be observed.

In the last Chapter, we consider a spin valve, one of the basic spintronic devices. A spin valve is a small ferromagnet-normal metal-ferromagnet junction which exhibits strong magnetoresistive effects: the conductance of the junction can vary strongly when one changes the directions of magnetization in the two ferromagnets. It is widely believed that in metallic devices hyperfine interaction manifests itself merely as a weak source of spin relaxation and that it does not influence the electronic transport properties of the devices directly. We study transport through the spin valve and we investigate the effect of hyperfine interaction between electrons and nuclei in the normal-metal part. We show that a switching of the magnetization directions of the ferromagnets causes nuclear spins to precess. The effect of this precession on the current through the system is large enough to be observed in experiment.

Jeroen Danon

July 2009

Samenvatting

In dit proefschrift onderzoeken we effecten van de wisselwerking tussen elektronspin en kernspin in twee nanoscopische systemen, de *quantum dot* en het *spinventiel*.

Een quantum dot is een kleine potentiaalput waarin elektronen opgesloten kunnen worden. Een van de voorgestelde toepassingen van quantum dots is de implementatie van qubits van elektronspin. Aangezien de meeste vrijheidsgraden van de omgeving van de quantum dot alleen maar koppelen aan de *lading* van het elektron, werd algemeen aangenomen dat zijn *spin* goed geïsoleerd zou zijn van de omgeving en daarom gebruikt zou kunnen worden als betrouwbaar qubit. Echter, uit experimenten bleek dat ook elektronspin-qubits zeer snelle decoherentie vertonen. Het lijkt erop dat het belangrijkste probleem bestaat uit de kernspins in het materiaal waarvan de quantum dot gemaakt is: een miljoen willekeurig fluctuerende kernspins koppelen via de hyperfijnwisselwerking aan de elektronspin, en manifesteren zich op die manier als een klein maar willekeurig magnetisch veld. Dit veld zorgt ervoor dat er snel onzekerheid ontstaat in de fase van de elektronspin, en veroorzaakt dus snelle decoherentie van de qubit. Echter, hyperfijnwisselwerking werkt twee kanten op: de elektronspin, op zijn beurt, beïnvloedt ook de kernspins. Een aantal recente experimenten heeft duidelijk laten zien hoe de kernspins in een quantum dot dynamisch gepompt kunnen worden door de elektronspindynamica. Men realiseerde zich al snel dat het wellicht mogelijk is om deze wisselwerking tussen de elektron- en kernspin zo te gebruiken dat de fluctuaties in het kernveld onderdrukt worden. Op die manier zou de coherentietijd van de elektronspin aanzienlijk verlengd kunnen worden.

In Hoofdstuk 4 van dit proefschrift onderzoeken we de gekoppelde spindynamica van het elektron en de kernen in een enkele quantum dot, wanneer het systeem in het regime van elektronspinresonantie is. We laten zien hoe de niet-evenwichtige elektronspindynamica kan leiden tot een sterk pompen van de kernspins. Bij een klein frequentieverschil wordt het systeem door het opgebouwde kernveld van de resonantie af gedreven. Opvallend is dat bij een groter frequen-

tieverschil het effect juist tegengesteld is: het systeem wordt bistabiel, en in een van de twee stabiele staten zorgt het kernveld ervoor dat de Zeemansplitsing van het elektron juist precies op resonantie gehouden wordt. In deze staat zijn de kernspinfluctuaties sterk onderdrukt, en is de kernspinrelaxatie versneld.

Vervolgens, in Hoofdstukken 5 en 6, kijken we naar hetzelfde effect in een dubbele quantum dot. Experimenteel observeren we, wanneer elektronspinresonantie toegepast wordt, meerdere stabiele staten van kernspinpolarisatie en ‘zelfafstemming’ door het kernveld in een groot gebied van frequenties, zelfs wanneer het externe statische magneetveld of the excitatiefrequentie afwisselend groter en kleiner gemaakt worden. Blijkbaar past het kernveld zich constant aan zodat de resonantieconditie vervuld blijft. We leggen deze observaties uit in een uitgebreid theoretisch model voor de polarisatie in de twee dots, in de limiet van sterke drijving. Dit model beschrijft ook ongebruikelijke kenmerken van de data, zoals snelle schakeling en een ‘verkeerd’ teken van polarisatie. Onze resultaten kunnen leiden tot toepassingen van dit polarisatie-effect, waaronder bijvoorbeeld nauwkeurige manipulatie van en controle over de kernvelden.

In Hoofdstuk 7 presenteren we de eerste stap van een analyse van vergelijkbare effecten, waargenomen in quantum dots in materialen met een sterke spin-baan wisselwerking. We bestuderen elektrontransport in zo’n systeem in het regime van Pauli spin blokkade. Experimenteel is gebleken dat sterke spin-baan wisselwerking de spinfysica in de dots drastisch kan veranderen: wanneer een klein extern magneetveld wordt aangelegd, dan wordt de blokkade opgeheven. Dit is vervelend, aangezien spin blokkade een nuttig hulpmiddel is voor manipulatie en uitlezing van elektronspins. In ons model nemen we het effect van spin-baan wisselwerking mee in een veranderde interdot tunnelkoppeling. We laten zien wat de rol is van spin-baan wisselwerking, het externe magneetveld, de kernvelden en spinrelaxatie, in de transporteigenschappen van het systeem. Onze resultaten komen kwalitatief overeen met de experimentele waarnemingen en we stellen ook een manier voor om het gebied waarin spin blokkade geobserveerd kan worden aanzienlijk uit te breiden.

In het laatste Hoofdstuk beschouwen we een spinventiel, een van de basisapparaten in de spintronica. Een spinventiel is een kleine ferromagneet-normaal metaal-ferromagneet junctie, die sterke magnetoresistieve eigenschappen heeft: de geleiding van de junctie kan sterk variëren wanneer de richting van de magnetisaties van de twee ferromagneten veranderd wordt. Het wordt algemeen aangenomen dat in metallische structuren de hyperfijnwisselwerking zich slechts manifesteert als een zwakke bron van spinrelaxatie en dat het de elektronische transporteigenschappen niet direct beïnvloedt. We bestuderen het transport door het spinventiel en onderzoeken het effect van hyperfijnwisselwerking tussen de

elektronen en kernen in het middengedeelte. We laten zien dat een verandering van de richting van de magnetisaties van de ferromagneten ervoor zorgt dat de kernspins gaan precesseren. Het effect van deze precessie op de stroom door het systeem is groot genoeg om duidelijk waargenomen te worden in een experiment.

Jeroen Danon
Juli 2009

Curriculum Vitae

Jeroen Danon

- June 2, 1977 Born in Delft, The Netherlands
- 1989 – 1995 Gymnasium at the *Gymnasium Haganum*, Den Haag
- 1995 – 2005 M.Sc. Applied Physics (*Cum Laude*),
Delft University of Technology
Graduate research under supervision of prof. dr. Yu. V. Nazarov
“*Detection of Quantum Noise*”
- 2005 – 2009 Ph.D. research at Delft University of Technology
under supervision of prof. dr. Yu. V. Nazarov
“*Nuclear Spin Effects in Nanostructures*”

List of publications

1. *Locking electron spins into resonance by electron-nuclear feedback*
I. T. Vink, K. C. Nowack, F. H. L. Koppens, J. Danon, Yu. V. Nazarov,
and L. M. K. Vandersypen
Accepted for publication in Nature Physics.
2. *Multiple nuclear polarization states in a double quantum dot*
J. Danon, I. T. Vink, F. H. L. Koppens, K. C. Nowack,
L. M. K. Vandersypen, and Yu. V. Nazarov
Phys. Rev. Lett. **103**, 046601 (2009)
3. *Pauli spin blockade in the presence of strong spin-orbit coupling*
J. Danon and Yu. V. Nazarov
Phys. Rev. B **80**, 041301(R) (2009)
4. *Nuclear tuning and detuning of the electron spin resonance:
Theoretical consideration*
J. Danon and Yu. V. Nazarov
Phys. Rev. Lett. **100**, 056603 (2008)
5. *Nuclear spin effect in a metallic spin valve*
J. Danon and Yu. V. Nazarov
Phys. Rev. Lett. **97**, 146602 (2006)
6. *Quantum tunneling detection of two-photon and two-electron processes*
J. Tobiska, J. Danon, I. Snyman, and Yu. V. Nazarov
Phys. Rev. Lett. **96**, 096801 (2006)

